

UCSF

UC San Francisco Electronic Theses and Dissertations

Title

Functional Remineralization of Carious Dentin

Permalink

<https://escholarship.org/uc/item/4s42x5wt>

Author

Pugach, Megan Kardon

Publication Date

2007-12-11

Peer reviewed|Thesis/dissertation

Functional Remineralization of Carious Dentin

by

Megan Kardon Pugach

DISSERTATION

Submitted in partial satisfaction of the requirements for the degree of

DOCTOR OF PHILOSOPHY

in

Oral and Craniofacial Sciences

in the

GRADUATE DIVISION

Copyright 2007

by

Megan Kardon Pugach

Dedication

This dissertation is dedicated to Meemom, who is the inspiration of my life. You introduced me to the world of science before I could walk. Although you are not physically here with me, you have been by my side encouraging me throughout this experience, and always will be. I miss you every day. I love you.

Acknowledgements

I would like to acknowledge the following grants for funding my research: T32-DE07204, T32-DE07306, RO1-DE16849, and PO1-DE09859.

I wish to thank my mentor, Grayson Marshall, for his constant support, advice, and guidance. In addition, I would like to thank Sally Marshall for support, advice and mentorship, Larry Watanabe for mentorship, help with sample preparation and technical issues, Grace Nonomura for advice, help with sample preparation and tooth collection, Stefan Habelitz for mentorship and contributions with artificial caries (Chapter 3), remineralization (Chapter 5) and collagen imaging (Chapter 4), Sunita Ho for mentorship and contributions with collagen imaging (Chapter 4), Kuniko Saeki for advice and mentorship, John Featherstone for contributions with artificial caries (Chapter 3) and remineralization (Chapter 5), Pamela DenBesten and Wu Li for advice, mentorship, and help with biochemistry, Joel Ager for contributions with UVRRS and SAXS (Chapter 4), John Kinney for contributions with SAXS (Chapter 4), James Strother for contributions with CD zone characterization (Chapter 2), Shabnam Zartoshtimanesh for contributions with high resolution collagen imaging (Chapter 4), Daniel Fried and Cynthia Darling for contributions with TMR (Chapters 2-4), Stuart Gansky for contributions with statistics (Chapter 2), May Wong and Luiz Bertassoni for contributions with remineralization experiments (Chapter 5), Lauren Jenni Imai and Linda Prentice for contributions with trichrome staining (Chapter 4), and Silvia Foppiano for support, advice and mentorship.

Most importantly I would like to thank my family, Jesse, Leslie and Rick Pugach, for being my constant support network, always there to pick me up, provide unconditional love and cheer me on. I could not have done this without them.

Dissertation Abstract

A primary goal of dental tissue engineering is the biological reconstruction of tooth substrate destroyed by caries or other diseases affecting tooth mineralization. Traditionally, dentists treat caries by using invasive techniques to remove the diseased dental tissue and restore the lesion, ideally preventing further progression of decay. Success in strategies associated with remineralization of enamel and root caries have contributed to the less invasive prospect of remineralization of dentinal carious lesions. The central hypothesis of this dissertation is that carious dentin lesions can be remineralized if the lesions contain residual mineral. Caries Detector (CD) stained zones (pink, light pink, transparent and normal) of arrested carious dentin lesions were characterized according to microstructure by atomic force microscopy (AFM) imaging, mineral content by digital transverse microradiography, and nanomechanical properties by AFM-based nanoindentation. CD-stained and unstained zones had significantly different microstructure, mineral content and nanomechanical properties. Furthermore, the most demineralized carious zone contained residual mineral. To obtain reproducible, standardized dentin caries lesions, we characterized the lesions from an artificial carious dentin lesion model using a 0.05M acetate demineralization buffer. The artificial caries-like lesions produced by the buffer had similar mineral content and nanomechanical properties in the stained and unstained zones as natural dentin lesions. Both natural and artificial lesions had significant correlations between mineral content and nanomechanical properties. Mineral crystallite size and shape was examined by small angle x-ray

scattering. Both natural and artificial carious dentin had different mineral sizes than normal dentin. Collagen in natural and artificial carious dentin lesions was examined by trichrome stain, AFM high-resolution imaging, and UV resonance Raman spectroscopy, to determine if fibrils were intact and mineralization levels. It appeared that the collagen in the most demineralized pink zones of the lesions was intact and contained intrafibrillar mineral. Natural and artificial carious dentin lesions were treated with remineralization solutions containing different amounts of Ca^{2+} and PO_4^{3-} , with and without CO_3^{2-} and with and without 2 ppm fluoride. The hydrated nanomechanical properties of the lesions were partially restored. This suggests that the most CD-stained zones of arrested dentin caries lesions may be remineralizable. These results suggest that remineralization as an approach of minimally invasive dentistry using non-invasive treatments to restore dental tissues is possible.

Table of Contents

Dedication	iii
Acknowledgements	iv
Dissertation Abstract	vi
Table of Contents	viii
List of Tables	ix
List of Figures	x
Chapter 1	1
Introduction	1
Summary of dissertation	7
Chapter 2	17
Natural dentin caries zones: Caries Detector stain, mineral, microstructure and mechanical properties.	17
Figures and Tables	33
Chapter 3	38
Comparison of artificial carious dentin lesions with natural carious dentin lesions: mineral content and nanomechanical properties.	38
Figures and Tables	52
Chapter 4	59
Collagen in carious dentin lesions	59
Figures and Tables	82
Chapter 5	95
Remineralization of artificial and natural carious dentin lesions	95
Figures and Tables	110
Chapter 6	118
Summary and future directions	118
Summary and Discussion	119
Future Directions	125
Significance of this research.....	128
Conclusions	129
Figure	133
UCSF Library Release	<i>Error! Bookmark not defined.</i>

List of Tables

Table 2-1. Means according to CD stain. _____	37
Table 3-1. Average elastic modulus and mineral content of artificial caries-like lesions according to CD stain. _____	58
Table 4-1. Gap-overlap height differences of dentin collagen from pink zones. _____	84
Table 4-2. Summary of data from SAXS measurements. _____	94
Table 5-1. Metastable supersaturated remineralization solutions. _____	110
Table 5-2. Hydrated elastic modulus in GPa of artificial carious dentin lesions treated with remineralization solutions. _____	111
Table 5-3. Hydrated nanohardness in GPa of artificial carious dentin lesions treated with remineralization solutions. _____	112
Table 5-4. Increase in hydrated elastic modulus and nanohardness of natural carious dentin lesions treated with one remineralization solution. _____	113

List of Figures

Figure 2-1. Morphological features of carious dentin_____	33
Figure 2-2. Nanomechanical properties of carious dentin_____	35
Figure 2-3. Mineral content of carious dentin_____	36
Figure 3-1. Artificial dentin caries sample preparation_____	52
Figure 3-2. Kinetics of artificial dentin caries acetate buffer_____	53
Figure 3-3. Nanomechanical properties of artificial carious dentin_____	55
Figure 3-4. Mineral content of artificial carious dentin_____	56
Figure 4-1. Trichrome staining of carious dentin_____	82
Figure 4-2. High-resolution AFM imaging of carious dentin collagen_____	83
Figure 4-3. UVRR spectra of citric acid demineralized dentin_____	85
Figure 4-4. UVRR spectra of 24 hr citric acid demineralized dentin_____	86
Figure 4-5. Relative UVRR spectra peak heights_____	87
Figure 4-6. UVRR spectra of carious dentin_____	88
Figure 4-7. SAXS images_____	89
Figure 4-8. Azimuthally averaged SAXS patterns_____	90
Figure 4-9. SAXS mineral crystallite thickness_____	91
Figure 4-10. Mineral content of SAXS samples_____	92
Figure 4-11. SAXS mineral crystallite shape_____	93
Figure 5-1. AFM images of remineralized artificial carious dentin lesions_____	114
Figure 5-2. Nanomechanical properties of remineralized artificial carious dentin lesions_____	115

Figure 5-3. *AFM images of remineralized natural carious dentin lesions* ____ 116

Figure 5-4. *Nanomechanical properties of remineralized natural carious dentin lesions* _____ 117

Figure 6-1. *AFM load-displacement curves of carious dentin* _____ 133

Chapter 1

Introduction

Dental caries is a transmissible, multifactorial disease that affects 85% of adults in the United States (Services, 2002). Traditionally, dentists treat caries by using invasive techniques to remove the diseased and surrounding dental tissue and restore the lesion with a synthetic material, ideally preventing further progression of decay. A primary goal of minimally invasive dentistry is the biological reconstruction of tooth substrate destroyed by caries. Success in strategies associated with remineralization of enamel and root caries (Featherstone and Rodgers, 1981; O'Reilly and Featherstone, 1987), and studies on the roles of calcified matrix proteins in *de novo* mineralization of bone or dentin have contributed to the less invasive possibility of remineralization of dentinal carious lesions (Hunter and Goldberg, 1993; Lussi *et al.*, 1988; Mukai and ten Cate, 2002).

The most abundant non-collagenous protein (NCP) in the dentin matrix, dentin phosphoprotein (DPP), is considered to have a crucial role in dentin mineralization due to its highly anionic, Ca^{2+} , and collagen-binding properties (Lussi *et al.*, 1988; Van den Bos, 1994). A mutation in the gene encoding DPP has been implicated in Dentinogenesis Imperfecta type II (DGI-II), a heritable autosomal dominant disease that is characterized by defects in dentin structure and mineralization (Thotakura *et al.*, 2000; Waltimo *et al.*, 1995). Furthermore, mice lacking DPP display DGI-II-like hypomineralized dentin (Sreenath *et al.*, 2003). Recent work suggests that DGI-II teeth lack intrafibrillar mineral (Kinney *et al.*, 2001a) and this substantially reduces the mechanical properties of the hydrated tissue (Kinney *et al.*, 2003). However, the exact mechanism involved in

DPP-induced dentin mineralization or remineralization, has yet to be clearly determined.

When dentin was demineralized *in vitro* by acetic acid, one of the organic acids produced by cariogenic bacteria, DPP could not be extracted from the dentin matrix (McCurdy *et al.*, 1990). However, this phosphoprotein can be removed by re-extraction of EDTA-demineralized dentin matrices (Clarkson *et al.*, 1998). DPP is tightly bound to the collagen and has initiated mineralization on agarose bead-collagen substrates in previously reported experiments (Linde *et al.*, 1989; Van den Bos, 1994). These studies indicate that insoluble DPP tightly bound to collagen may nucleate mineral crystal growth within the collagen fibrils, the so-called intrafibrillar mineral (IF), as opposed to extrafibrillar mineral (EF), which forms outside of or around the collagen fibrils (Bradt JH, 1995; Landis *et al.*, 1993; Olszta *et al.*, 2003). These mineral nuclei may be able to direct remineralization, assuming no mineralization inhibitors such as soluble NCPs are present. The central hypothesis of the proposed research is that **remineralization of carious dentin that restores the normal hydrated elastic modulus of dentin can be accomplished if the dentin lesion contains intact collagen fibrils that have residual intrafibrillar mineral.**

Background

Dentin mineralization

Physiological calcification involves crystal deposition within the extracellular matrices of bone and teeth. The mineral in dentin is carbonated

apatite, similar to bone and calcified tendon, and is either intrafibrillar (in the gaps between collagen molecules), or extrafibrillar (attached to the collagen fibrils) (Lees *et al.*, 1997; Wassen *et al.*, 2000). Dentin apatite crystal dimensions have been reported to be between 20 and 5nm, with both plate-like and needle-like morphologies (Arsenault, 1989; Kinney *et al.*, 2001b; LeGeros, 1991).

Calcium and phosphate promote mineral induction by increasing the ion concentration in a metastable supersaturated solution, while fluoride acts as a catalyst (Saito *et al.*, 2003). Type I collagen alone will not nucleate mineral formation from metastable calcium phosphate solutions that do not spontaneously precipitate (Saito *et al.*, 1997). During dentinogenesis, the first mineral is said to nucleate and grow from within the collagen fibrils via the gap zones (Butler, 1995). In mineralizing turkey tendon, once the intrafibrillar (IF) space within the fibrils has been filled with mineral, the space around the fibrils, extrafibrillar (EF), is then mineralized (Landis *et al.*, 1993). The EF mineral is thought to be more easily removed by acid demineralization, as in caries, while the IF mineral is more difficult to remove.

Dentin caries

Acids generated by bacterial plaque following ingestion of fermentable carbohydrates begin the caries process (Featherstone *et al.*, 1990). Whether the lesions will progress, stay the same or reverse, is determined by a balance between protective (salivary proteins, antibacterials, fluoride) and pathological (acidogenic bacteria, fermentable carbohydrates) factors (Featherstone, 2004).

Mineral dissolution of the enamel is the essential first step of the process. Dentin mineral is more soluble than enamel mineral, since it contains more carbonate in the mineral and the crystallite size is much smaller (Hoppenbrouwers *et al.*, 1986). The tooth root is mostly dentin overlain with a thin coat of cementum. The demineralization process in natural root caries is diffusion controlled, as it is for enamel caries (Featherstone and Cussler, 1987). The presence of supersaturated levels of calcium and phosphate in the demineralizing buffer assists in the development of the diffusion control of the caries process. Since the rate of mineral loss can be twice as fast from the dentin as from the enamel, and dentin has much less mineral to begin with, dentin caries is a serious problem.

Before the underlying dentin matrix collagen can be degraded by collagenases, dentin has to be partially demineralized (Klont and ten Cate, 1991). Collagen fibrils in the “inner” region of carious dentin (less porous/ light pink zone by Caries Detector) appear to maintain their characteristic cross-striated banding pattern, found in normal dentin and unmineralized collagen (tendon). However, the “outer” layer (more porous, dark pink zone) contains collagen in which the banding pattern is no longer visible, which is indicative that the structure of the collagen fibrils has been disrupted by denaturation and degradation (Nakornchai *et al.*, 2004). Confirming this observation, one study found that the collagen in outer carious dentin is both quantitatively and qualitatively altered, but in the inner carious dentin, no significant difference was observed in the amino acid composition and cross-linking compared with normal

dentin collagen (Nakornchai *et al.*, 2004). However, it is important to note that the banding pattern of collagen fibrils can be obscured by a coating of mineral and non-collagenous proteins adhering to the fibril. Therefore, a lack of banding as imaged by atomic force microscopy must be carefully interpreted.

Dentin remineralization

Recent evidence suggests that dentin remineralization occurs by neither spontaneous precipitation, nor nucleation of mineral on the organic matrix but by growth of residual crystals in the lesions (Daculsi *et al.*, 1979; Hunter *et al.*, 1986; Klont and ten Cate, 1991; Levine and Rowles, 1973; Stetler-Stevenson and Veis, 1986). If phosphoproteins as inhibitors are removed, mineralization occurs on the demineralized organic matrix (Clarkson *et al.*, 1991; DeSteno *et al.*, 1975; Lussi and Linde, 1993; Saito *et al.*, 1998). Inaba (Inaba *et al.*, 1996) suggested that the removal of organic material with NaOCl enhances dentin remineralization significantly.

One recent study (Mukai and ten Cate, 2002) found that advanced root dentin carious lesions, produced *in vitro*, were remineralizable despite a virtual lack of remaining mineral in the lesion. The artificial lesions could be repaired to an apparent 50 to 85% of normal mineral, and the remineralization occurred in the surface area, the lesion body and the inner zone adjacent to the sound dentin (Mukai and ten Cate, 2002). According to transverse microradiography (TMR) analysis of mineral content of the lesions, mineral deposition first occurred in the surface layer and then moved to the lesion body when the surface layer reached

mineral content levels similar to sound dentin. Therefore, the authors concluded that the mineral precipitated on the lesion surface until there was no more space for crystal growth, and then proceeded to the body of the lesion.

Remineralization in the lesion body may reflect the number of nucleation sites available for crystal growth following demineralization, since the supersaturated remineralizing solution does not spontaneously precipitate (Clarkson *et al.*, 1998). Mukai and ten Cate (Mukai and ten Cate, 2002) proposed that since the surface did not seem to hypermineralize, the tubules remained open and available for ion transport. Although this study showed that remineralization of root caries lesions is possible, even when there is a high degree of mineral loss, the “quality” (i.e. mechanical properties) of the remineralized tissue was not assessed. It remains unclear whether the mineral was located within the fibrils, surrounding them, or how the structure and morphology of the remineralized tissue compared to normal dentin.

Summary of dissertation

The primary function of teeth is mastication. We thus define functional remineralization as a process of crystallization of apatite mineral in a diseased mineralized tissue to restore its mechanical properties and function, allowing for unimpeded mastication.

The purpose of this research is to identify the conditions required for functional remineralization of dentin, in order to re-establish the unique properties of unaffected (sound) dentin. Functional remineralization of dentin is considered

ideal because it should maintain the unique association between organic (type I collagen network with NCPs) and inorganic matrices (carbonated apatite crystals) in dentin. Dentin is a hydrated tissue, and work has shown that some tissues may vary appreciably in their apparent mechanical properties depending on whether they are hydrated or dry, the appropriate conditions for measurement of restoration of mechanical (Marshall *et al.*, 2001; Angker *et al.*, 2004). Functional remineralization will be considered to have been achieved when treatments yield hydrated nanomechanical properties of the remineralized dentin tissue that are not significantly different from normal dentin.

Residual apatite nuclei within collagen fibrils may be critical for remineralization, so it is important to establish which zones of carious lesions contain remaining mineral. In Chapter 2 the hypothesis was tested that even the most demineralized zones of dentin caries lesions have residual mineral. Zones of natural carious dentin lesions were identified by Caries Detector (CD) stain, and were characterized by relating microstructural properties (peritubular dentin presence, tubule occlusion and intratubular roughness) to nanomechanical properties as measured by atomic force microscopy (AFM) nanoindentation, mineral content as measured by x-ray tomographic microscopy (XTM), and transverse digital microradiography (TMR). The CD stain could identify with varying nanomechanical properties, mineral content, and microstructural features. Furthermore, the most demineralized CD stained-zone, showing a pink color, contained residual mineral and mineral content, that was significantly correlated with nanomechanical properties.

In our studies, natural carious dentin lesions varied considerably in size, shape and severity. Since the ultimate goal of this research was to remineralize carious dentin lesions, standardized, reproducible lesions in which the variables could be controlled, were needed. We chose a dentin demineralization model that has been shown to produce artificial caries-like lesions in dentin (McIntyre *et al.*, 2000). In Chapter 3 we tested the hypothesis that this artificial carious dentin model can create lesions with similar zones as natural lesions, and that the most demineralized zone of artificial lesions contains residual mineral. Zones of artificial carious dentin lesions as identified by CD stain were characterized, relating nanomechanical properties as measured by AFM nanoindentation, to mineral content as measured by XTM and TMR. Also in Chapter 3, mineral crystallite dimensions in both natural and artificial carious dentin lesions were determined by small angle x-ray scattering (SAXS). Artificial carious dentin lesion zones had similar mechanical properties, mineral content and mineral crystallite size as natural carious dentin lesion zones. However, the artificial lesions created by this model did not contain a region of transparent dentin (i.e. slightly demineralized with occluded tubules) and these lesions shown a thin light pink colored zone (i.e. demineralized inner dentin) compared to natural lesions.

In carious dentin lesions, especially those most severe, collagenases are both released from the dentin matrix (Tjaderhane *et al.*, 1998), and are produced by the acidogenic bacteria (Nyvad and Fejerskov, 1990; Schupbach *et al.*, 1989). Thus far, it is unclear if the CD-stained pink zone of carious dentin lesions contain intact collagen fibrils that have not been exposed to collagenase, or if the

collagen has been degraded. The state of the collagen is important to determine whether intact collagen fibrils bound to IF mineral nuclei are present for remineralization. In Chapter 4, collagen in carious dentin lesions (natural and artificial) was analyzed to determine if there are differences between carious and non-carious dentin. UV-resonance Raman spectroscopy (UVRRS) was used to investigate changes in collagen peptide bonds from hydration and dehydration of carious and non-carious dentin. Masson's trichrome staining was used to visualize the collagen in each dentin caries zone and compare these CD stained zones. The trichrome stain was also used to detect degraded collagen. AFM imaging of dentin collagen in carious dentin of both natural and artificial lesions was used to visualize collagen gap and overlap height differences. An increase in gap-overlap height difference is indicative of a loss of intrafibrillar mineral and has been shown to vary from 0 to 7 nm (Balooch *et al.*, 2004). The collagen in the most demineralized pink zones of arrested carious dentin lesions seemed intact, indicating that remineralization in these zones may be possible.

To investigate the remineralization potential of the most demineralized, pink zones of artificial and natural carious dentin lesions, we treated the lesions with remineralization solutions. In Chapter 5 the hypothesis was tested that the most demineralized zones of artificial and natural dentin caries can be remineralized such that the hydrated elastic properties will be partially restored, and will be further enhanced by the addition of fluoride to the remineralization solution. Artificial lesions were remineralized with one of 6 remineralization solutions containing varying concentrations of Ca^{2+} (2.2 mM or 1.5 mM), and

PO_4^{3-} (1.45 mM or 0.9 mM), with or without 2 ppm F^- , and with or without 22 mM CO_3^{2-} at pH 7.4 for 1 to 28 days. Hydrated nanomechanical properties were tested by AFM-based nanoindentation before remineralization to establish baseline elastic modulus (E) and hardness (H) values of the artificially demineralized lesions. The remineralization solution that resulted in the largest increase in hydrated E and H from baseline was chosen for remineralization experiments of natural carious dentin lesions. For these experiments, hydrated E and H were measured before remineralization and after 1 to 28 days. Artificial lesions were partially remineralizable, and this remineralization was enhanced by the addition of fluoride to the remineralization solution. Natural lesions were partially remineralizable, to a lesser degree than artificial lesions, after treatment with a remineralization solution containing fluoride.

Chapter 6 includes discussion, conclusions and future studies.

Significance of this research

The existing mineral nuclei or crystals may facilitate *functional* mineral growth, from within collagen fibrils (IF) and continuing outward to the EF compartment (Kinney *et al.*, 2003). Without existing mineral nucleation sites, as in completely demineralized collagen, remineralized tissue is likely the result of *precipitative* mineral growth, filling only the extrafibrillar compartment with mineral. This tissue may have structural and nanomechanical similarities to DGI-II dentin. On the other hand, functional remineralization is considered to be optimal.

The clinical applications of this area of biomineralization are vast, including therapies for defective bone and dentin diseases, such as dentinal caries. Theoretically, it would be possible to remineralize dentin demineralized by cariogenic acids, as long as the mechanisms and components involved in initial dentin mineralization were understood and the remaining components in the carious lesions were known. Caries-demineralized dentin generally contains varying and unknown concentrations of residual mineral and proteins. Therefore, it is important to identify the remaining components in carious dentin lesions and their effects on remineralization of different regions of the lesions, such that optimal remineralization conditions are determined, and future caries treatments can be minimally invasive.

D. REFERENCES

Angker L, Nijhof N, Swain MV, Kilpatrick NM (2004a). Influence of hydration and mechanical characterization of carious primary dentine using an ultra-micro indentation system (UMIS). *Eur J Oral Sci* 112(3):231-6.

Arsenault AL (1989). A comparative electron microscopic study of apatite crystals in collagen fibrils of rat bone, dentin and calcified turkey leg tendons. *Bone Miner* 6(2):165-77.

Balooch MB, G; Habelitz, S; Marshal, SJ; and Marshall, GW (2004). Intrafibrillar demineralization study of single human dentin collagen fibrils by AFM. *MRS Symposium Proceedings*.

Balooch M, Demos SG, Kinney JH, Marshall GW, Balooch G, Marshall SJ (2001). Local mechanical and optical properties of normal and transparent root dentin. *J Mater Sci Mater Med* 12(6):507-14.

Bradt JH MM, Teresiak A, Pompe W (1995). Biomimetic mineralization of collagen by combine fibril assembly and calcium phosphate formation. *Chem Mater* 11(2694-2701).

Butler WT (1995). Dentin matrix proteins and dentinogenesis. *Connect Tissue Res* 33(1-3):59-65.

Clarkson BH, Feagin FF, McCurdy SP, Sheetz JH, Speirs R (1991). Effects of phosphoprotein moieties on the remineralization of human root caries. *Caries Res* 25(3):166-73.

Clarkson BH, Chang SR, Holland GR (1998). Phosphoprotein analysis of sequential extracts of human dentin and the determination of the subsequent remineralization potential of these dentin matrices. *Caries Res* 32(5):357-64.

Daculsi G, Kerebel B, Kerebel LM (1979). Mechanisms of acid dissolution of biological and synthetic apatite crystals at the lattice pattern level. *Caries Res* 13(5):277-89.

DeSteno CV, Fragin F, Butler WT (1975). Mineralization of dentin, bone and tendon in vitro. *Calcif Tissue Res* 17(2):161-3.

Featherstone JD, Rodgers BE (1981). Effect of acetic, lactic and other organic acids on the formation of artificial carious lesions. *Caries Res* 15(5):377-85.

Featherstone JD, Cussler EL (1987). Subsurface demineralization in porous apatite-gel suspensions. *Caries Res* 21(6):494-501.

Featherstone JD, Glana R, Shariati M, Shields CP (1990). Dependence of in vitro demineralization of apatite and remineralization of dental enamel on fluoride concentration. *J Dent Res* 69 Spec No(620-5; discussion 634-6.

Featherstone JD (2004). The caries balance: the basis for caries management by risk assessment. *Oral Health Prev Dent* 2 Suppl 1(259-64.

Hoppenbrouwers PM, Driessens FC, Borggreven JM (1986). The vulnerability of unexposed human dental roots to demineralization. *J Dent Res* 65(7):955-8.

Hunter GK, Nyburg SC, Pritzker KP (1986). Hydroxyapatite formation in collagen, gelatin, and agarose gels. *Coll Relat Res* 6(3):229-38.

Hunter GK, Goldberg HA (1993). Nucleation of hydroxyapatite by bone sialoprotein. *Proc Natl Acad Sci U S A* 90(18):8562-5.

Inaba D, Ruben J, Takagi O, Arends J (1996). Effect of sodium hypochlorite treatment on remineralization of human root dentine in vitro. *Caries Res* 30(3):218-24.

Kinney JH, Pople JA, Driessen CH, Breunig TM, Marshall GW, Marshall SJ (2001a). Intrafibrillar mineral may be absent in dentinogenesis imperfecta type II (DI-II). *J Dent Res* 80(6):1555-9.

Kinney JH, Pople JA, Marshall GW, Marshall SJ (2001b). Collagen orientation and crystallite size in human dentin: a small angle X-ray scattering study. *Calcif Tissue Int* 69(1):31-7.

Kinney JH, Habelitz S, Marshall SJ, Marshall GW (2003). The importance of intrafibrillar mineralization of collagen on the mechanical properties of dentin. *J Dent Res* 82(12):957-61.

Klont B, ten Cate JM (1991). Susceptibility of the collagenous matrix from bovine incisor roots to proteolysis after in vitro lesion formation. *Caries Res* 25(1):46-50.

Landis WJ, Song MJ, Leith A, McEwen L, McEwen BF (1993). Mineral and organic matrix interaction in normally calcifying tendon visualized in three dimensions by high-voltage electron microscopic tomography and graphic image reconstruction. *J Struct Biol* 110(1):39-54.

Lees S, Capel M, Hukins DW, Mook HA (1997). Effect of sodium chloride solutions on mineralized and unmineralized turkey leg tendon. *Calcif Tissue Int* 61(1):74-6.

LeGeros RZ (1991). Calcium phosphates in oral biology and medicine. *Monogr Oral Sci* 15(1-201).

Levine RS, Rowles SL (1973). Further studies on the remineralization of human carious dentine in vitro. *Arch Oral Biol* 18(11):1351-6.

Linde A, Lussi A, Crenshaw MA (1989). Mineral induction by immobilized polyanionic proteins. *Calcif Tissue Int* 44(4):286-95.

Lussi A, Crenshaw MA, Linde A (1988). Induction and inhibition of hydroxyapatite formation by rat dentine phosphoprotein in vitro. *Arch Oral Biol* 33(9):685-91.

Lussi A, Linde A (1993). Mineral induction in vivo by dentine proteins. *Caries Res* 27(4):241-8.

Marshall GW, Habelitz S, Gallagher R, Balooch M, Balooch G, Marshall SJ (2001). Nanomechanical properties of hydrated carious human dentin. *J Dent Res* 80(8):1768-71.

McCurdy SP, Clarkson BH, Speirs RL, Feagin FF (1990). Phosphoprotein extraction from the dentine/cementum complex of human tooth roots. *Arch Oral Biol* 35(5):347-57.

- McIntyre JM, Featherstone JD, Fu J (2000). Studies of dental root surface caries. 1: Comparison of natural and artificial root caries lesions. *Aust Dent J* 45(1):24-30.
- Mukai Y, ten Cate JM (2002). Remineralization of advanced root dentin lesions in vitro. *Caries Res* 36(4):275-80.
- Nakornchai S, Atsawasuwan P, Kitamura E, Surarit R, Yamauchi M (2004). Partial biochemical characterisation of collagen in carious dentin of human primary teeth. *Arch Oral Biol* 49(4):267-73.
- Nyvad B, Fejerskov O (1990). An ultrastructural study of bacterial invasion and tissue breakdown in human experimental root-surface caries. *J Dent Res* 69(5):1118-25.
- O'Reilly MM, Featherstone JD (1987). Demineralization and remineralization around orthodontic appliances: an in vivo study. *Am J Orthod Dentofacial Orthop* 92(1):33-40.
- Olszta MJ, Douglas EP, Gower LB (2003). Scanning electron microscopic analysis of the mineralization of type I collagen via a polymer-induced liquid-precursor (PILP) process. *Calcif Tissue Int* 72(5):583-91.
- Saito T, Arsenault AL, Yamauchi M, Kuboki Y, Crenshaw MA (1997). Mineral induction by immobilized phosphoproteins. *Bone* 21(4):305-11.
- Saito T, Yamauchi M, Crenshaw MA (1998). Apatite induction by insoluble dentin collagen. *J Bone Miner Res* 13(2):265-70.
- Saito T, Toyooka H, Ito S, Crenshaw MA (2003). In vitro study of remineralization of dentin: effects of ions on mineral induction by decalcified dentin matrix. *Caries Res* 37(6):445-9.
- Schupbach P, Guggenheim B, Lutz F (1989). Human root caries: histopathology of initial lesions in cementum and dentin. *J Oral Pathol Med* 18(3):146-56.
- Services USDHHS (2002). In: USDoHaH Services editor: National Institute of Dental and Craniofacial Research, Nations Institutes of Health, Rockville, MD.
- Sreenath T, Thyagarajan T, Hall B, Longenecker G, D'Souza R, Hong S, *et al.* (2003). Dentin sialophosphoprotein knockout mouse teeth display widened predentin zone and develop defective dentin mineralization similar to human dentinogenesis imperfecta type III. *J Biol Chem* 278(27):24874-80.

Stetler-Stevenson WG, Veis A (1986). Type I collagen shows a specific binding affinity for bovine dentin phosphophoryn. *Calcif Tissue Int* 38(3):135-41.

Thotakura SR, Mah T, Srinivasan R, Takagi Y, Veis A, George A (2000). The non-collagenous dentin matrix proteins are involved in dentinogenesis imperfecta type II (DGI-II). *J Dent Res* 79(3):835-9.

Tjaderhane L, Larjava H, Sorsa T, Uitto VJ, Larmas M, Salo T (1998). The activation and function of host matrix metalloproteinases in dentin matrix breakdown in caries lesions. *J Dent Res* 77(8):1622-9.

Van den Bos TaB, W. (1994). Bound phosphoproteins enhance mineralization of alkaline phosphatase-collagen complexes in vivo. *J Bone Miner Res* 9(12):1205-9.

Waltimo J, Ranta H, Lukinmaa PL (1995). Ultrastructure of dentin matrix in heritable dentin defects. *Scanning Microsc* 9(1):185-97; discussion 197-8.

Wassen MH, Lammens J, Tekoppele JM, Sakkers RJ, Liu Z, Verbout AJ, *et al.* (2000). Collagen structure regulates fibril mineralization in osteogenesis as revealed by cross-link patterns in calcifying callus. *J Bone Miner Res* 15(9):1776-85.

Chapter 2

Natural dentin caries zones: Caries Detector stain, mineral, microstructure and mechanical properties.

This Chapter has been submitted to the Journal of Dental Research for publication: Pugach MK, Strother JM, Darling CL, Gansky SA, Fried D, Marshall SJ and Marshall GW. Carious dentin zones: mineral, structure and properties.

ABSTRACT

Caries Detector (CD) staining of dentin lesions is used as an aid in determining how much dentin to remove before restoration. We investigated physical and microstructural properties of carious dentin in each of four different zones revealed by CD staining. Six arrested dentin carious lesions and 2 normal controls were CD stained. Each zone (pink, light pink, transparent, apparently normal) was analyzed by atomic force microscopy (AFM) imaging for microstructure; AFM-nanoindentation for mechanical properties; and transverse digital microradiography (TMR) for mineral content. Each zone had significantly different microstructural and nanomechanical properties, and mineral content. Hydrated elastic modulus (E) and mineral content from normal dentin to pink CD-stained dentin ranged from 19.1 (1.6) GPa to 1.3 (1.8) GPa and 43.6 (2.1) vol. % to 11.9 (2.6) vol. %, respectively. Even the most demineralized pink zone contained considerable residual mineral.

INTRODUCTION

Modern management of caries involves non-invasive techniques and maximum conservation of tooth structure. Differentiation between heavily infected outer carious dentin and demineralized, inner affected dentin, reduces the risk of pulp exposure, maximizing the reparative potential of the pulp (McComb, 2000). The different layers of carious dentin lesions have been classified using clinical and laboratory techniques (Anderson *et al.*, 1985;

Fusayama and Terachima, 1972), but recommendations may conflict or overlap so it is important to understand the nature and variations in such lesions.

Caries staining products have been developed (Fusayama and Terachima, 1972) to assist clinicians during caries removal, but it is unclear what characteristics of the lesion are stained, or how staining is related to microstructural features of various zones of the carious lesion. Not all stainable dentin is infected with caries (Kidd *et al.*, 1993), but it has also been demonstrated that absence of stain does not ensure elimination of bacteria (Anderson *et al.*, 1985).

Aided by commercially available caries stain, Zheng *et al.* (2003) described staining characteristics as pink staining, light pink staining, transparent and apparently normal dentin, and compared the nanoindentation properties of moderately active and arrested carious lesions. Hardness values for intertubular dentin increased from the pink staining zone to the layer of normal dentin (outer to inner). In another study, mechanical properties across dentin carious lesions decreased as the surface of the lesion was approached (Angker *et al.*, 2004b).

Hydration and dehydration affect mechanical properties of dentin, especially demineralized dentin (Kinney *et al.*, 1993; Kinney *et al.*, 1996; Marshall, 1993). Type I collagen normally exists in an aqueous environment, and is often associated with proteoglycans that contain a large amount of bound water. Therefore, properties measured under hydrated conditions provide more realistic estimates of those found *in vivo* (Marshall *et al.*, 2001).

The hypothesis for this study is that CD staining allows discrimination of

carious zones with distinct microstructural characteristics, mechanical properties and mineral contents. We investigated the zones revealed by CD staining in carious lesions classified as arrested. We related these zones to their microstructural features determined by AFM, nanomechanical properties determined by AFM-nanoindentation and mineral concentration.

MATERIALS AND METHODS

Tooth selection and sample preparation

Teeth were collected following protocols approved by the UCSF Committee on Human Research. Eight unrestored third molars (6 with carious lesions, 2 non-carious controls) were obtained from research subjects requiring extractions for dental treatment. The freshly extracted teeth were sterilized by gamma radiation (White *et al.*, 1994) and stored in Hank's balanced salt solution at 4°C (Habelitz *et al.*, 2002). After longitudinally sectioning the tooth through the center of its lesion using a water-cooled saw (Isomet Low Speed saw; Buehler, Lake Bluff, IL, USA) with a 0.15-mm thick diamond blade, a tooth with an obvious carious lesion that appeared, by eye, to extend 50-75% through the dentin thickness was eligible for the lesion group (Zheng *et al.*, 2003). A 2-mm thick longitudinal section through the center of the lesion was sectioned further into at least two 2-mm by 2-mm sticks. Additional 2-mm by 2-mm sticks were sectioned from normal dentin controls from similar locations as the lesions. The surface to be studied was polished, using a sequence of waterproof SiC papers under running water with grit sizes of 600, 800, and 1200 and subsequently 1

and 0.25 μm diamond pastes on a polishing pad. The prepared surface was stained by Caries Detector (CD) (Kuraray, Osaka, Japan). Specimens (~20 teeth) were prepared as described above until six lesions (two sticks per lesion) exhibiting apparently arrested caries (heavily discolored, firm consistency, lightly stained by CD) were identified for the lesion group. A digital image of each prepared surface was recorded (Fig. 2-1a).

Classification of dentin carious lesion zones

Four zones were identified in the lesions based on their optical appearance and degree of staining of the dentin with CD as previously described (Zheng *et al*, 2003): pink (P), light pink (L), transparent (T), and apparently normal (N) zones. The reason for the different appearance due to staining is thought to be due to differences in porosity. The most demineralized zones (pink and light pink) take up the stain readily, while the transparent zone does not stain since this zone has its dentin tubules occluded by mineral. The transparent zone protects the deeper dentin (apparently normal) from taking up the stain.

Carious dentin microstructure analysis by AFM

AFM images (Digital Instruments, Nanoscope III, Santa Barbara, CA, modified with a Triboscope head, Hysitron, Minneapolis, MN) and nanoindentation clusters were made at ~ 350 μm intervals from the DEJ to the pulp (a distance of ~1.5 mm to 3.5 mm). Using the Triboscope Indenter tip of the AFM, a 30 μm by 30 μm AFM image of each area was taken in dry and hydrated

conditions before and after indentation. The hydrated image before indentation was used to examine microstructure of the dentin in each area. Microstructural criteria included tubule occlusion, peritubular dentin presence and intertubular roughness.

For each AFM image, the total number of tubules was determined. To assess tubule occlusion (TO), each tubule was given a rating of 4 if it was completely open; 3 if partially occluded; 2 if plugged (peritubular dentin or tubule margin was visible); and 1 if completely closed or covered (Fig. 2-1b). For peritubular dentin (PT) assessment, the ratings were 4 if the tubule had complete peritubular dentin surrounding it; 3 if it was partially surrounded by peritubular dentin; 2 if there was no peritubular dentin, but the tubule shape appeared to be normal; and 1 if there was no peritubular dentin and the tubule had a distorted shape (Fig. 2-1c). This peritubular dentin rating system was designed to account for the difference between a loss of peritubular dentin in the initial stages of demineralization and the tubule distortion characteristic of more advanced demineralization caused by dentin caries. For both tubule occlusion and peritubular, average tubule rating was determined for each AFM image. The ratings were then related to other physical and mechanical properties and CD stain.

Intertubular roughness (R_a) was determined from the AFM images. Three 5 μm by 5 μm regions of intertubular dentin the same images used for tubule occlusion and peritubular analyses were used to analyze intertubular R_a (Oliveira

et al., 2003) using the roughness analysis option from AFM software (Nanoscope III, version 5.12r3, Digital Instruments, Santa Barbara, CA, USA).

Measurement of reduced elastic modulus and hardness

The modified AFM was used for nanoindentation to determine reduced elastic modulus (E) and hardness (H) along the stick used for the microstructural evaluations following methods previously described (Balooch *et al* 1998; Marshall *et al*, 2001). A Berkovich diamond tip was used for the indentations, which were performed both dry and in a liquid cell filled with deionized water. All measurements used a trapezoidal force profile with peak loads between 50 μN and 500 μN and 3 s indentation times. These peak loads produced nanoindentations with similar displacement values as is normally measured in sound dentin in our lab. Each indentation yielded a load-deformation curve, from which the reduced elastic modulus, E, was calculated from the slope of the unloading curve and the hardness, H, was determined according to the following equations (Doerner, 1986):

$$E = \sqrt{\pi}/(2\sqrt{a}) \cdot S$$

$$H = F_{\max}/a,$$

where S represents the stiffness or slope of the unloading curve based on the method of Oliver (1992), *a* is the contact area of the indentation, and F_{\max} is the maximum force. The nanoindentation procedure was calibrated using a silica standard as previously described (Marshall *et al*, 2004). Indentations were made at $\sim 350 \mu\text{m}$ intervals along a line from near the pulp chamber to the carious

occlusal surface. At each area along the line, a cluster of 5 indentations was made to determine the hardness and modulus of intertubular dentin. If indentations were made onto peritubular dentin, it was noted and not included with intertubular dentin mechanical properties. We collected AFM images before and after the indentations to ensure that they were uniform, well-defined, and at the desired site within the intertubular dentin, as previously described (Marshall *et al.*, 2001).

Measurement of mineral concentration

A custom built digital transverse microradiography (TMR) system was used to measure mineral loss in the natural dentin carious lesions (Darling *et al.*, 2006). The prepared 2 x 2 mm sticks were cut into sections of ~ 200 μm thickness, protecting the top surface which had been evaluated by nanoindentation. The thickness of each section was measured with a digital micrometer with 1 μm resolution. Microradiographs were taken using Cu K_{α} radiation from a Philips 3100 x-ray generator and a Photonics Science FDI X-ray digital imager (Microphotonics, Allentown, PA). The x-ray digital imager consists of a 1392x1040 pixel interline CCD directly bonded to a coherent micro fiber-optic coupler that transfers the light from an optimized gadolinium oxysulphide scintillator to the CCD sensor. The image size is 2.99 x 2.24 mm with a pixel resolution of 2.15- μm . A high-speed motion control system with Newport UTM150 and 850G stages and an ESP300 controller coupled to a video microscopy and laser targeting system was used for precise positioning of the

specimens in the field of view of the imaging system. The TMR images were converted from 12-bit intensity values representing x-ray attenuation through the section, to Vol.% mineral using a calibration plot and the section thickness. Analysis was performed using Igor Pro software (Wavemetrics, Lake Oswego, OR).

Statistical analysis

ANOVA ($p < 0.05$), was used to detect differences between CD stained regions (N, T, L, P) for each property (R_a , E and H (hydrated and dry), and Vol.% mineral). Pearson's correlation coefficient (r) and Spearman's rank (r_s) for ordinal data were used to assess the relationship of physical properties (E and H (wet and dry), and Vol.% mineral) with morphological properties (CD stain, R_a). The relationship of peritubular and tubule occlusion with CD stained regions (N, T, L, P) was assessed with r_s using a bootstrap procedure to select one tubule per stick and calculating r_s ; this process was repeated 20,000 times and the distribution of r_s was determined with the mean and 5% and 95% bounds reported.

RESULTS

Table 2-1 shows mean values for each of the characterization criteria (microstructural, mechanical, mineral content) used in this study to evaluate carious dentin zones. As expected, with increasing levels of demineralization, peritubular rating ($r_s = 0.58$), mechanical properties, and mineral content

decreased. The results for peritubular and R_a as related to Caries Detector stain are shown (Fig. 2-1d and 2-1e). The correlation coefficient between peritubular dentin rating and Caries Detector stains was $r_s=0.58$ (95% confidence bounds: 0.51, 0.65) indicating a significant association. The correlation coefficient between tubule occlusion and CD stain was 0.36 (95% CB: -0.09, 0.72), which was not significantly different than zero with this sample size. Average intertubular R_a of the pink zone was significantly greater than that of normal and transparent ($p<0.05$), and the correlation coefficient for relating R_a to Caries Detector stain was also significant ($p<0.05$) (Fig. 2-1e).

Figure 2-2a shows typical elastic modulus profiles of normal control dentin and a carious dentin lesion, from nanoindentations in both hydrated and dry conditions, starting ~3 mm below the DEJ, following a line towards the surface of the lesion. Dry elastic modulus values for pink were significantly less than for normal, ($p < 0.05$) (Figure 2-2b), while wet elastic modulus values of pink were significantly less than light pink, transparent and normal ($p<0.05$) (Fig. 2-2b). Both wet and dry elastic modulus had statistically significant correlation coefficients ($p<0.05$) when related to Caries Detector stain.

Figures 2-3a and 2-3b show a microradiograph from a representative carious dentin lesion with a volume % mineral line profile through the lesion center. ANOVA showed significant differences in volume % mineral measurement between pink and light pink, and light pink and transparent ($p<0.05$) (Fig. 2-3c). Mineral content was significantly ($p<0.05$) linearly correlated with elastic modulus (Fig. 2-3d), wet and dry ($r^2=0.89$ and 0.82 , respectively).

DISCUSSION

Previous studies have suggested that the mechanical properties of a calcified tissue are associated with its mineral content (Angker *et al.*, 2004a; Arends and ten Bosch, 1992; Featherstone *et al.*, 1983; Kinney *et al.*, 1996; Kodaka *et al.*, 1992). Angker *et al.*, (2004a) has reported that mechanical properties are significantly affected by wet or dry testing conditions. In the present study, elastic modulus and hardness of hydrated dentin could better distinguish between light pink and pink stains than dry measurements. Another possible reason that dry AFM measurements do not correlate as well with CD stain is that when dentin is demineralized and dehydrated the collagen in the demineralized layers collapses and mechanical property measurements do not accurately reflect the demineralization state of the dentin. Instead they are measurements of the underlying, less demineralized dentin (Marshall *et al.*, 2001). A linear correlation may not be adequate to describe the relationship between elastic modulus and mineral content, especially under hydrated conditions. In comparison to nanoindentation results, the CD stain sometimes gave false positives in normal dentin near the pulp chamber, as well as false negatives in slightly demineralized dentin that has not become porous enough to pick up the stain. These discrepancies are consistent with previous reports on staining characteristics (McComb, 2000).

We analyzed AFM images from the nanoindented areas and rated each tubule for peritubular dentin and tubule occlusion. In our study, peritubular dentin

ratings were significantly related to Caries Detector stain, but tubule occlusion was not. Tubule occlusion was most apparent in transparent dentin leading to its transparent optical appearance. While we did see tubule coverage and distortion in Caries Detector stained dentin, the tubules in the stained regions were not filled, but sometimes contained loosely attached mineral or organic material. Therefore the tubule occlusion ratings did not correlate well with Caries Detector stain.

Kinney *et al.* (1996) suggested that intertubular dentin modulus and hardness are major determinants for the values for dentin as a whole, and that there is minimal, if any contribution of the peritubular dentin to the overall elastic properties. In this study we were careful to make the nanoindents in intertubular dentin to accurately assess mechanical properties of the dentin tissue. However, it is also important to account for the presence or absence of peritubular dentin in a given area as its dissolution is an early microstructural indicator of demineralization (Marshall *et al.*, 1998). Likewise, occlusion of the tubules by mineral deposits due to the demineralization/ remineralization cycle from pH changes in the saliva (ten Cate *et al.*, 1988); (Featherstone *et al.*, 1990; Featherstone, 2004) during the caries process is an important indicator of transparent dentin formation (Fusayama, 1991).

Our study shows that when dentin becomes capable of taking up the Caries Detector stain peritubular dentin is absent, perhaps in part because the lack of peritubular dentin leaves larger pores through which the Caries Detector stain can diffuse. While peritubular dentin ratings were a good indicator of

demineralization, they could not distinguish between the partially demineralized light pink colored dentin and the more demineralized outer pink zone of the dentin. Once peritubular dentin is removed by demineralization, it may not reform, even if the dentin is remineralized. Intertubular roughness (R_a) measurements using AFM showed that R_a also could distinguish between each of the zones of the lesions as demineralization increased the surface roughness in the polished specimens.

Greater understanding of the Caries Detector staining process is needed to improve their clinical utility. This study emphasizes the importance of measuring dentin properties in hydrated conditions. Dry measurements of modulus or hardness may result in misleadingly high values, especially in the more demineralized zones. A significant finding of this study is that the pink zone of these carious dentin lesions contained about 25% of the mineral content of normal dentin. Previous studies of bone have shown that the mineral of the calcified tissue is partitioned between two sites: intrafibrillar mineral, which is confined within or immediately adjacent to the gap zones of the collagen fibrils; and extrafibrillar mineral, which lies within the interstitial spaces separating the fibrils (Landis *et al.*, 1996). Bonar *et al.* (Bonar *et al.*, 1985) estimated that extrafibrillar mineral, makes up as much as 75% of the total mineral, leaving 25% intrafibrillar mineral. Therefore, in our study, the pink zone may have remaining intrafibrillar mineral, which may have important consequences on remineralization and restoration of mechanical properties (Kinney *et al.*, 2003a).

CONCLUSIONS

In conclusion, this study showed that Caries Detector stain was correlated with microstructure, mechanical properties and mineral content. Furthermore, carious dentin in the pink zone contained residual mineral. This study also confirmed the importance of mechanical properties being measured under hydrated conditions. In a clinical setting these results may suggest a more conservative approach to removal of the most demineralized zones (pink) of carious dentin before the placement of a restoration.

D. REFERENCES

- Anderson MH, Loesche WJ, Charbeneau GT (1985). Bacteriologic study of a basic fuchsin caries-disclosing dye. *J Prosthet Dent* 54(1): 51-5.
- Angker L, Nijhof N, Swain MV, Kilpatrick NM (2004a). Influence of hydration and mechanical characterization of carious primary dentine using an ultra-micro indentation system (UMIS). *Eur J Oral Sci* 112(3):231-6.
- Angker L, Nockolds C, Swain MV, Kilpatrick N (2004b). Correlating the mechanical properties to the mineral content of carious dentine--a comparative study using an ultra-micro indentation system (UMIS) and SEM-BSE signals. *Arch Oral Biol* 49(5):369-78.
- Arends J, ten Bosch JJ (1992). Demineralization and remineralization evaluation techniques. *J Dent Res* 71 Spec No(924-8).
- Bonar LC, Lees S, Mook HA (1985). Neutron diffraction studies of collagen in fully mineralized bone. *J Mol Biol* 181(2):265-70.
- Darling CL, Huynh GD, Fried D (2006). Light scattering properties of natural and artificially demineralized dental enamel at 1310 nm. *J Biomed Opt* 11(3):34023.
- Doerner W (1986). A method for interpreting the data from depth-sensing indentation instruments. *J Mater Res* 1(601-615).

Featherstone JD, ten Cate JM, Shariati M, Arends J (1983). Comparison of artificial caries-like lesions by quantitative microradiography and microhardness profiles. *Caries Res* 17(5):385-91.

Featherstone JD, Glena R, Shariati M, Shields CP (1990). Dependence of in vitro demineralization of apatite and remineralization of dental enamel on fluoride concentration. *J Dent Res* 69 Spec No(620-5; discussion 634-6.

Featherstone JD (2004). The caries balance: the basis for caries management by risk assessment. *Oral Health Prev Dent* 2 Suppl 1(259-64.

Fusayama T, Terachima S (1972). Differentiation of two layers of carious dentin by staining. *J Dent Res* 51(3):866.

Habelitz S, Marshall GW, Jr., Balooch M, Marshall SJ (2002). Nanoindentation and storage of teeth. *J Biomech* 35(7):995-8.

Kidd EA, Joyston-Bechal S, Beighton D (1993). Microbiological validation of assessments of caries activity during cavity preparation. *Caries Res* 27(5):402-8.

Kinney JH, Balooch M, Marshall GW, Marshall SJ (1993). Atomic-force microscopic study of dimensional changes in human dentine during drying. *Arch Oral Biol* 38(11):1003-7.

Kinney JH, Balooch M, Marshall SJ, Marshall GW, Jr., Weihs TP (1996). Hardness and Young's modulus of human peritubular and intertubular dentine. *Arch Oral Biol* 41(1):9-13.

Kodaka T, Debari K, Yamada M, Kuroiwa M (1992). Correlation between microhardness and mineral content in sound human enamel (short communication). *Caries Res* 26(2):139-41.

Landis WJ, Hodgens KJ, Arena J, Song MJ, McEwen BF (1996). Structural relations between collagen and mineral in bone as determined by high voltage electron microscopic tomography. *Microsc Res Tech* 33(2):192-202.

Marshall GW, Habelitz S, Gallagher R, Balooch M, Balooch G, Marshall SJ (2001). Nanomechanical properties of hydrated carious human dentin. *J Dent Res* 80(8):1768-71.

Marshall GW, Jr. (1993). Dentin: microstructure and characterization. *Quintessence Int* 24(9):606-17.

Marshall GW, Jr., Wu-Magidi IC, Watanabe LG, Inai N, Balooch M, Kinney JH, *et al.* (1998). Effect of citric acid concentration on dentin demineralization,

dehydration, and rehydration: atomic force microscopy study. *J Biomed Mater Res* 42(4):500-7.

McComb D (2000). Caries-detector dyes--how accurate and useful are they? *J Can Dent Assoc* 66(4):195-8.

Oliveira SS, Pugach MK, Hilton JF, Watanabe LG, Marshall SJ, Marshall GW, Jr. (2003). The influence of the dentin smear layer on adhesion: a self-etching primer vs. a total-etch system. *Dent Mater* 19(8):758-67.

Oliver W, Pharr, GM (1992). An improved technique for determining hardness and elastic modulus using load and displacement sensing indentation experiments. *J Mater Res* 7(1564).

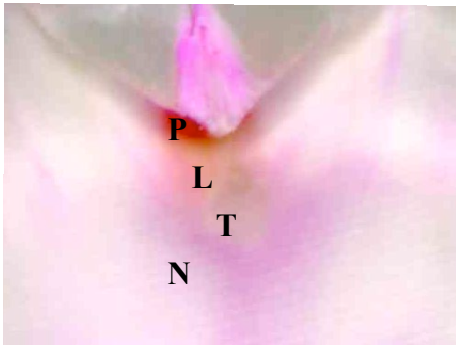
ten Cate JM, Timmer K, Shariati M, Featherstone JD (1988). Effect of timing of fluoride treatment on enamel de- and remineralization in vitro: a pH-cycling study. *Caries Res* 22(1):20-6.

White JM, Goodis HE, Marshall SJ, Marshall GW (1994). Sterilization of teeth by gamma radiation. *J Dent Res* 73(9):1560-7.

Zheng L, Hilton JF, Habelitz S, Marshall SJ, Marshall GW (2003). Dentin caries activity status related to hardness and elasticity. *Eur J Oral Sci* 111(3):243-52.

Figures and Tables

(a)



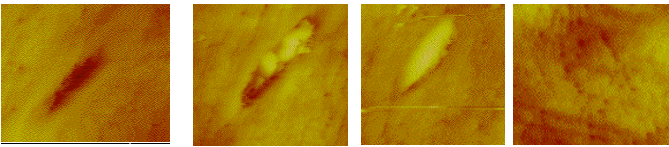
4

3

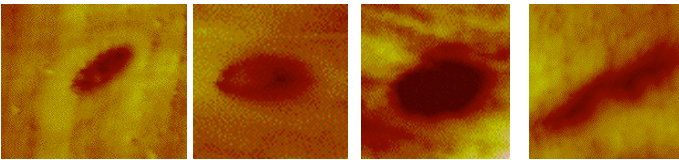
2

1

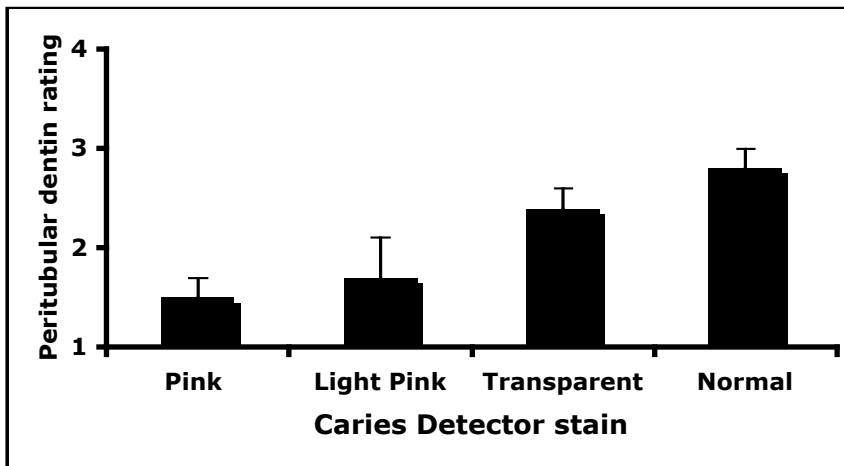
(b) Tubule occlusion



(c) Peritubular dentin



(d)



(e)

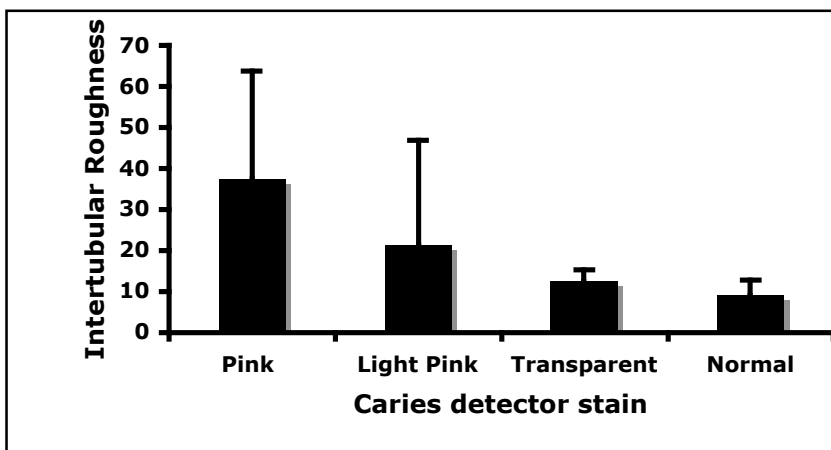


Figure 2-1. Carious morphological features. (a) CD stained lesion with 4 carious dentin zones: pink (P), light pink (L), transparent (T) and apparently normal (N); (b-c) AFM height images (n=61) showing examples of (b) tubule occlusion, 4=open, 3=partial, 2=closed, 1=covered; (c) peritubular dentin, 4=complete, 3=partial, 2=none, 1=distorted, (images 30 x 30 μm), (d) peritubular dentin ratings for each CD stain, with 95% confidence intervals, (e) intertubular roughness (R_a) measurements of CD stain zones (pink zone was significantly more rough than transparent and normal zones, paired t-test, $p < 0.05$).

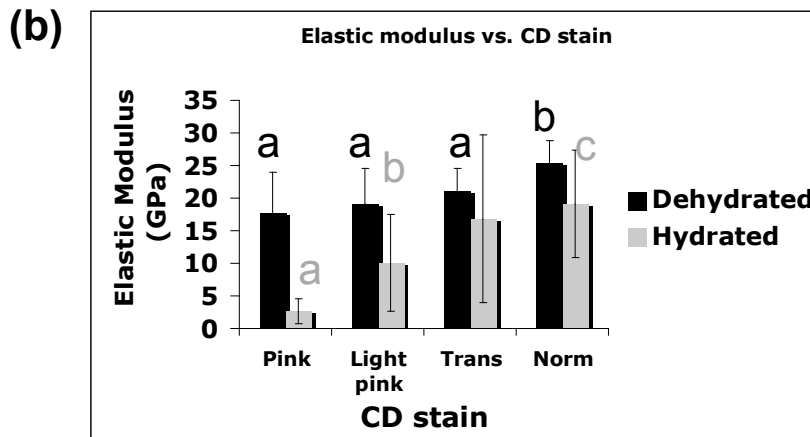
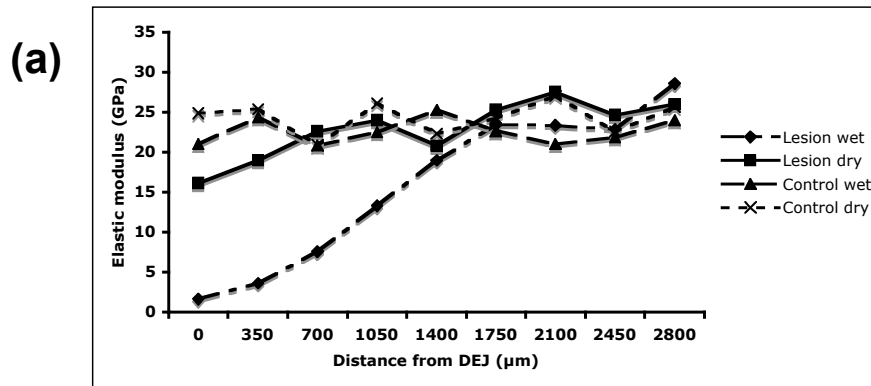


Figure 2-2. Nanomechanical properties of carious dentin lesions – AFM nanoindentation in hydrated and dry conditions. (a) Elastic modulus (E) in GPa of 1 lesion, wet and dry, and control (normal dentin). (b) E for each CD stain (different letters ^{a, b} of same color indicate significant differences, paired t-test, $p < 0.05$)

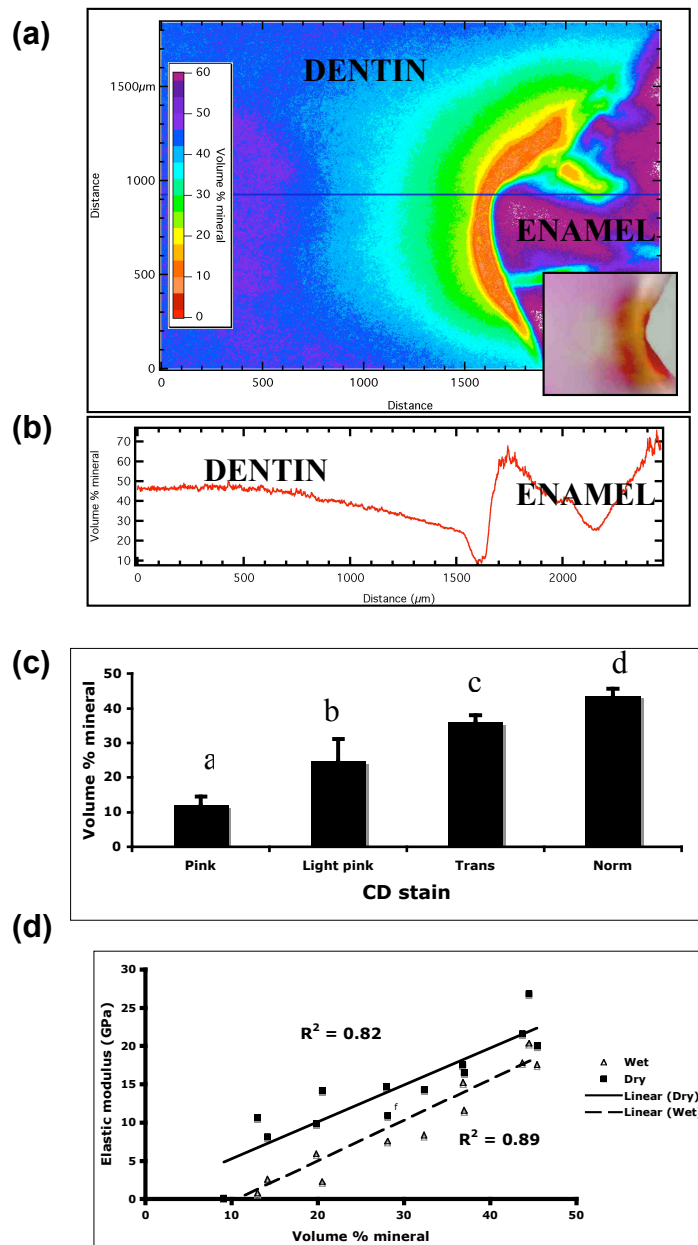


Figure 2-3. Digital transverse microradiography (TMR). (a) Volume % mineral color gradient TMR image showing a representative carious dentin lesion, inset shows corresponding CD-stained lesion; (b) Line profile showing volume % mineral along the line shown in (a), distance in μm along lesion from above pulp to just above DEJ, (c) Volume % mineral averages by CD stain. Different letters (a, b, c, d) indicate significant differences, $p < 0.05$; (d) mineral content compared with elastic modulus dry and wet.

Table 2-1. Means according to CD stain.

Feature	CD Stain			
	Normal	Transparent	Light Pink	Pink
Peritubular Dentin rating ¹	2.8 (2.7-3.0)	2.4 (2.1-2.8)	1.7 (1.6-1.9)	1.5 (1.0-1.3)
Tubule Occlusion rating ¹	3.3 (3.1-3.4)	2.9 (2.6-3.2)	2.6 (2.4-2.8)	2.1 (1.6-2.7)
Intertubular R _a (nm) ²	8.9 (3.7) ^a	12.3 (3.1) ^a	21.2 (25.8)	37.6 (26.2) ^b
Elastic modulus dry (GPa) ²	24.4 (3.3) ^a	20.4 (5.4) ^b	17.7 (5.7) ^b	14.3 (8.1) ^b
Elastic modulus wet (GPa) ²	19.2 (8.3) ^a	16.8 (12.9) ^b	10.1 (7.4) ^b	2.3 (1.9) ^c
Hardness dry (GPa) ²	0.83 (0.18) ^a	0.77 (0.43) ^b	0.55 (0.33) ^b	0.38 (0.18) ^c
Hardness wet (GPa) ²	0.84 (0.41) ^a	0.60 (0.45) ^a	0.57 (0.41) ^a	0.08 (0.04) ^b
Mineral content (vol.%) ²	43.6 (2.1) ^a	35.9 (2.2) ^b	24.7 (6.5) ^c	11.9 (2.6) ^d

¹ Bootstrap mean and 95% confidence boundaries.

² Means and SDs. For each property, different letters ^{a, b, c, d} indicate significant differences between stains.

Chapter 3

**Comparison of artificial carious dentin lesions with natural carious dentin lesions:
mineral content and nanomechanical properties.**

ABSTRACT

Natural dentin carious lesions have large variations, making it difficult to find many similar sample lesions for remineralization studies. Therefore, the goal of this chapter is to assess an artificial carious dentin lesion for use in evaluation of remineralization of carious dentin. Artificial caries-like dentin lesions were created with an acetate buffer at pH 5.0 and the demineralization kinetics were determined. Eight-week lesions approximately 650 μm deep were used for characterization and comparison to natural lesions. After Caries Detector (CD) staining the artificial lesions, three zones (pink, light pink, apparently normal) were identified and evaluated for nanomechanical properties by atomic force microscopy (AFM) nanoindentation and mineral content by transverse digital microradiography (TMR). Transparent dentin could not be identified visually or by AFM imaging in the artificial lesions. Normal, non-CD-stained dentin had a dry elastic modulus of 16.7 (4.4) GPa, a wet elastic modulus of 13.0 (5.5) GPa and mineral concentration of 44.1 (5.0) vol. %. Light pink CD-stained dentin had a dry elastic modulus of 13.6 (5.9) GPa, a hydrated elastic modulus of 11.0 (5.6) GPa and mineral concentration of 33.0 (6.5) vol. %. The width of the zone was small in comparison to natural carious lesions. Pink CD-stained dentin had a dry elastic modulus of 4.8 (2.4) GPa, hydrated elastic modulus of 0.6 (0.7) GPa, and a mineral concentration of 18.5 (5.0) vol. %. The gradient of mineral and mechanical property decrease was sharper in artificial lesions than in the arrested natural carious dentin lesions used for comparison. This study showed that the most demineralized pink zone of the artificial lesions, like natural lesions,

contained residual mineral. Also, the data implies that CD-staining of artificial and natural dentin caries lesions may allow for accurate prediction of mechanical properties and mineral content.

Introduction

Dentin caries is far more complex than enamel caries because dentin is made up of almost 50% organic components whereas enamel contains less than 5%, and remineralized dentin must maintain the interaction between organic and inorganic components. For *in vitro* dentin remineralization studies, it is necessary to obtain large reproducible dentin lesions in extracted teeth. Unfortunately, natural dentin carious lesions have large variations in width, depth, severity and color, making it difficult to find many similar sample lesions for the studies. Thus, there have been many attempts to create artificial enamel caries model systems using organic acids (Featherstone *et al.*, 1979; Featherstone and Rodgers, 1981; Featherstone *et al.*, 1982; ten Cate, 1982) and pH-cycling (Featherstone and Nelson, 1989; Featherstone *et al.*, 1990; Featherstone, 1994), that should recreate natural carious lesions reproducibly in enamel and dentin. Dentin artificial lesions have been evaluated and compared to natural lesions in extracted teeth by cross-sectional microhardness and qualitative polarized microscopy, and these profiles in both types of lesion were similar (McIntyre *et al.*, 2000).

McIntyre *et al.* (2000) used polarized light microscopy and microhardness testing to assess the ability of artificial demineralizing systems, without bacteria

or enzymes present, to produce lesions most closely resembling those that occur naturally. Both natural and artificial root caries lesions were characterized by a 'frontal zone', in which the dentin tubule structure is preserved. The acetate artificial caries system resulted in demineralization across the lesion similar to that observed in natural lesions of similar depths (Arends and ten Bosch, 1992). However, that study did not consider the nature of the breakdown of apatite crystals, nor the ultrastructural differences.

The purpose of this study was to characterize the mineral content, mechanical properties and CD stained zones of an artificial dentin caries model (McIntyre *et al.*, 2000), comparing it with natural dentin carious lesions, such that the limitations of the model can be determined before use in remineralization studies. Our hypothesis is that the artificial carious dentin model produces lesions with similar CD stained zones and mineral gradients as natural carious dentin lesions.

Materials and Methods

Creation of artificial lesions and sample preparation

Extracted, non-carious third molars were used for this study. The teeth were extracted from patients as part of their normal dental treatments and followed a protocol approved by the UCSF Committee on Human Research. After extraction the teeth were sterilized using gamma irradiation (White *et al.*, 1994) and stored in Hank's balanced salt solution at 4°C until preparation. Enamel was removed using a high-speed saw with a diamond blade, just above

the DEJ. This was approximated by making sure that fissures extended below the cut surface, leaving the surface with exposed dentin with enamel islands and enamel surrounding the dentin. The cut surfaces were carefully polished with 600-grit silicon carbide paper until the enamel island in the center of the tooth had been removed. This was confirmed by light microscopy.

A 2 mm x 2 mm window was created with acid resistant nail varnish centered on the area where the central enamel island had been removed (Fig. 3-1). This was done to simulate an occlusal natural carious lesion in a fissure, which when it reaches the DEJ, spreads laterally and into the dentin. The nail varnish was painted on the tooth in two coats, except for the window. The roots were then mounted in poly-methyl methacrylate resin to prevent infiltration of the cariogenic acid through the root tip and to keep the occlusal surface in constant contact with the acid. Each specimen (n = 6/group) was placed in a 50 ml tube with 40 ml 0.05M acetate buffer that contained 2.2 mM calcium and phosphate at pH 5.0. The demineralization solution was changed weekly for 4, 8 or 12 weeks.

After the specimens had been in the artificial caries acid buffer for 4, 8 or 12 weeks, they were stored in deionized water with thymol to prevent bacterial growth.

Determination of lesion depth by polarized light microscopy

Sections about 200 μm thick were cut through the centers of the artificial lesions that had been created for the different time points. Lesion depths were determined by polarized light microscopy while the sections containing the

lesions were immersed in water. Images were analyzed using image analysis software (Image-Pro, Media Cybernetics, Bethesda, MD).

Classification of dentin carious lesion zones

The surface to be studied was polished, sequentially, using waterproof silicon carbide papers under running water with grit sizes of 600, 800, and 1200 and diamond pastes of 1 and 0.25 μm . The sections were stained with Caries Detector (CD) (Kuraray, Kurashiki, Japan) stain for 10 s, followed by rinsing in deionized water for 30 s, and the lesions were qualitatively assessed under the microscope. Based on prior work (Zheng *et al.*, 2003) zones were identified in the lesions based on their optical appearance and degree of staining of the dentin with CD. In the AFM, normal dentin had smooth intertubular dentin, peritubular dentin was present, and tubules were open. The transparent zone, the tubules were mostly filled with mineral and the intertubular dentin was coarser. The light pink zone had some intratubular mineral, little or no peritubular dentin, and coarse intertubular dentin. The pink zone, peritubular dentin and intertubular mineral were not present. The zones were classified by 2 independent observers.

Measurement of reduced elastic modulus and hardness of carious dentin by AFM

A Nanoscope III AFM (Digital Instruments, Santa Barbara, CA, USA) modified with a Triboscope head for nanoindentation (Hysitron, Minneapolis, MN, USA) (Balooch *et al.*, 1998; Marshall *et al.*, 2001) was used to study the

mechanical properties of each area across each lesion. A Berkovich diamond tip was used for the indentations, which were performed both dry and in a liquid cell filled with deionized water. All measurements used a trapezoidal force profile with peak loads between 50 μN and 500 μN and 3 s indentation times. Each indentation yielded a load-deformation curve, from which the reduced elastic modulus, E , was calculated from the slope of the unloading curve and the hardness, H , was determined according to the following equations (Doerner, 1986):

$$E = \sqrt{\pi}/(2\sqrt{a}) \cdot S$$

$$H = F_{\max}/a,$$

where S represents the stiffness or slope of the unloading curve based on the method of Oliver and Pharr (1992), a is the contact area of the indentation, and F_{\max} is the maximum force. The nanoindentation procedure was calibrated using a silica standard as previously described (Marshall *et al*, 2001). Indentations were made at approximately equal intervals of less than 200 μm along a line from near the pulp chamber to the occlusal surface across the area that contained the artificial lesion. At each area along the line, we made a cluster of approximately 5 indentations to determine the hardness and modulus of intertubular dentin in the area. If measurements were made in areas of peritubular dentin, it was noted and not included with intertubular dentin mechanical properties. We collected AFM images before and after the indentations to ensure that they were uniform and well-defined and were at the desired site within the intertubular dentin as

previously done (Marshall *et al.*, 2001). Indents placed in peritubular dentin or intratubular dentin were not used.

Digital transverse microradiography (TMR) of carious dentin

TMR studies were based on the work of Fried and colleagues (Darling *et al.*, 2006; Jones *et al.*, 2006; Ngaotheppitak *et al.*, 2005). The thickness of each ~ 200 μm section was measured with a digital micrometer with 1 μm resolution. A custom built TMR system was used to measure mineral loss in the artificial dentin caries lesions. Micrographs were taken using Cu K α radiation from a Philips 3100 x-ray generator and a Photonics Science FDI X-ray digital imager (Microphotonics, Allentown, PA), as previously described (Chapter 2). The TMR images were converted from 12-bit intensity values representing x-ray attenuation through the section, to volume % mineral using a calibration plot and the section thickness. Analyses were performed using Igor Pro software (Wavemetrics, Lake Oswego, OR).

Statistical analysis

ANOVA ($p < 0.05$) was used to detect differences between CD stains (N, T, L, P) for each property (elastic modulus and hardness, hydrated and dry, and Vol.% mineral). Pearson's correlation coefficient and Spearman's rank (r^2) for ordinal data were used to correlate physical properties (elastic modulus and hardness, wet and dry, and Vol.% mineral) with CD stain and mineral content versus E.

Results

Lesion depth measurements and kinetics of the acetate buffer system

Fig. 3-2 shows lesion depth determined by PLM plotted against the square-root of time and gave a linear fit of the data (depth (μm) = $18.08(t^{1/2}) - 24.41$, $r^2 = 0.99$) (Fig. 3-2d) that represented the demineralization kinetics of the cariogenic acid buffer used for this study. Artificial lesions that were approximately 650 μm deep, created by 8 weeks of exposure to the 0.05M acetate buffer containing 2.2 mM calcium phosphate at pH 5.0 (Fig. 3-2a-c), were chosen for the remainder of the experiments comparing artificial and natural carious dentin lesions.

Nanomechanical property measurements

There was a very small light pink zone in all of the artificial lesions and a large pink zone covering most of the depth of the artificial lesion. No transparent dentin could be identified in the artificial lesions either visually or based on microstructural characteristics by AFM imaging. Table 3-1 shows a summary of property measurements and comparisons both within and between artificial and natural carious lesion zones. Figure 3-3a shows elastic modulus profiles across carious lesions of representative samples from both artificial and natural lesions, as well as a non-carious control. Figure 3-3b shows wet and dry elastic modulus and hardness values for the zones according to CD stain for the artificial lesions. The hydrated elastic modulus and hardness of the pink zone were significantly

different than both the light pink zone and normal dentin ($p < 0.05$) but light pink dentin was not significantly different from normal dentin. Mechanical properties of caries zones were not significantly different between artificial and natural lesions, except for the normal dentin zones, which had lower properties.

Mineral content measurements by microradiography

Volume % mineral false color images are shown for a representative artificial lesion (Fig. 3-4a) and natural lesion (Fig. 3-4c). The corresponding line scans through the corresponding lesions are shown Fig. 3-4b and 3-4c. Mineral content from all the lesions according to CD stain is shown in Fig. 3-4d. Both hydrated ($r^2 = 0.66$) and dry ($r^2 = 0.75$) artificial carious dentin had significant correlations between mineral content and elastic modulus (Fig. 3-4e). The volume percent mineral values are shown in Table 3-1 with corresponding natural lesion values (Chapter 2), for zones according to CD stain. There were significant differences ($p < 0.05$) between normal dentin and both pink and light pink stains, as well as between pink and light pink. Furthermore, between artificial and natural carious dentin zones, there were differences in mineral content.

Discussion

We found that use of an acetate buffer previously developed for artificial root caries lesions allowed us to create artificial dentin caries lesions, based on a highly linear relationship of demineralization depth vs. $t^{1/2}$. The artificial lesions

created in coronal dentin were similar in shape, size and depth to artificial lesions created in root dentin (McIntyre *et al.*, 2000), using the same demineralization buffer.

When stained with CD the artificial lesions contained three zones (pink, light pink, apparently normal) in contrast with natural lesions which have a fourth zone of transparent dentin between the light pink and apparently normal dentin. One problem to consider when using artificial dentin caries systems is that natural caries occurs in living teeth, while artificial caries are created in non-vital specimens. The most likely reason for the absence of a transparent zone in the artificial lesions is that they were created by continuous immersion in a demineralization buffer at pH 5. However, natural carious lesions undergo pH cycling in the mouth, which causes both demineralization and remineralization as a result of changes in calcium-phosphate supersaturation with respect to hydroxyapatite. These cyclical phenomena cause occlusion of tubules with precipitated mineral in caries-affected dentin, resulting in transparent optical properties. Therefore, the artificial dentin caries model will likely need to be modified with the addition of a pH-cycling system.

Nanomechanical properties decreased as demineralization increased and significant differences in mineral content and mechanical properties were associated with the different CD stained zones of artificial lesions as in natural lesions. Also like natural lesions, there were significant linear relationships between mineral content and both wet ($r^2=0.66$) and dry ($r^2=0.75$) elastic modulus of artificial lesions.

Although it is important to consider the differences between natural and artificial systems, it is crucial to have consistent samples, as long as the limitations of the model system are identified. This study showed that the most demineralized pink zone of the artificial lesions, like natural lesions, contained residual mineral. Also, the data implies that CD-staining of artificial and natural dentin caries lesions may allow for accurate prediction of mechanical properties and mineral content.

Some notable differences between artificial carious dentin and natural carious dentin lesions are that there is little to no light pink zone, as well as the lack of the transparent zone in artificial lesions as discussed above. This results in a sharper gradient (in distance from DEJ to pulp) of mechanical property and mineral content reduction between normal dentin and the most demineralized (pink zone) dentin. These lesions may be in fact more similar to active dentin carious lesion than arrested lesions. Subsequent experiments will utilize further modifications in fluoride concentration, acid type, or addition of proteolytic enzymes to produce dentin lesions with similar zones and zone sizes as both arrested and active natural lesions.

Conclusions

This study identified similarities between an artificial carious dentin lesion model and arrested natural carious dentin lesion in mineral content and mechanical properties of pink colored zones of Caries Detector stained dentin. While there are limitations to this artificial carious dentin model that have been

identified, it would be suitable for producing artificial caries-like lesions for the purposes of carious dentin remineralization studies.

D. REFERENCES

Arends J, ten Bosch JJ (1992). Demineralization and remineralization evaluation techniques. *J Dent Res* 71 Spec No (924-8).

Balooch M, Wu-Magidi IC, Balazs A, Lundkvist AS, Marshall SJ, Marshall GW, *et al.* (1998). Viscoelastic properties of demineralized human dentin measured in water with atomic force microscope (AFM)-based indentation. *J Biomed Mater Res* 40(4):539-44.

Darling CL, Huynh GD, Fried D (2006). Light scattering properties of natural and artificially demineralized dental enamel at 1310 nm. *J Biomed Opt* 11(3):34023.

Doerner W (1986). A method for interpreting the data from depth-sensing indentation instruments. *J Mater Res* 1(601-615).

Featherstone JD, Duncan JF, Cutress TW (1979). A mechanism for dental caries based on chemical processes and diffusion phenomena during in-vitro caries simulation on human tooth enamel. *Arch Oral Biol* 24(2):101-12.

Featherstone JD, Rodgers BE (1981). Effect of acetic, lactic and other organic acids on the formation of artificial carious lesions. *Caries Res* 15(5):377-85.

Featherstone JD, Cutress TW, Rodgers BE, Dennison PJ (1982). Remineralization of artificial caries-like lesions in vivo by a self-administered mouthrinse or paste. *Caries Res* 16(3):235-42.

Featherstone JD, Nelson DG (1989). Recent uses of electron microscopy in the study of physico-chemical processes affecting the reactivity of synthetic and biological apatites. *Scanning Microsc* 3(3):815-27; discussion 827-8.

Featherstone JD, Glana R, Shariati M, Shields CP (1990). Dependence of in vitro demineralization of apatite and remineralization of dental enamel on fluoride concentration. *J Dent Res* 69 Spec No(620-5; discussion 634-6).

Featherstone JD (1994). Fluoride, remineralization and root caries. *Am J Dent* 7(5):271-4.

Featherstone JD (1996). Modeling the caries-inhibitory effects of dental materials. *Dent Mater* 12(3):194-7.

Jones RS, Darling CL, Featherstone JD, Fried D (2006). Remineralization of in vitro dental caries assessed with polarization-sensitive optical coherence tomography. *J Biomed Opt* 11(1):014016.

Marshall GW, Habelitz S, Gallagher R, Balooch M, Balooch G, Marshall SJ (2001). Nanomechanical properties of hydrated carious human dentin. *J Dent Res* 80(8):1768-71.

McIntyre JM, Featherstone JD, Fu J (2000). Studies of dental root surface caries. 1: Comparison of natural and artificial root caries lesions. *Aust Dent J* 45(1):24-30.

Ngotheppitak P, CL Darling and D Fried (2005). Measurement of the severity of natural smooth surface (interproximal) caries lesions with polarization sensitive optical coherence tomography. *Lasers Surg Med* 37(1):78-88.

O'Reilly MM, Featherstone JD (1987). Demineralization and remineralization around orthodontic appliances: an in vivo study. *Am J Orthod Dentofacial Orthop* 92(1):33-40.

Oliver W, Pharr, GM (1992). An improved technique for determining hardness and elastic modulus using load and displacement sensing indentation experiments. *J Mater Res* 7(1564).

ten Cate JMaD, P.P. (1982). Alternating demineralization and remineralization of artificial enamel lesions. . *Caries Res* 16(201-210).

Figures and Tables

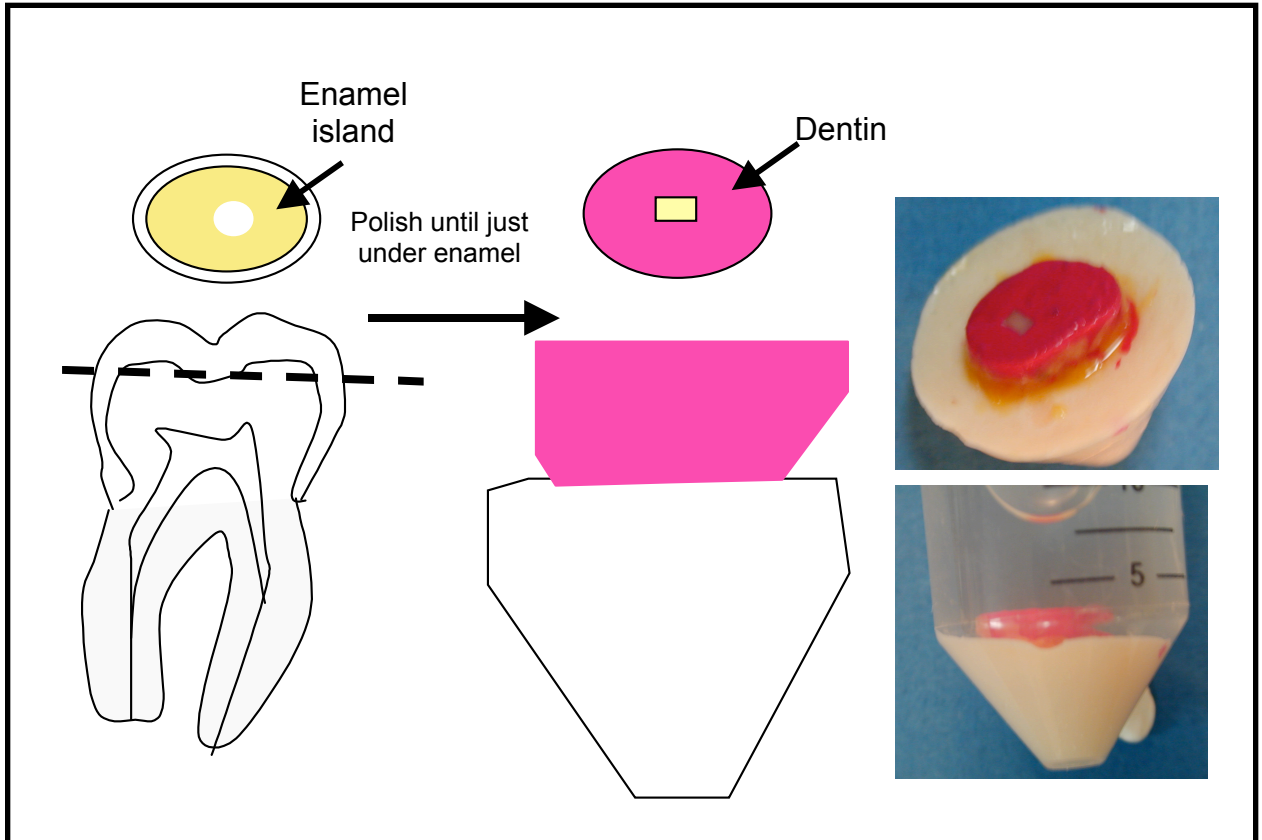


Figure 3-1. Artificial dentin carious lesion sample preparation. Non-carious 3rd molars had enamel removed, polished away, and dentin below the central fissure was isolated with acid resistant nail varnish. Teeth were embedded in resin and immersed in a demineralization buffer for up to 12 weeks.

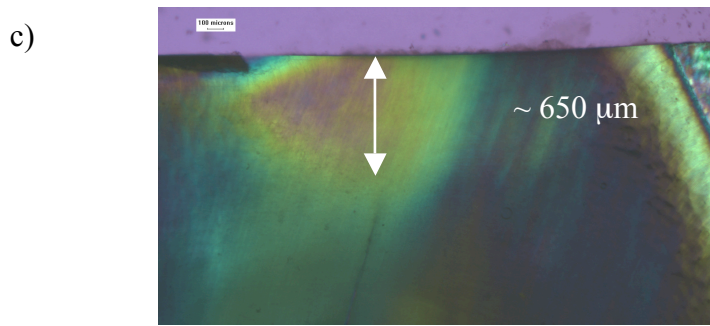
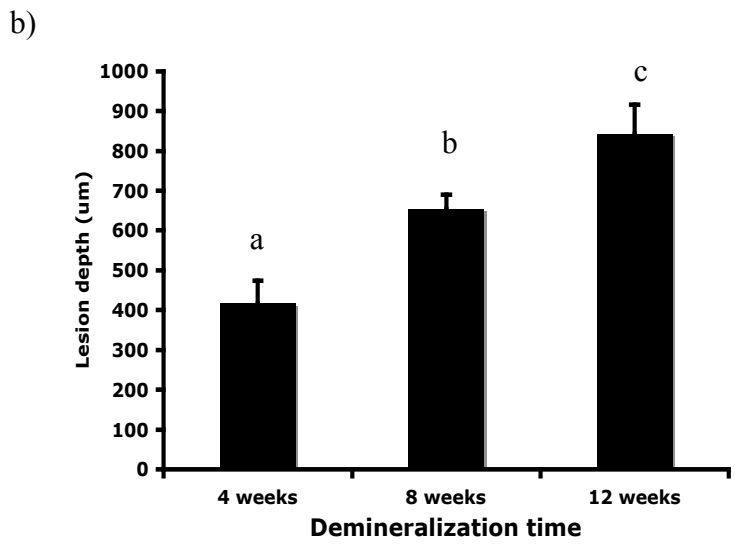
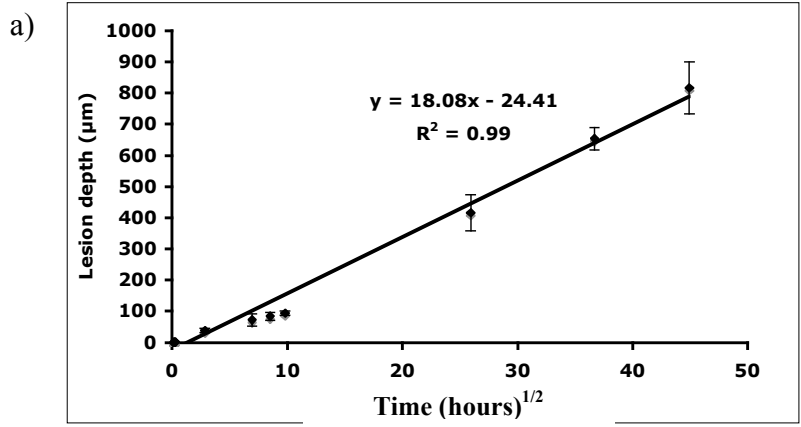


Figure 3-2. Kinetics of artificial dentin caries progression in acid buffer 0.05M Acetate with 2.2 mM calcium phosphate, pH 5.0. a) Kinetics curve: lesion depth (µm) versus square root of time in hours, b) Lesion depth (µm) versus demineralization time at 4, 8 and 12 weeks, different letters (a, b, c) indicate a significant difference ($p < 0.05$); c) polarized light microscopy (PLM)

image of a typical lesion after 8 weeks of demineralization with 0.05 M acetate with 2.2 mM calcium phosphate at pH 5.0.

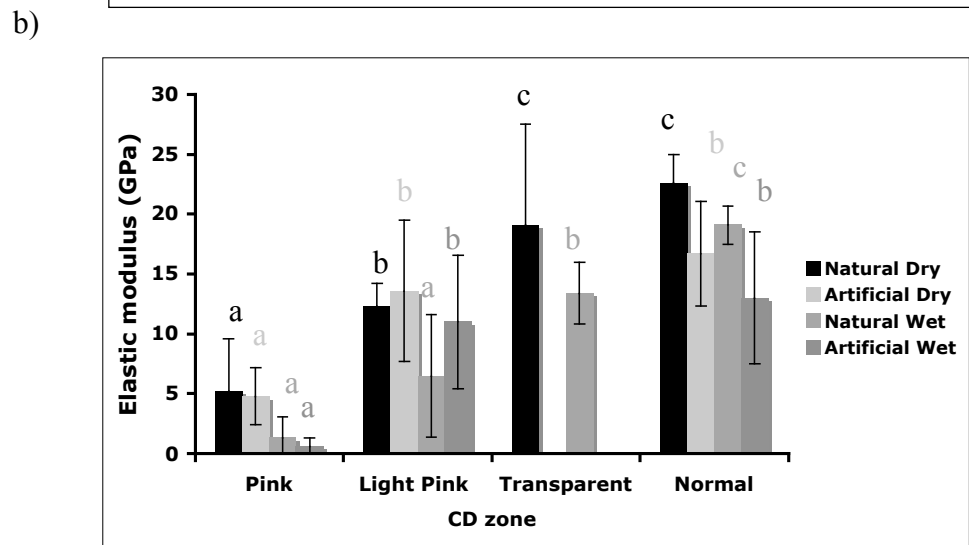
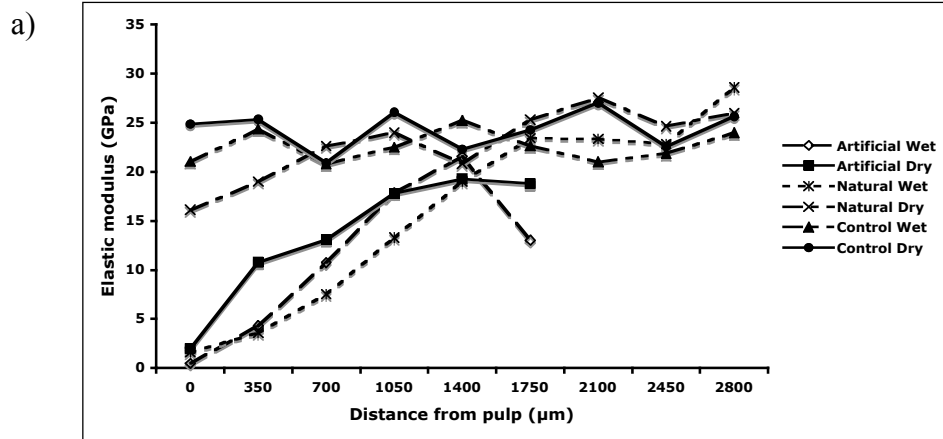
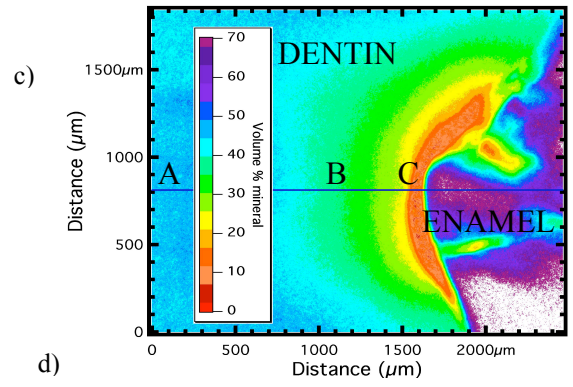
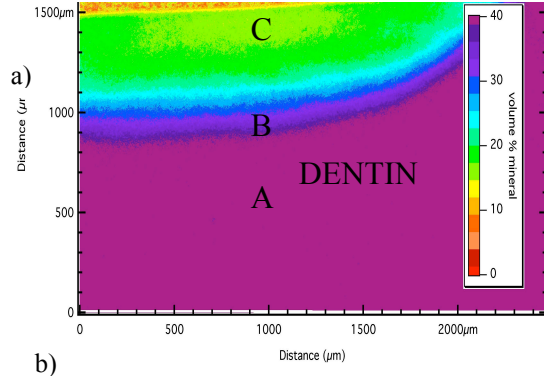
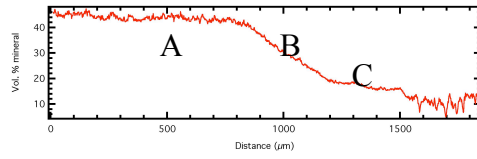


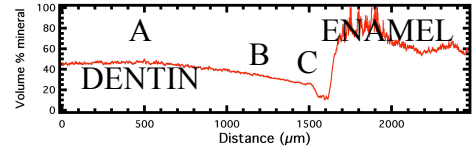
Figure 3-3. AFM nanoindentation of artificial caries-like dentin lesions compared to natural lesions and control. a) Typical elastic modulus (in GPa) line profiles through an artificial lesion, a natural lesion and a control non-lesion, under wet and dry conditions; b) Elastic modulus of artificial lesions according to CD stain compared with natural lesions, under wet and dry conditions. Different letters (a, b, c, d) of the same color indicate significant differences between CD stains ($p < 0.05$).



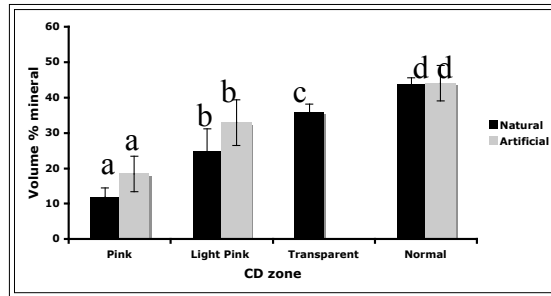
b)



d)



e)



f)

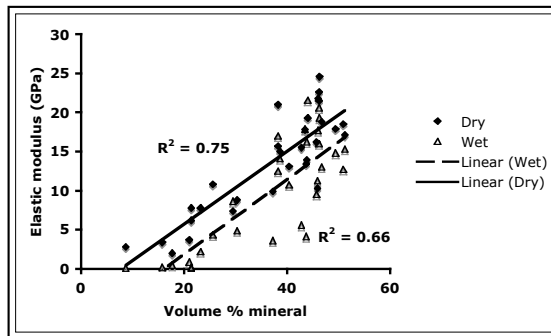


Figure 3-4. Digital transverse microradiography (TMR) of artificial and natural carious dentin lesions. a) Representative TMR image of an artificial lesion with volume % mineral color scale ranging from 45 % to 0 %; b) volume % mineral line profile (μm) through artificial lesion in a); c) representative TMR image of a natural lesion with volume % mineral color scale ranging from 45 % to 0 %; d) volume % mineral line profile (μm) through artificial lesion in c). For a-d, A is in normal dentin, B is in light pink dentin, and C is in pink dentin. Also, please note Vol. % mineral scale differences between artificial and natural lesions. e) volume % mineral of artificial lesions according to CD stain, compared with natural lesions. Different letters (a, b, c, d) indicate a significant differences between CD stains ($p < 0.05$). f) Significant ($p < 0.05$) linear correlations between elastic modulus and mineral content for both hydrated and dry artificial carious dentin.

Table 3-1. Average elastic modulus (GPa), wet and dry, and mineral content (vol. % mineral) of artificial caries-like lesions according to CD stain, compared with normal dentin caries lesions.

CD stain	Elastic modulus (GPa) dry	Elastic modulus (GPa) wet	Hardness (GPa) dry	Hardness (GPa) Wet	Volume % mineral
<i>Artificial</i>					
Pink	4.8 (2.4) ^{aA}	0.6 (0.7) ^{aA}	0.24(0.10) ^{aA}	0.02 (0.02) ^{aA}	18.5 (5.0) ^{aA}
Light pink	13.6 (5.9) ^{bA}	11.0 (5.6) ^{bA}	0.37(0.17) ^{aA}	0.49 (0.28) ^{bA}	33.0 (6.5) ^{bA}
Transparent	N/A	N/A	N/A	N/A	N/A
Normal	16.7 (4.4) ^{bA}	13.0 (5.5) ^{bA}	0.62(0.16) ^{bA}	0.61 (0.20) ^{bA}	44.1 (5.0) ^{cA}
<i>Natural</i>					
Pink	5.2 (4.4) ^{aA}	1.3 (1.8) ^{aA}	0.38(0.18) ^{aA}	0.08 (0.04) ^{aB}	11.9 (2.6) ^{aB}
Light pink	12.3 (1.9) ^{bA}	6.5 (5.1) ^{aA}	0.55(0.33) ^{bA}	0.57 (0.41) ^{bA}	24.7 (6.5) ^{bB}
Transparent	19.1 (8.4) ^c	13.4 (2.6) ^b	0.77(0.43) ^b	0.60 (0.45) ^b	35.9 (2.2) ^c
Normal	22.6 (2.4) ^{cB}	19.1 (1.6) ^{cB}	0.83(0.18) ^{cB}	0.84 (0.41) ^{bA}	43.6 (2.1) ^{dA}

Within artificial or natural lesions, for each property, different letters (a, b, c, d) indicate significant differences between CD stains ($p < 0.05$). Comparing zones between artificial and natural lesions, for each property, different letters (^{A,B}) indicate a significant difference ($p < 0.05$).

Chapter 4

Collagen in carious dentin lesions

Introduction

Dentin is a hydrated composite of collagen fibrils, non-collagenous proteins and apatite. The interaction between organic and inorganic components of dentin results in its unique elastic properties but this interaction has not been studied in dentin. Studies on mineralizing turkey tendon have shown that apatite is distributed in two locations: intrafibrillar (IF) mineral within or near the gap zones of the collagen fibrils and extrafibrillar (EF) mineral between the fibrils (Landis *et al.*, 1996). In turkey tendon, when collagen is initially mineralized, IF mineral is bound to gap zones of dentin collagen fibrils via negatively charged non-collagenous proteins (NCPs) (Landis, 1986). One NCP, a phosphoprotein, is bound to collagen gap zones and the complex of collagen, NCP and mineral is difficult to remove unless the collagen is degraded by collagenase (Clarkson *et al.*, 1998). Clarkson and co-workers (Clarkson *et al.*, 1998) showed that the remineralization potential of demineralized intact dentin collagen, with only EF mineral and NCPs removed by treatment with EDTA, was far greater than dentin collagen digested with collagenase. In carious dentin lesions, especially active lesions, collagenases are released from the dentin matrix (Tjaderhane *et al.*, 1998) and produced by the acidogenic bacteria (Nyvad and Fejerskov, 1990; Schupbach *et al.*, 1989). Thus far, it is unclear if the CD-stained pink zones of carious dentin lesions (characterized in Chapters 2 and 3) contain intact collagen fibrils that have not been exposed to collagenase, or if the collagen has been degraded. Furthermore, it has not been determined if mineral remaining in the pink zone of dentin caries is IF mineral. Thus, the hypothesis of this study is that

the pink zone of arrested dentin caries contains mostly intact collagen fibrils with IF mineral.

Type-I collagen typically comprises approximately 90% of the organic matrix of human dentin. Its role in influencing the mechanical properties of bone (Bailey and Knott, 1999; Oxlund *et al.*, 1996; Paschalis *et al.*, 2001; Paschalis *et al.*, 2004; Zioupos *et al.*, 1999) and dentin (Balooch, 2004; Habelitz *et al.*, 2002; Katz *et al.*, 2003; Walters and Eyre, 1983) has been well studied. The collagen molecule is composed of a triple helix, two α 1 chains and one α 2 chain, each of which is approximately 1000 residues long. These molecules then self-assemble into thin (10-300 nm in diameter) collagen fibrils, and often aggregate into large fibers that can be several micrometers in diameter (Veis *et al.*, 1997). The regular arrangement of tropocollagen molecules within the fiber lead to regular bands with periodicity of 67 nm, with gap and overlap regions that can be observed by various microscopy methods including AFM (Habelitz *et al.*, 2002). Collagen molecules are covalently cross-linked between lysine residues, with the cross-links contributing to its tensile strength (Eyre *et al.*, 1984; Knott and Bailey, 1998).

Fusayama *et al.* (Fusayama and Terachima, 1972) described two layers of carious dentin that were characterized in Chapter 2: the pink zone, or outer carious layer, which was most demineralized but contained residual mineral, and the light pink, or inner carious layer which contained demineralized dentin and substantial mineral remaining. These two layers have been characterized through the biochemical study of collagen fibers (Kuboki *et al.*, 1977). There was

no significant difference in the amino acid composition and pattern between the collagen fibers of the outer carious dentin, inner carious dentin, and sound dentin. However, significant differences were observed in the intermolecular cross-links of collagen fibers between the sound dentin and the two layers of carious dentin. In comparison to sound dentin, the inner carious dentin had decreased cross-links and increased precursors of cross-links. Furthermore, the outer carious dentin had significant decreases in both cross-links and precursors (Kuboki *et al.*, 1977), which suggested an irreversible degeneration of the collagen in this layer. Since functional remineralization of carious dentin requires interaction between the organic and inorganic components of dentin, collagen fibril degradation will decrease the potential for physiological remineralization.

Recently, Suppa *et al.* (2006) used immunohistochemistry to detect antigenic alterations to the dentin collagen in caries. The distribution of collagen fibrils in sclerotic dentin due to caries was significantly lower than in normal dentin. The carious dentin layers have also been characterized histochemically by Mallory-Azan staining. This technique stained the outer carious dentin red, indicating denatured collagen fibers; and the inner carious dentin was stained blue, indicating sound collagen fibers as in normal dentin (Ohushi 1973), although it is unclear how influential a role tissue porosity plays with this stain.

In this chapter, to investigate the state of the collagen in artificial and natural carious dentin lesions, four techniques were used: histochemical staining, atomic force microscopy (AFM), ultraviolet resonance Raman spectroscopy (UVRRS), and small-angle x-ray scattering (SAXS), which also provided shape and size

information of mineral crystallites associated with the collagen. A recent study showed that gap-overlap height changes increase during demineralization as IF is removed (Balooch *et al.*, 2004). Thus fibrils that are initially smooth in topography show increasing evidence of the banded structure and gap-overlap height goes from ~0 nm to 5-7 nm. These measurements were used in conjunction with Raman microspectroscopy to confirm the loss of intrafibrillar mineral. Therefore, AFM imaging of collagen fibril topography was used to determine if remnant IF mineral was in each zone.

Ultraviolet excitation has been used to enhance the vibrational intensities of certain parts of proteins through resonance effects (Asher *et al.*, 2004). In ultraviolet resonance Raman (UVR) spectroscopy, excitation wavelengths near 200 nm can be used to selectively enhance the amide I vibration near 1660 cm⁻¹ (Asher *et al.*, 2004). UVRRS has been used to study the effects of aging and disease on bone mineralization (Akkus *et al.*, 2004; Timlin *et al.*, 2000) and to evaluate the strain caused by the inorganic component under mechanical deformation (Morris *et al.*, 2004; Pezzotti and Sakakura, 2003). In situ UVRRS measurements of human cortical bone (Ager *et al.*, 2005) and dentin (Ager *et al.*, 2006) have reported age-induced changes in the amide I band. Furthermore, the amide I feature also increased in dentin that had been demineralized and dehydrated (Ager *et al.*, 2006). UVRRS was used in this study to evaluate the strain of the collagen network in demineralized dentin.

Small angle x-ray scattering (SAXS) has been performed on fully mineralized human dentin to quantify its collagen and mineral architecture

(Kinney *et al.*, 2001b). SAXS results were consistent with the standard model of type I collagen mineralization, in which the 67-nm periodically spaced gaps are the sites for primary apatite crystal nucleation and growth. Another study (Kinney *et al.*, 2001a) used SAXS to investigate the collagen/mineral relationship in dentinogenesis imperfecta type II dentin, which had 33% lower mineral. In contrast to normal dentin, the low-angle diffraction peaks at harmonics of 67 nm were not found in DI-II dentin, which is consistent with an absence of intrafibrillar mineral in DI-II dentin. SAXS was used in this work to evaluate the mineral crystallites and the interaction between collagen and mineral in carious dentin.

Materials and Methods

3rd molars were extracted from patients requiring such treatment as part of their normal dental treatments following a protocol approved by the UCSF Committee on Human Research. All teeth were sterilized by gamma radiation and stored in Hank's balanced salt solution at 4°C (Habelitz *et al.*, 2002; White *et al.*, 1994).

Masson's Trichrome Stain

Samples were cut longitudinally through the center of the carious lesion using a water-cooled saw (Isomet Low Speed saw; Buehler Ltd., Lake Bluff, IL, USA) with a 0.15-mm thick diamond blade. Molars that contained no prior restorations, with an obvious carious lesion that appeared, by eye, to extend into the dentin by 50-75% of the dentin thickness were eligible for the study. The

opposing half of the lesion was stained with Caries Detector stain and imaged to compare with the trichrome stain. A 2-mm thick longitudinal section of the carious dentin lesion was prepared for Masson's trichrome staining by removing all visible enamel. Five specimens were included in the study and demineralized with Cal-EX II solution (Fisher Diagnostics; Fair Lawn, NJ, USA) and RDO Rapid Decalcifier (Apex Engineering Products Corporation; Aurora, IL, USA). Masson's trichrome stain was completed for histological evaluation of the carious lesions (Sheehan, 1980). Slides of the specimens were prepared and histological evaluation was done with light microscopy (Olympus BX51 Research microscope, Center Valley, PA, USA). Each zone of the carious lesions was examined at a magnification of 60x for characterization.

High-resolution AFM imaging of carious dentin collagen

Carious surfaces were prepared for high-resolution imaging by ultramicrotome sectioning. AFM studies were performed using a Nanoscope III with a calibrated piezo-scanner (Digital Instruments, Santa Barbara, CA). Contact mode images in air were obtained with Si_3N_4 -tips, (Digital Instruments). High-resolution imaging in water was difficult and did not yield measurable images. Collagen fibril repeat distance was measured from section analysis of images using data that had been modified only by plane fitting. Section analysis was used to determine the step height between the gap and overlap zones of individual fibrils. Axial repeat distances of individual collagen fibrils were determined from AFM images by Fourier transform analysis (AFM software 4.48r,

Digital Instruments) of spectral frequencies along a line centered on the fibril axis (Habelitz *et al.*, 2002).

UV-Resonance Raman Spectroscopy

The UV Raman system, which has been used by our colleagues at the Lawrence Berkeley National Laboratory to study bone and dentin (Ager *et al.*, 2005; Ager *et al.*, 2006), used an argon ion laser, which provided excitation at 244 nm. Specimens were mounted on a rotating stage; the control samples, hydrated type I collagen membranes (from bovine Achilles tendon; Ace Surgical Supply), were pressed flat and mounted on the same stage. The laser power at the sample was below 5 mW. Comparison of sequential data frames allowed experimental conditions to be developed under which spectra did not change over the experimental time period. A typical protocol was 3 frames of 30 sec duration each. The data frames were averaged and a small linear background was defined by the signal at 500 and 2000 cm^{-1} (where little Raman scattering from the sample is expected) and subtracted. Presented spectra were normalized to the height of the CH_2 wag peak at $\sim 1460 \text{ cm}^{-1}$.

Demineralization studies were performed on 2 mm thick occlusal dentin disks prepared from non-carious 3rd molars using 10% citric acid with exposure times between 15 sec and 24 hr. Hydrated type I collagen membranes (from bovine Achilles tendon; Ace Surgical Supply) were used as a comparison standard for fully demineralized tissue. Carious dentin lesions, both natural and artificial, were also evaluated at different zones throughout the lesions.

Small angle x-ray scattering

Two extracted non-carious human third molars with no visible evidence of caries and 5 extracted human third molars with arrested dentin caries were used in this study. Artificial dentin lesions were generated in non-carious third molars following sterilization. The tooth roots were cut off above the CEJ, using a high-speed saw with a diamond blade. The enamel was also cut off just above the DEJ. This was approximated by making sure that fissures extended below the cut surface, leaving the surface with exposed dentin with enamel islands and enamel surrounding the dentin. The occlusal surfaces of the dentin disks were carefully polished with 600-grit silicon carbide paper until an enamel island in the center of the tooth had been removed. This surface was then polished, sequentially, using waterproof silicon carbide papers under running water with grit sizes of 600, 800, and 1200 and diamond pastes of 1 and 0.25 μm . Each dentin disk was immersed in 2 ml 0.05M acetate buffer that contained 2.2 mM calcium and phosphate at pH 5.0 for 8 hours. This buffer has been shown to produce artificial caries-like lesions in dentin (McIntyre *et al.*, 2000). A previous study (Chapter 3) showed that demineralization of dentin by this buffer at this pH for 8 hours produces artificial carious dentin lesions approximately 38 μm deep with pink zones approximately 2 μm thick.

Small angle x-ray scattering was performed on beam line 1-4 at the Stanford Synchrotron Radiation Laboratory. The synchrotron radiation from a bending magnet was focused in the vertical axis by applying a small curvature to

a reflecting mirror in the optical train. The x-ray beam was scanned across the specimens from the DEJ to the pulp in 0.5 mm steps. The SAXS data from each location was collected on two-dimensional imaging plate detectors and analyzed by the methods described below. Crystallite shape was inferred from the logarithmic dependence of the scattering intensity with respect to the incident x-ray path (Fratzl *et al.*, 1991). The shape factor provides dimensionality, D. For D=1, the particle is roughly one-dimensional (length), and for D=2, the particle is two-dimensional (area) (Kinney *et al.*, 2001a). It has been customary to refer to the one-dimensional scattering behavior as arising from needle-like shapes, and the two-dimensional scattering behavior as arising from plate-like crystals (Fratzl *et al.*, 1992). The surface-to-volume ratio of the mineral crystallites, S/V was determined from the Porod constant which was determined by curve fitting the q^{-4} dependence of the scattering intensity at large q (Guinier and Fournet, 1955). The data were prepared as Kratky plots and the total scattering yield was calculated. Using the total scattering yield and the Porod constant the thickness parameter was estimated from the stereological relationship $T=V/2S$ (Kinney *et al.*, 2001a).

Results

Masson's Trichrome Stain

Trichrome staining was used to characterize the histological characteristics of the four zones (pink, light pink, transparent, apparently normal) of a carious lesion distinguished by Caries Detector (Kuraray, Osaka, Japan).

Fig. 4-1 shows the histological slides of these zones. Fig. 4-1(a) shows the transitions between the four zones of a typical carious lesion at low magnification (10x).

The apparently normal zone shown in Fig. 4-1(b) shows the peritubular dentin surrounding the dentinal tubules, as shown by the red staining. The intertubular dentin, composed of primarily type I collagen reinforced by mineral, is evident by the blue staining with red staining in the intertubular spaces.

Fig. 4-1(c) shows the transparent zone with the similar appearance of peritubular and intertubular dentin areas as the apparently normal zone, but with a less intense red staining, suggesting a possible dissolution of apatite mineral. In addition, there is mineral within the dentinal tubules depicted by the red stain. Fig. 4-1(d) shows the light pink zone in which the tubules are partially filled with intratubular mineral (ITM) (red) and the peritubular dentin and intertubular dentin appear to exhibit further mineral dissolution shown by the increased blue staining. In Fig. 4-1(e), the pink zone exhibits a lack of peritubular dentin and significant loss of mineral in the intertubular dentin as most of the collagen is stained blue. Intratubular mineral is also absent.

High-resolution AFM imaging of carious dentin collagen

High-resolution AFM imaging revealed partially demineralized collagen fibrils from the outer demineralized layer (pink zone) carious dentin lesions Fig. 4-2(a). Fig. 4-2(b) shows a section analysis (AFM software 4.48r, Digital Instruments) along a line placed parallel to the fibril axis, with an axial repeat

distance of approximately 67 nm, as shown by the distance between the two red arrows. Table 4-1 shows gap-overlap height differences of dentin collagen fibrils from the pink zones of four different lesions, which averaged approximately 2.7 nm (± 2.0), suggesting that significant mineral was removed, but possibly incompletely (Balooch *et al.*, 2004).

UV-Resonance Raman Spectroscopy

UVRRS was used to examine dentin demineralized with citric acid, in an effort to further understand the mineral loss process during dentin demineralization (Ager *et al.*, 2006). UVRR spectra of hydrated dentin specimens that were demineralized by exposure to citric acid are shown in Fig. 4-3(a) for specimens that were kept hydrated after demineralization. It can be seen that the $\text{PO}_4^{3-} \nu_1$ peak at ca. 960 cm^{-1} is present in dentin exposed for 1 min but absent for exposures of 30 min and longer. As shown in the inset, which represents the intensities of the PO_4^{3-} , Y8a and amide I peaks, the height of the amide I peak remains relatively constant in hydrated dentin as a function of citric acid exposure time. Similarly, the Y8a peak intensity remained relatively constant as well.

As shown in Fig. 4-3(b), in dentin that was allowed to dry after citric acid exposure, the height of the overlapping Y8a/amide I peak was increased, as compared to the untreated control sample. Peak fitting revealed that most of this increase was due to an increase in the amide I peak height (inset). The effect of dehydration was reversible (Fig. 4-4); that is, in a sample for which citric acid

exposure and dehydration increased the height of the Y8a/amide I peak, rehydration caused the peak to be reduced back to near its initial intensity.

As a control experiment, the effect of citric acid exposure on hydrated, unmineralized type 1 collagen from bovine tendon was investigated. No significant differences were found between the spectra at any of the acid treated time points with that of untreated hydrated collagen. While this suggests that citric acid exposure does not have a direct effect on the collagen structure in dentin, it is possible that the citric acid treatment could have an effect on the non-collagenous proteins that are present in dentin.

The Y8a and amide I peak heights from five demineralization experiments: two performed hydrated, one performed after hydration, and one with data from hydrated and dehydrated samples from the same run are summarized in Fig. 4-5. The control values represent the means of the unexposed dentin used in this study. Data from dentin demineralized for 30 min and longer (from Fig. 4-3) were used to form the “wet” and “dry” sample sets. Referring to Fig. 4-5, demineralization produces a significant increase in the amide I peak height after dehydration, but not if the samples are kept hydrated. The Y8a feature decreased compared to the control; this trend was significant ($p < 0.05$) in the wet sample set. As with the sequentially demineralized dentin substrates, carious dentin lesions also displayed an increase in the amide I peak height after dehydration (Fig. 4-6).

Small angle x-ray scattering

The SAXS images of scattering are shown in Fig. 4-7 for carious, transparent and normal dentin. The ring corresponding to the 3rd harmonic of the 67nm reflection relating to the periodicity of gap zones in the collagen fibrils is shown in transparent (66.5 nm) and normal dentin (66.4 nm), but was not evident in more demineralized zones, P and LP (Fig. 4-7). A graph of the scattering intensity as a function of q for an x-ray beam incident parallel to the mineralization front is shown in Fig. 4-8 for a natural carious dentin lesion (Fig. 4-8(a)) and an artificial carious dentin lesion (Fig. 4-8(b)), which did not contain transparent dentin. The peak corresponding to the 3rd harmonic of the 67 nm periodicity was seen in normal and transparent dentin but not in carious (P and LP) dentin. Insets show mineral concentrations, measured by transverse microradiography, across the lesions.

Mineral crystallite thickness for carious (3.6 ± 1.1 nm), transparent (3.7 ± 1.4 nm) and normal dentin (3.2 ± 0.5 nm) is shown in Fig. 4-9. There were no significant differences between any types of dentin. Mineral content measured by transverse microradiography is shown in Fig. 4-10. For each type of dentin, carious (P and LP) ($28 \pm 7\%$), transparent ($36 \pm 3\%$), and normal ($42 \pm 2\%$), mineral content was significantly different ($p < 0.05$). Mineral crystallite shape was needle-like in all dentin types, but carious dentin had a significantly different ($p < 0.05$, t-test) aspect ratio (3.3) than normal dentin (4.0), indicating that shorter crystallites are present in carious dentin (Fig. 4-11). Aspect ratio was determined by correlating crystallite shape (rod-like) with diameter. Table 4-2 summarizes the SAXS data for each dentin type.

Discussion

Trichrome staining has been used to identify intact collagen in bone and dentin (Wang *et al.* 2006; Wang *et al.* 2003). Trichrome staining of carious dentin identified the same four zones as distinguished by Caries Detector from the image of the opposing cut surface of the lesion that was Caries Detector stained. The use of Masson's trichrome stain enabled the visualization of the variation in dentin tissue density in the different carious dentin zones. The blue stain was representative of a loose, textured tissue with higher permeability, such as collagen, and the red stain for mineral of a more dense tissue, such as collagen reinforced with apatite crystals or mineral in peritubular and intertubular mineral.

The gradual change in mineral dissolution was evident from the trichrome staining of the carious dentin (Figure 4-1). Apparently normal dentin consisted of tubules lined with mineral from peritubular dentin and fully mineralized intertubular dentin. The transparent zone exhibited partial dissolution of the peritubular and intertubular dentin shown by decreased density of the apatite crystals. Also, there was increased intertubular mineral deposition. The light pink zone was characterized by the further dissolution of peritubular and intertubular dentin exhibited by the lack of red staining. Intratubular mineral was present to a lesser extent than in the transparent zone. However, intratubular mineral was absent in the pink zone. The lack of red staining was indicative of extensive demineralization of the peritubular and intertubular dentin.

The trichrome staining characterized the four zones of carious dentin demonstrating the different microstructures of the zones similar to those reported by previous studies (Marshall *et al.*, 1997; Ogawa *et al.*, 1983; Shimizu *et al.*, 1981). Although little attention has been given to trichrome staining of carious dentin in the literature, the present study showed that there is a possible parallel between the identification of the zones with Caries Detector and trichrome stain. However, further investigation is necessary to fully evaluate this comparison of stains.

In this study, high-resolution AFM imaging of dentin collagen from the pink zones of carious dentin lesions revealed partially demineralized fibrils that displayed the characteristic periodicity of ~67 nm. The average gap-overlap height difference of 2.7 nm indicated significant mineral remaining in the fibrils. In a recent study, *in situ* atomic force microscopy (AFM) was used to investigate the kinetics of demineralization of human dentin collagen fibrils. Topographic images showed a gradual increase in gap-overlap depth of the fibril. The gap-overlap depth varied linearly with the square root of time until there were no further changes at 7 nm. Furthermore, reconstituted collagen without mineral had a 5-7 nm gap-overlap depth (Balooch *et al.*, 2004). These data suggest that high-resolution AFM imaging and gap-overlap depth measurement could be an indirect way to determine the presence of intrafibrillar mineral.

When dentin is demineralized by acid exposure, apatite mineral is dissolved and water or acid occupies the space formerly occupied by the mineral. In the course of dentin demineralization, mineral is thought to be removed first

from the extrafibrillar compartment with NCPs, and the intrafibrillar mineral is removed last since it is protected by the collagen. In completely demineralized dentin, water molecules are able to enter the fibril. If demineralized dentin is dehydrated, the surface collapses and the collagenous matrix shrinks until it is supported by the partially or completely mineralized dentin below it (Weiner and Wagner 1998; Kanca, 1992; Marshall *et al.*, 1997). For more complete demineralization, we expect a more complete collapse of the intertubular demineralized dentin matrix (Marshall *et al.*, 1998).

This depiction of the demineralization process is supported by mechanical and structural studies (Angker *et al.*, 2004; Kinney *et al.*, 1999; Marshall *et al.*, 1998; Zheng *et al.*, 2003). For example, analysis of hydrated and dehydrated dentin collagen revealed that dehydration affects fibril diameter and repeat distance in a reciprocal way (Habelitz *et al.*, 2002). Tapping mode images obtained with atomic force microscopy (AFM) showed significant differences in the distribution of fibril diameter and axial repeat distance, depending on the hydration state of the substrate. After dehydration the periodicity shortened for some fibrils and showed an overall wider distribution. According to some studies (Bella *et al.*, 1995; Orgel *et al.*, 2000), hydrated fibrils have a higher degree of structural organization, while dehydration causes structural disorder and mechanical stresses. Upon dehydration, loss of adsorbed and chemically bound water molecules destabilizes the quaternary structure of collagen molecules and lowers the degree of organization in the fibril.

The present UVRRS data are consistent with this picture. The stability of the UVRRS spectra in hydrated, demineralized dentin and the reversible changes in the UVRRS spectra with hydration/dehydration (Fig. 4-2) are consistent with the idea that water can support the collagen structure. The increase in amide I peak intensity upon dehydration indicates structural disorder and mechanical stresses with the demineralized collagen fibrils. The mineralized collagen fibrils are able to retain their structure, even after dehydration, because of the mineral supporting the fibril. This is also consistent with the recent observation of a structured layer of water between the mineral and organic phases of bone (Wilson *et al.*, 2005). The presence or absence of mineral (even intrafibrillar mineral) therefore does not have a direct effect on the amide I peak intensity. On the other hand, other perturbations of the collagen environment, as produced by dehydrating demineralized dentin or, as reported previously, by exposing dentin to non-physiological solvents such as ethanol and acetone (Nalla *et al.*, 2005), clearly increase the amide I intensity.

Based on the physical model for demineralization presented above, we would expect, and in fact observe, an increase in the amide I peak height in dehydrated and demineralized dentin, because of the increased interaction between collagen fibrils caused by distortion from shrinkage and intrafibrillar movement. Finally, we note that the Y8a peak decreases in hydrated demineralized dentin suggesting that the Y8a intensity may be specifically affected by intrafibrillar mineral. Artificial and natural carious dentin lesions behaved similarly to citric acid demineralized dentin samples. The more

demineralized zones, pink and light pink, had increased amide I intensity upon dehydration, whereas the fully mineralized zones did not.

SAXS measurements of carious dentin have not confirmed the presence of mineral crystallites in the gap zones of collagen fibrils of the most demineralized pink zone of caries. Diffraction peaks representing the 3rd harmonic of the 67 nm periodicity were not apparent in carious dentin (pink and light pink zones). However the existence of mineral in the gap regions of these zones cannot be ruled out, especially since AFM imaging indicates considerable remnant intrafibrillar mineral. This discrepancy could be explained by disorientation of the carious region to the direction of the x-ray beam (Kinney et al., 2001b), brought about by the dehydration of the dentin, which was necessary to perform SAXS measurements. Further investigation is necessary, using TEM to image crystallites at high resolution. Transparent dentin had increased diffraction peaks representing the 3rd harmonic of the 67 nm periodicity, perhaps because the decrease in EF mineral may have lead to an enhancement of the relative intensity of IF mineral.

In conclusion, using histochemical staining, AFM imaging, UVRRS, and SAXS to characterize the collagen in carious dentin, it appears that the collagen fibrils were intact. Based on the current evidence, the presence of intrafibrillar mineral in carious dentin collagen cannot be proven, however, the high-resolution AFM images of demineralized collagen suggested remnant intrafibrillar mineral.

D. REFERENCES

Ager JW, Nalla RK, Breeden KL, Ritchie RO (2005). Deep-ultraviolet Raman spectroscopy study of the effect of aging on human cortical bone. *J Biomed Opt* 10(3):034012.

Ager JW, 3rd, Nalla RK, Balooch G, Kim G, Pugach M, Habelitz S, Marshall GW, Kinney JH, Ritchie RO (2006). On the increasing fragility of human teeth with age: a deep-UV resonance Raman study. *J Bone Miner Res* 21(12):1879-87.

Akkus O, Adar F, Schaffler MB (2004). Age-related changes in physicochemical properties of mineral crystals are related to impaired mechanical function of cortical bone. *Bone* 34(3):443-53.

Angker L, Nijhof N, Swain MV, Kilpatrick NM (2004). Influence of hydration and mechanical characterization of carious primary dentine using an ultra-micro indentation system (UMIS). *Eur J Oral Sci* 112(3):231-6.

Asher SA, Mikhonin AV, Bykov S (2004). UV Raman demonstrates that alpha-helical polyalanine peptides melt to polyproline II conformations. *J Am Chem Soc* 126(27):8433-40.

Bailey AJ, Knott L (1999). Molecular changes in bone collagen in osteoporosis and osteoarthritis in the elderly. *Exp Gerontol* 34(3):337-51.

Balooch MB, G; Habelitz, S; Marshal, SJ; and Marshall, GW (2004). Intrafibrillar demineralization study of single human dentin collagen fibrils by AFM. *MRS Symposium Proceedings*.

Bella J, Brodsky B, Berman HM (1995). Hydration structure of a collagen peptide. *Structure* 3(9):893-906.

Clarkson BH, Chang SR, Holland GR (1998). Phosphoprotein analysis of sequential extracts of human dentin and the determination of the subsequent remineralization potential of these dentin matrices. *Caries Res* 32(5):357-64.

Eyre DR, Paz MA, Gallop PM (1984). Cross-linking in collagen and elastin. *Annu Rev Biochem* 53(717-48).

Fusayama T, Terachima S (1972). Differentiation of two layers of carious dentin by staining. *J Dent Res* 51(3):866.

Habelitz S, Balooch M, Marshall SJ, Balooch G, Marshall GW, Jr. (2002). In situ atomic force microscopy of partially demineralized human dentin collagen fibrils. *J Struct Biol* 138(3):227-36.

Kanca J, 3rd (1992). Improving bond strength through acid etching of dentin and bonding to wet dentin surfaces. *J Am Dent Assoc* 123(9):35-43.

Katz JL, Spencer P, Nomura T, Wagh A, Wang Y (2003). Micromechanical properties of demineralized dentin collagen with and without adhesive infiltration. *J Biomed Mater Res A* 66(1):120-8.

Kinney JH, Balooch M, Marshall GW, Marshall SJ (1999). A micromechanics model of the elastic properties of human dentine. *Arch Oral Biol* 44(10):813-22.

Kinney JH, Pople JA, Driessen CH, Breunig TM, Marshall GW, Marshall SJ (2001a). Intrafibrillar mineral may be absent in dentinogenesis imperfecta type II (DI-II). *J Dent Res* 80(6):1555-9.

Kinney JH, Pople JA, Marshall GW, Marshall SJ (2001b). Collagen orientation and crystallite size in human dentin: a small angle X-ray scattering study. *Calcif Tissue Int* 69(1):31-7.

Knott L, Bailey AJ (1998). Collagen cross-links in mineralizing tissues: a review of their chemistry, function, and clinical relevance. *Bone* 22(3):181-7.

Kuboki Y, Ohgushi K, Fusayama T (1977). Collagen biochemistry of the two layers of carious dentin. *J Dent Res* 56(10):1233-7.

Landis WJ (1986). A study of calcification in the leg tendons from the domestic turkey. *J Ultrastruct Mol Struct Res* 94(3):217-38.

Landis WJ, Hodgens KJ, Arena J, Song MJ, McEwen BF (1996). Structural relations between collagen and mineral in bone as determined by high voltage electron microscopic tomography. *Microsc Res Tech* 33(2):192-202.

Marshall GW, Jr., Inai N, Wu-Magidi IC, Balooch M, Kinney JH, Tagami J, *et al.* (1997). Dentin demineralization: effects of dentin depth, pH and different acids. *Dent Mater* 13(6):338-43.

Marshall GW, Jr., Wu-Magidi IC, Watanabe LG, Inai N, Balooch M, Kinney JH, *et al.* (1998). Effect of citric acid concentration on dentin demineralization, dehydration, and rehydration: atomic force microscopy study. *J Biomed Mater Res* 42(4):500-7.

McIntyre JM, Featherstone JD, Fu J (2000). Studies of dental root surface caries. 1: Comparison of natural and artificial root caries lesions. *Aust Dent J* 45(1):24-30.

Morris MD, Finney WF, Rajachar RM, Kohn DH (2004). Bone tissue ultrastructural response to elastic deformation probed by Raman spectroscopy. *Faraday Discuss* 126(159-68; discussion 169-83).

- Nalla RK, Porter AE, Daraio C, Minor AM, Radmilovic V, Stach EA, Tomsia AP, Ritchie RO. (2005). Ultrastructural examination of dentin using focused ion-beam cross-sectioning and transmission electron microscopy. *Micron* 36(7-8):672-80.
- Nyvad B, Fejerskov O (1990). An ultrastructural study of bacterial invasion and tissue breakdown in human experimental root-surface caries. *J Dent Res* 69(5):1118-25.
- Ogawa K, Yamashita Y, Ichijo T, Fusayama T (1983). The ultrastructure and hardness of the transparent layer of human carious dentin. *J Dent Res* 62(1):7-10.
- Orgel JP, Wess TJ, Miller A (2000). The in situ conformation and axial location of the intermolecular cross-linked non-helical telopeptides of type I collagen. *Structure* 8(2):137-42.
- Oxlund H, Mosekilde L, Ortoft G (1996). Reduced concentration of collagen reducible cross links in human trabecular bone with respect to age and osteoporosis. *Bone* 19(5):479-84.
- Paschalis EP, Verdelis K, Doty SB, Boskey AL, Mendelsohn R, Yamauchi M (2001). Spectroscopic characterization of collagen cross-links in bone. *J Bone Miner Res* 16(10):1821-8.
- Paschalis EP, Shane E, Lyritis G, Skarantavos G, Mendelsohn R, Boskey AL (2004). Bone fragility and collagen cross-links. *J Bone Miner Res* 19(12):2000-4.
- Pezzotti G, Sakakura S (2003). Study of the toughening mechanisms in bone and biomimetic hydroxyapatite materials using Raman microprobe spectroscopy. *J Biomed Mater Res A* 65(2):229-36.
- Schupbach P, Guggenheim B, Lutz F (1989). Human root caries: histopathology of initial lesions in cementum and dentin. *J Oral Pathol Med* 18(3):146-56.
- Shimizu C, Yamashita Y, Ichijo T, Fusayama T (1981). Carious change of dentin observed on longspan ultrathin sections. *J Dent Res* 60(11):1826-31.
- Suppa P, Ruggeri A, Jr., Tay FR, Prati C, Biasotto M, Falconi M, *et al.* (2006). Reduced antigenicity of type I collagen and proteoglycans in sclerotic dentin. *J Dent Res* 85(2):133-7.
- Timlin JA, Carden A, Morris MD, Rajachar RM, Kohn DH (2000). Raman spectroscopic imaging markers for fatigue-related microdamage in bovine bone. *Anal Chem* 72(10):2229-36.

Tjaderhane L, Larjava H, Sorsa T, Uitto VJ, Larmas M, Salo T (1998). The activation and function of host matrix metalloproteinases in dentin matrix breakdown in caries lesions. *J Dent Res* 77(8):1622-9.

Veis A, Sfeir C, Wu CB (1997). Phosphorylation of the proteins of the extracellular matrix of mineralized tissues by casein kinase-like activity. *Crit Rev Oral Biol Med* 8(4):360-79.

Walters C, Eyre DR (1983). Collagen crosslinks in human dentin: increasing content of hydroxypyridinium residues with age. *Calcif Tissue Int* 35(4-5):401-5.

Wang IE, Mitroo S, Chen FH, Lu HH and Doty SB (2006). Age-dependent changes in matrix composition and organization at the ligament-to-bone insertion. *J Orthop Res* 24:1745-1755.

Wang Y and Spencer P. Hybridization efficiency of the adhesive/dentin interface with wet bonding. *J Dent Res* 82(2): 141-145.

White JM, Goodis HE, Marshall SJ, Marshall GW (1994). Sterilization of teeth by gamma radiation. *J Dent Res* 73(9):1560-7.

Wilson EE, Awonusi A, Morris MD, Kohn DH, Tecklenburg MM, Beck LW (2005). Highly ordered interstitial water observed in bone by nuclear magnetic resonance. *J Bone Miner Res* 20(4):625-34.

Zheng L, Hilton JF, Habelitz S, Marshall SJ, Marshall GW (2003). Dentin caries activity status related to hardness and elasticity. *Eur J Oral Sci* 111(3):243-52.

Zioupou P, Currey JD, Hamer AJ (1999). The role of collagen in the declining mechanical properties of aging human cortical bone. *J Biomed Mater Res* 45(2):108-16.

Figures and Tables

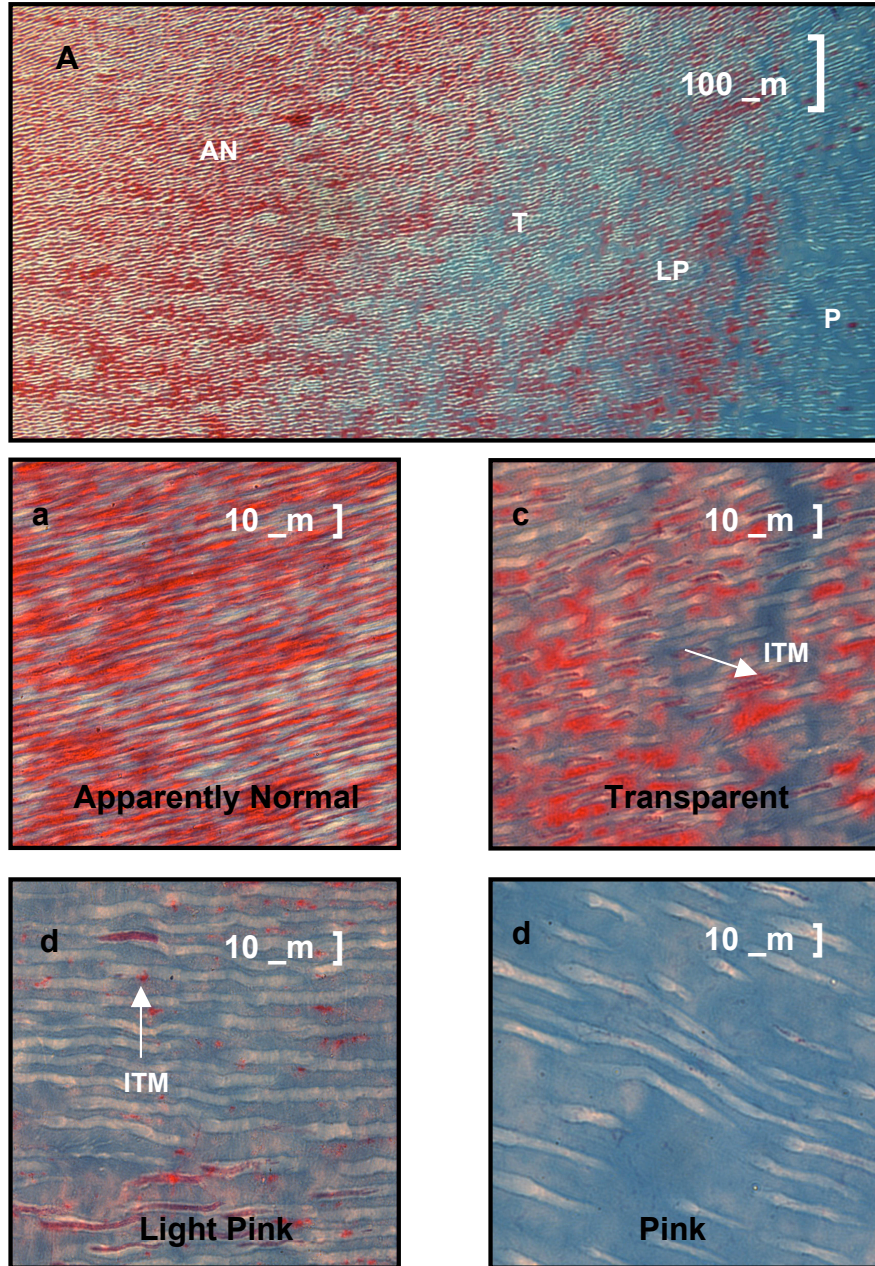


Fig. 4-1. Histological images of the carious dentin zones stained by Masson's trichrome. (a) Progression from the apparently normal (AN) zone to the pink (P) zone at 10x magnification. (b) Apparently normal zone at 60x magnification. (c) Transparent zone at 60x magnification. Red stain in tubules shows mineral occlusion. (d) Light pink zone at 60x magnification. (e) Pink zone at 60x magnification. Lack of red stain shows loss of peritubular dentin and mineral from intertubular dentin. P, pink zone; LP, light pink zone; T, transparent zone; AN, apparently normal zone; ITM, intratubular mineral.

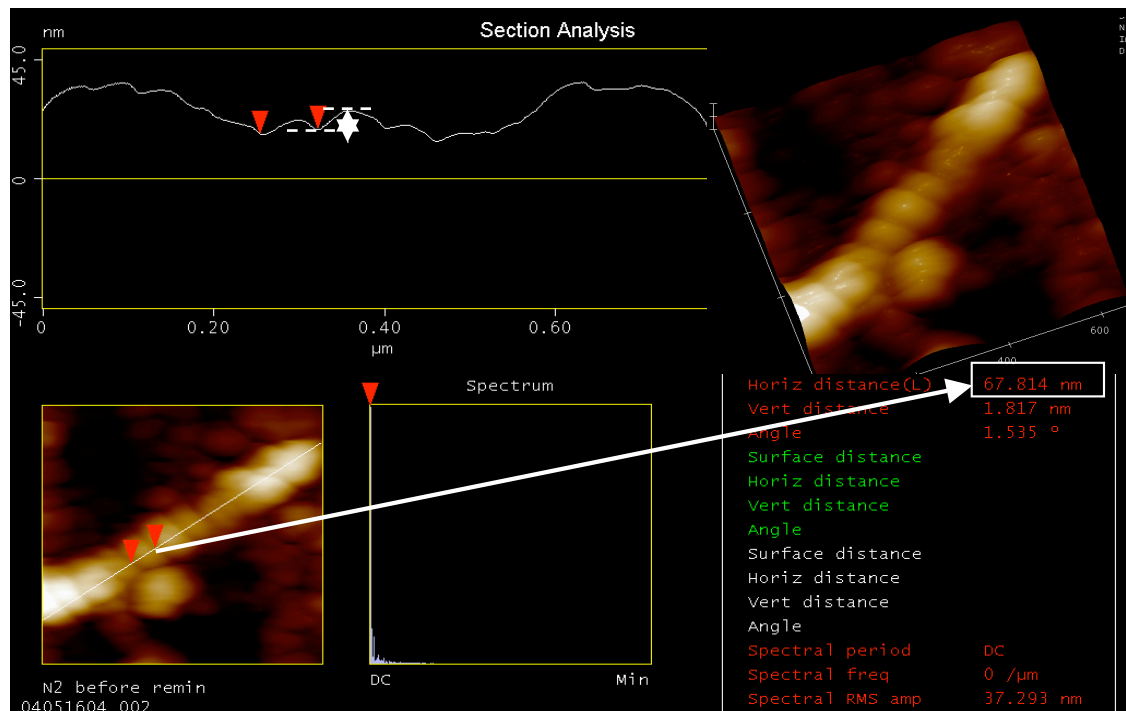


Fig. 4-2. High-resolution AFM imaging of pink zone carious dentin collagen. Section analysis along the axis of the collagen fibril shows a wave-like repeat pattern. The periodicity of the gap-overlap distance was determined to be 67.8 nm. The step height between the gap and overlap zones was around 2.7 (± 2.0) nm (inset: topographic image of a typical collagen fibril from pink zone carious dentin).

Table 4-1. Gap-overlap height differences of dentin collagen from pink zones.

	Gap-overlap height difference (nm)	sd
lesion 1	2.6	1.7
lesion 2	2.9	2.5
lesion 3	2.4	1.5
lesion 4	3.0	2.2
Total	2.7	2

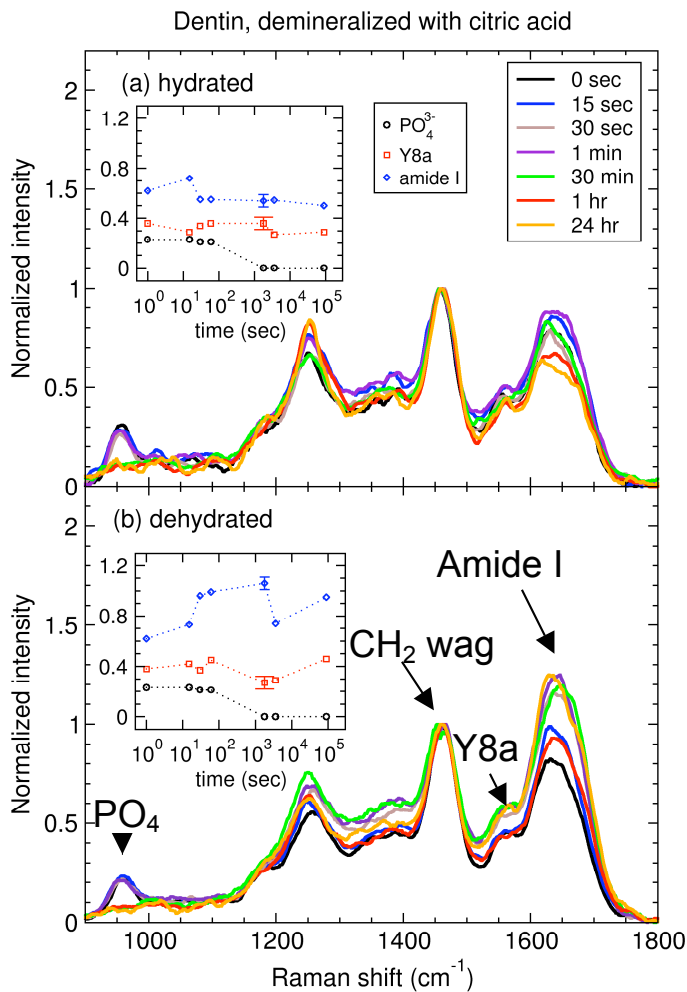


Fig. 4-3 UVRR spectra (244 nm excitation) of dentin exposed to citric acid to induce demineralization: (a) demineralized dentin maintained in its hydrated state and (b) demineralized dentin allowed to dry. The relative peak heights of the phosphate peak at 960 cm^{-1} , Y8a (1610 cm^{-1}), and amide I (ca. 1660 cm^{-1}) are shown in the insets as a function of exposure time. The collapse of the dentin structure produced by demineralization and dehydration produces an increase in the amide I peak height (from Ager *et al.*, 2006).

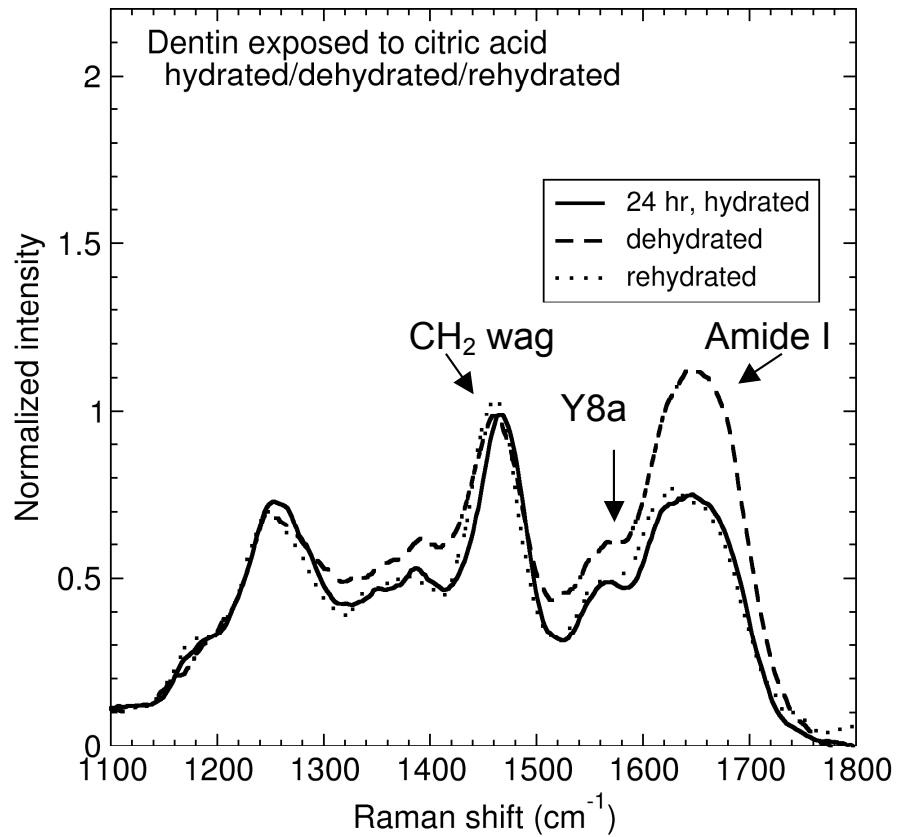


Fig. 4-4. UVRR spectra (244 nm excitation) of dentin exposed to citric acid for 24 hr to induce demineralization, subsequently dehydrated, and then rehydrated. The increase in the height of the overlapped Y8a/amide I feature upon dehydration is reversible (from Ager *et al.*, 2006).

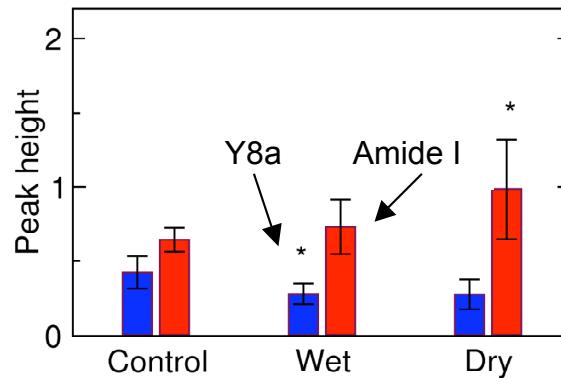


Fig. 4-5. Normalized peak heights for the Y8a (blue) and amide I (red) feature obtained from non-linear least squares fitting of UVRR spectra (Fig. 4-3) obtained from demineralized dentin. Significant differences in means compared to the Control group (t-test) * $p < 0.05$ (from Ager *et al.*, 2006).

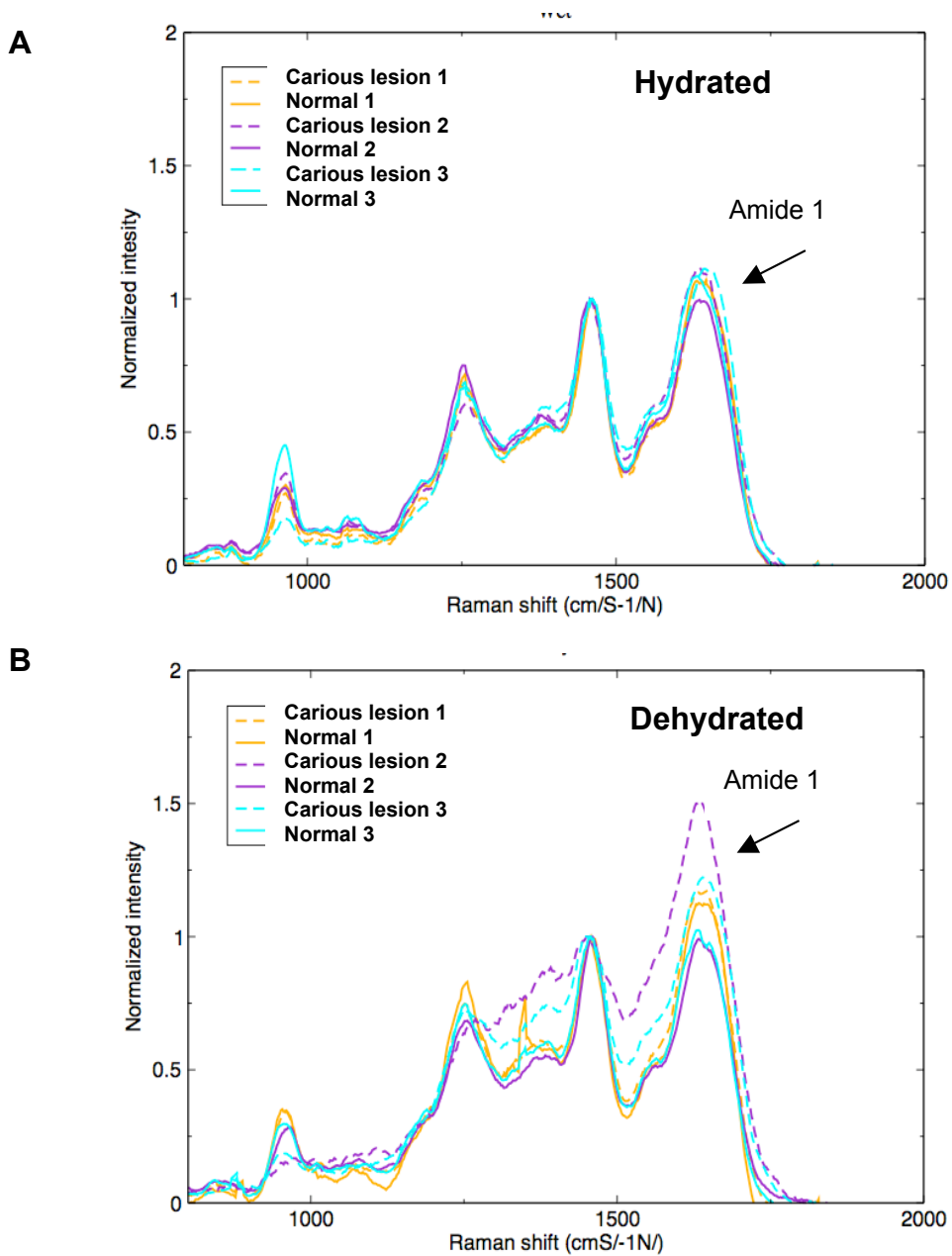


Figure 4-6. URRS of 3 carious dentin lesions showing both carious and non-carious dentin under (A) hydrated and (B) dehydrated conditions. (A) Under hydrated conditions the amide I peak is of similar intensity for both carious and non-carious dentin. (B) Under dehydrated conditions the amide I peak intensity of the carious portion of the 3 lesions increases dramatically.

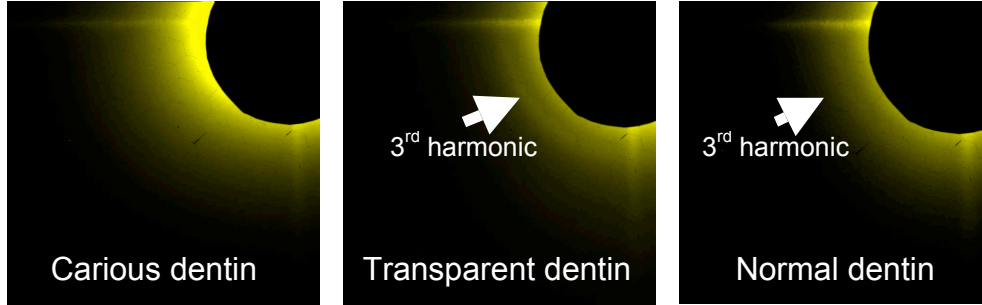


Figure 4-7. Representative SAXS scattering images of carious, transparent and normal dentin showing ring representing the 3rd harmonic, which appears as a faint line around the x-ray beam stop, of the ~67 nm periodicity of collagen fibrils apparent in transparent and normal dentin but not carious (pink and light pink) dentin.

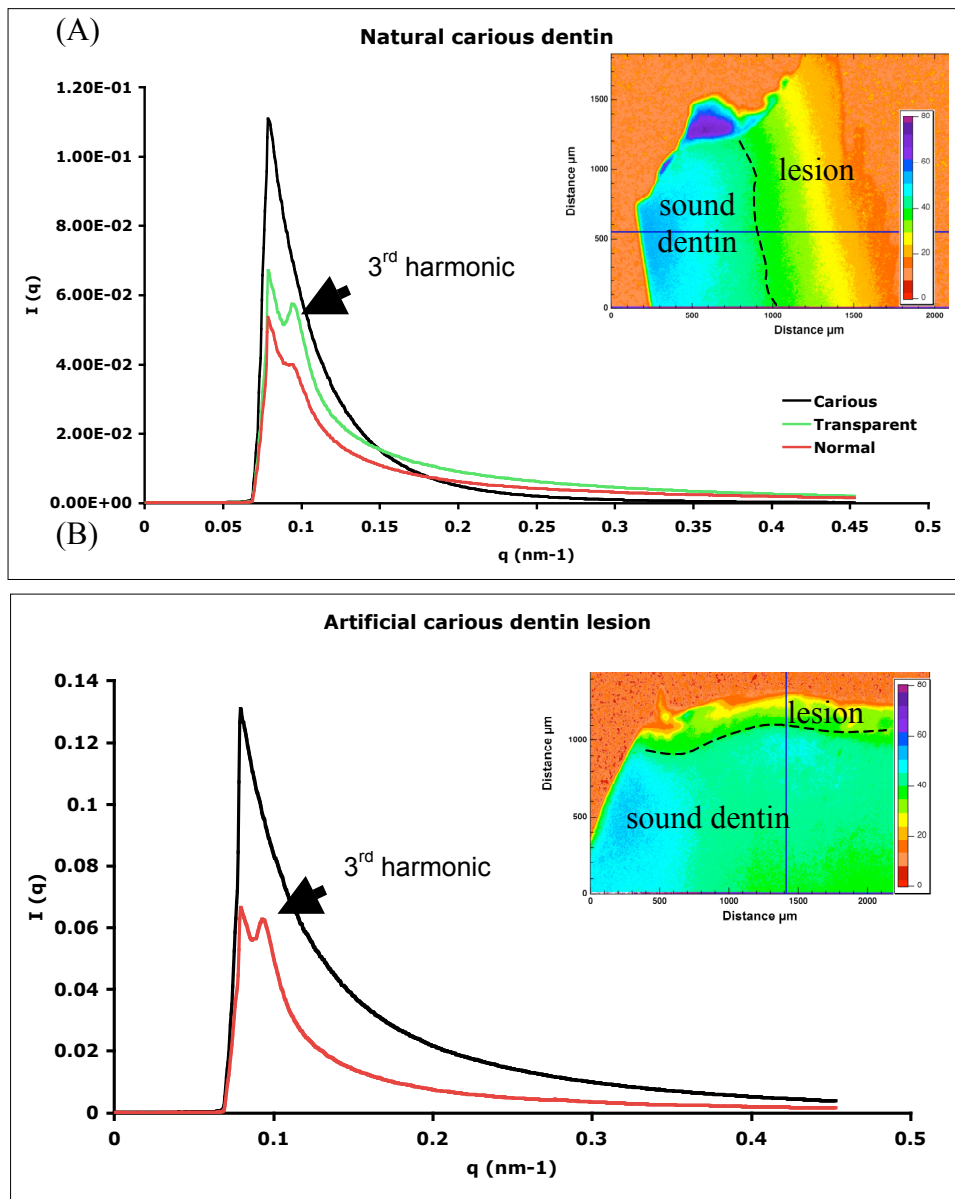


Figure 4-8. Azimuthally averaged SAXS patterns of natural (A) and artificial (B) carious dentin lesions showing the detectable ~ 22.6 nm 3^{rd} harmonic characteristic of the ~ 67 nm repeat pattern of collagen fibrils in normal and transparent dentin but not carious (pink and light pink) dentin.

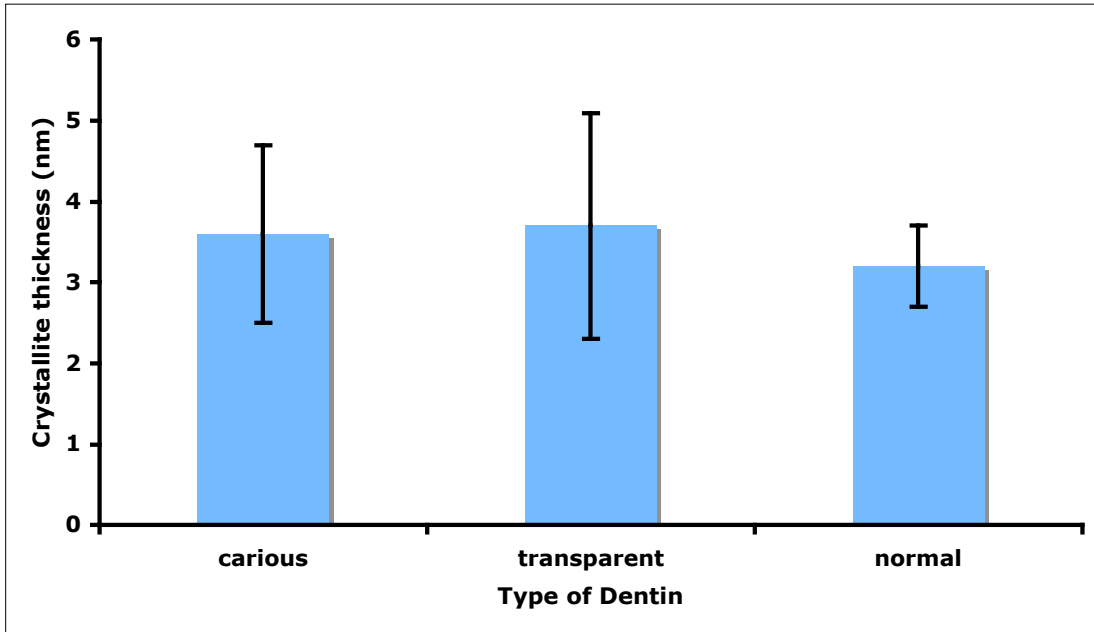


Figure 4-9. Mineral crystallite thickness (in nm) of carious (pink and light pink), transparent and normal dentin. There were no significant differences between the types of dentin.

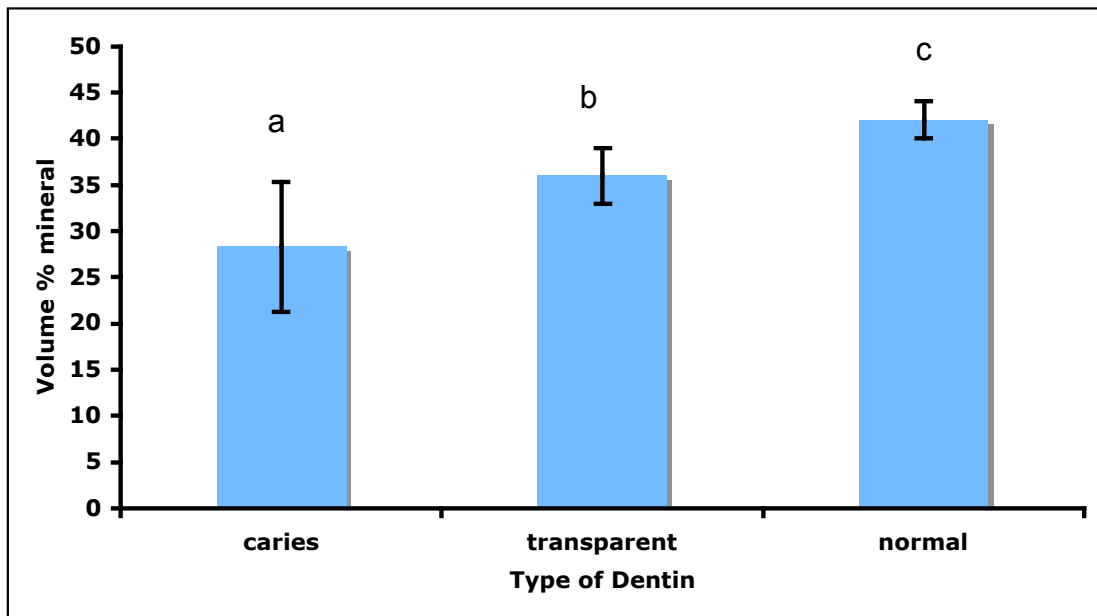


Figure 4-10. Mineral content of carious, transparent and normal dentin, in volume % mineral, measured by transverse digital microradiography. Different letters (a, b, c) indicate significant differences ($p < 0.05$).

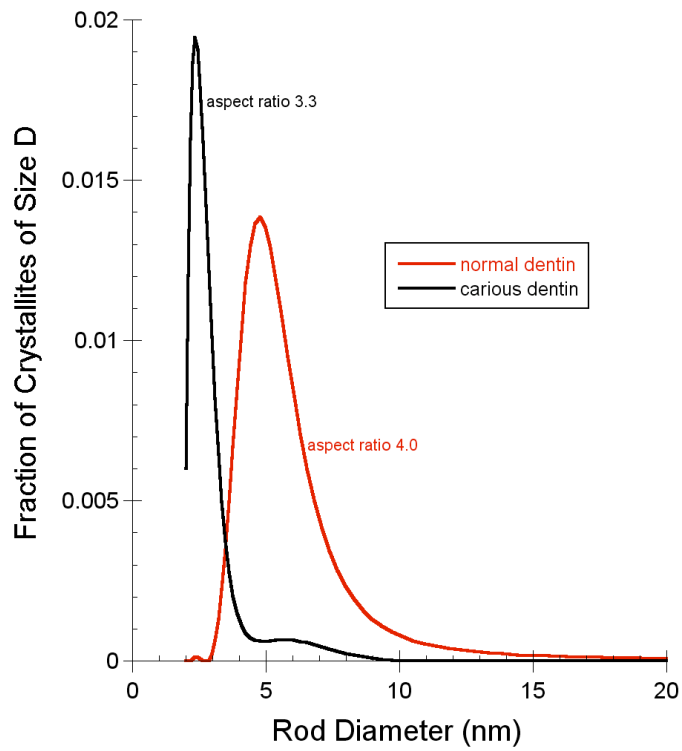


Figure 4-11. Mineral crystallite shape (rod-like) of size D vs. rod diameter (nm) in carious and normal dentin derived from SAXS measurements. Crystallite aspect ratios were significantly different (t-test, $p < 0.05$).

Table 4-2. Summary of data from SAXS measurements.

	Crystallite thickness (nm)	Gap spacing (nm)	Crystallite size (nm) aspect ratio	Volume % mineral
Cariou dentin	3.6 (1.1)		3.3	28 (7)
Transparent dentin	3.7 (1.4)	66.5 (0.5)		36 (3)
Normal Dentin	3.2 (0.5)	66.4 (0.5)	4.0	42 (2)

Chapter 5

Remineralization of artificial and natural carious dentin lesions.

Introduction

Available evidence suggests that dentin remineralization occurs neither by spontaneous precipitation nor nucleation of mineral on the organic matrix but by growth of residual crystals in the lesions (Daculsi *et al.*, 1979; Hunter and Goldberg, 1994; Klont and ten Cate, 1991; Levine and Rowles, 1973; Stetler-Stevenson and Veis, 1986). One study (Mukai and ten Cate, 2002) found that advanced root dentin carious lesions produced *in vitro* were remineralizable despite a virtual lack of remaining mineral in the lesion. The artificial lesions repaired an apparent 50 to 85% of normal mineral, and the remineralization occurred in the surface area, the lesion body and the inner zone adjacent to the sound dentin (Mukai and ten Cate, 2002). According to transverse microradiography (TMR) analysis of mineral content of the lesions, mineral deposition first occurred in the surface layer and then moved to the lesion body when the surface layer reached mineral content levels similar to sound dentin. Therefore, the authors concluded that the mineral was precipitated on the lesion surface until there was no more space for crystal growth (Mukai and ten Cate, 2002). Remineralization in the lesion body may reflect the number of nucleation sites available for crystal growth following demineralization (Clarkson *et al.*, 1998). Although this study showed that remineralization of root caries lesions is possible, even when there is a high degree of mineral loss, the “quality” (mineral content compared with nanomechanical properties) of the remineralized tissue was not assessed. It remains unclear whether the mineral was located within the

fibrils, surrounding them, or how the structure and morphology of the remineralized tissue compared to normal dentin.

The quality of the tissue formed when demineralized dentin collagen containing residual intrafibrillar mineral is remineralized, is predicted to be significantly different from that formed on demineralized dentin without intrafibrillar mineral. The existing mineral nuclei or crystals may facilitate *functional* mineral growth, from within collagen fibrils intrafibrillar (IF) and continuing outward to the extrafibrillar (EF) compartment (Kinney *et al.*, 2003). Without existing nuclei, in completely demineralized collagen, remineralized tissue is likely the result of *precipitative* mineral growth, filling only the extrafibrillar compartment with mineral. This tissue may have structural and nanomechanical properties similar to dentinogenesis imperfecta type II (DI). DI dentin nanomechanical properties are generally poor (Kinney *et al.*, 2003). Thus, such remineralization would not be considered optimal.

Dentinogenesis imperfecta type II (DI) dentin is thought to have poor interaction between collagen and hydroxyapatite due to the apparent lack of intrafibrillar mineral (Kinney *et al.*, 2001). In a recent study of DI dentin nanomechanical properties (Kinney *et al.*, 2003), elastic modulus modulus of dry DI dentin was 13.8 (2.0) GPa, while normal dentin was 23.9 (1.1) GPa. Elastic modulus of hydrated DI dentin was 5.7 (1.4) GPa, and normal dentin was 20.0 (1.0). Furthermore, elastic modulus of dry dentin was correlated with mineral content, while elastic modulus of hydrated dentin was not. For this reason we chose to use hydrated nanomechanical properties to measure the level of

remineralization that we believe to be functional; that which maintains the interaction between organic and inorganic components of dentin.

Materials and Methods

Artificial carious dentin lesions

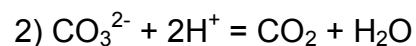
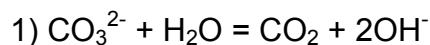
Extracted, non-carious third molars were used for this study. The teeth were extracted from patients requiring such treatment as part of their normal dental treatments following a protocol approved by the UCSF Committee on Human Research. After extraction the teeth were sterilized using gamma irradiation (White *et al.*, 1994) and stored in Hank's balanced salt solution at 4°C until preparation. The tooth roots were cut off above the CEJ, using a high-speed saw with a diamond blade. The enamel was also cut off just above the DEJ. This was approximated by making sure that fissures extended below the cut surface, leaving the surface with exposed dentin with enamel islands and enamel surrounding the dentin. The occlusal surfaces of the dentin disks were carefully polished with 600-grit silicon carbide paper until an enamel island in the center of the tooth had been removed. This surface was then polished, sequentially, using waterproof silicon carbide papers under running water with grit sizes of 600, 800, and 1200 and diamond pastes of 1 and 0.25 µm. The dentin disks were then quartered and half of each quarter disk was masked with double-stick tape to provide a reference layer control.

Each quarter dentin disk was immersed in 2 ml 0.05M acetate buffer that contained 2.2 mM Ca/ PO₄ (calcium/phosphate) at pH 5.0 for 8 hours (Chapter

3). This buffer has been shown to produce artificial caries-like lesions in dentin (McIntyre *et al.*, 2000). A previous study (Chapter 3) showed that demineralization of dentin by this buffer at this pH for 8 hours produces artificial carious dentin lesions with pink zones approximately 2 μm thick, according to the lesion depth measurements by AFM in Chapter 3.

Remineralization of artificial lesions

Demineralized lesions (n=3) were placed in 100 ml of one of 6 supersaturated metastable remineralizing solutions (Table 5-1) and removed at 7 time points between 1 and 28 days. The solutions were chosen based on previous studies and contained either 2.2 mM Ca^{2+} , 1.45 mM PO_4^{3-} and 150 mM KCl with or without 2 ppm NaF (Featherstone *et al.*, 1990) (pH 7.4) and with or without 22 mM CO_3^{2-} (pH 5.5-8.5); or 1.5 mM Ca^{2+} , 0.9 PO_4^{3-} and 150 mM KCl with or without 2 ppm NaF (pH 7.4). For each solution, saturation with respect to hydroxyapatite (HAP) and fluorapatite (FAP) at these pHs has been calculated (Table 5-1) (Larsen, 2001). Carbonate solutions were based on the protocol described by Tung (US Patent, 1995). Carbon dioxide is formed from CO_3^{2-} according to one of the following reactions, depending on the initial conditions:



The reaction continues until equilibrium has been reached. An alkaline carbonated phosphate solution was mixed with an aqueous solution containing high concentrations of calcium ions at an acidic pH, resulting in a solution

containing high calcium and phosphate concentrations at a lower pH (5-7.5). At a low pH, carbonate, phosphate, and calcium ions dissolved in the solution settle in the intrafibrillar region of the collagen fibrils. As carbon dioxide is formed and released into the air, the pH of the solution increased according to the chemical reactions described above. The pH changes in the solution were monitored using a pH meter.

Remineralization of natural lesions

Arrested natural carious dentin lesions (n=3) that exhibited mostly pink zones, with some light pink zone, were chosen. Enamel was removed and occlusal carious surfaces were characterized by AFM-based nanoindentation to obtain baseline measurements. One solution (2.2 mM Ca²⁺, 1.45 mM PO₄³⁻, 150 mM KCl, 2 ppm F⁻, pH 7.4) was chosen for remineralization of the natural lesions because it had the largest increase in hydrated elastic modulus after remineralization of artificial lesions. Samples were remineralized for 1 to 28 days and hydrated elastic modulus was measured after remineralization.

Measurement of reduced elastic modulus and hardness of carious dentin by AFM

A Nanoscope III AFM (Digital Instruments, Santa Barbara, CA, USA) modified with a Triboscope head for nanoindentation (Hysitron, Minneapolis, MN, USA) (Balooch *et al.*, 1998; Marshall *et al.*, 2001) was used to study the mechanical properties of each area across each lesion. A Berkovich diamond tip was used for the indentations, which were performed both dry and in a liquid cell

filled with deionized water. All measurements used a trapezoidal force profile with peak loads between 50 μN and 500 μN , depending on the softness of the surface (as described previously in Chapter 2), and 3 s indentation time increments (load = 3s, hold 3s, unload = 3s). Each indentation yielded a load-deformation curve, from which the reduced elastic modulus, E , was calculated from the slope of the unloading curve and the hardness, H , was determined according to the following equations (Doerner, 1986):

$$E = \sqrt{\pi}/(2\sqrt{a}) \cdot S$$

$$H = F_{\max}/a,$$

where S represents the stiffness or slope of the unloading curve based on the method of Oliver and Pharr (Oliver and Pharr, 1992), a is the contact area of the indentation, and F_{\max} is the maximum force. The nanoindentation procedure was calibrated using a silica standard as previously described (Marshall *et al.*, 2001). Indentations were made at approximately equal intervals of less than 200 μm along a line from near the pulp chamber to the occlusal surface across the area that contained the artificial lesion. At each area along the line, we made a cluster of approximately 5 indentations to determine the hardness and modulus of intertubular dentin in the area. If measurements were made in areas of peritubular or intratubular dentin, it was noted and not included with intertubular dentin mechanical properties. We collected AFM images before and after the indentations to ensure that they were uniform and well-defined and were at the desired site within the intertubular dentin, as previously described (Marshall *et*

al., 2001). AFM images were also used to compare the surface morphology before and after remineralization.

Statistics

ANOVA ($p < 0.05$) was used to detect differences between hydrated nanomechanical properties of lesions treated with remineralization solution and that of baseline (demineralized) and normal dentin values. Furthermore, ANOVA was used to detect difference between time points.

Results

Artificial carious dentin lesions

AFM images of surface topography of lesion surfaces treated with the remineralization solutions are shown in Figure 5-1. Figure 5-1a shows the dentin surface of an artificial lesion treated with the demineralization buffer for 8 hours at pH 5.0, and residual mineral particles are visible in the intertubular region and peritubular dentin is largely absent. The surface after remineralization in Solution 1 for 1 day is shown in Figure 5-1b, for 7 days in Figure 5-1c, and for 7 days in high resolution in Figure 5-1d. Hydrated nanomechanical properties of remineralized lesions were compared to controls, normal and baseline (demineralized 8h) dentin values. Normal hydrated dentin mechanical properties were $E = 18.9 (4.2) \text{ GPa}$ and $H = 0.76 (0.32) \text{ GPa}$. Baseline mechanical properties of demineralized dentin were $E = 0.2 (0.1) \text{ GPa}$ and $H = 0.02 (0.01) \text{ GPa}$. For the three remineralization solutions without fluoride, at the 7 time points ($n=3$) between 1 and 28 days, hydrated elastic modulus ranged from $0.2 (0.1) \text{ GPa}$ to $3.0 (2.7) \text{ GPa}$ for solution 1, $0.2 (0.3) \text{ GPa}$ to $3.3 (4.4) \text{ GPa}$ for solution 2 and

0.3 (0.2) to 3.3 (2.1) GPa for solution 3 (Figure 5-2a, Table 5-2). Hydrated nanohardness ranged from 0.02 (0.01) to 0.05 (0.05) GPa for solution 1, 0.02 (0.01) to 0.12 (0.15) GPa for solution 2 and 0.02 (0.01) to 0.10 (0.08) GPa for solution 3 (Figure 5-2b, Table 5-3).

The three remineralization solutions with 2 ppm fluoride, at the 7 time points (n=3 each) between 1 and 28 days, had hydrated elastic moduli that ranged from 1.2 (0.5) to 12.4 (3.4) GPa for solution 4, 0.3 (0.3) to 6.6 (7.5) GPa for solution 5, and 1.0 (0.6) to 6.7 (5.7) GPa for solution 6 (Figure 5-2a, Table 5-2). Hydrated nanohardness ranged from 0.05 (0.02) GPa to 0.37 (0.14) GPa for solution 4, 0.02 (0.01) to 0.28 (0.23) GPa for solution 5, and 0.03 (0.02) to 0.12 (0.10) GPa for solution 5 (Figure 5-2b, Table 5-3).

Natural carious dentin lesions

AFM topographic images of a representative natural carious dentin lesion before and after treatment with remineralization solution 4 are shown in Figure 5-3. After 28 days in 2.2 mM Ca^{2+} , 1.45 mM PO_4^{3-} , 150 mM KCl, 2 ppm F at pH 7.4 (solution 4), hydrated elastic modulus increased to 2.9 (1.7) GPa, nanohardness increased to 0.25 (0.18) GPa (Figure 5-4a, Table 4). This data includes both pink and light pink zones of the natural lesions. When the light pink zones were removed from the data set, hydrated E after 28 days was 1.2 (0.5) GPa, an increase of only around 1 GPa, and nanohardness increased 0.16 (0.02) GPa (Figure 5-4b).

Discussion

This study used AFM-based nanoindentation of hydrated dentin to measure remineralization of carious dentin lesions. Hydrated nanomechanical property measurements are thought to be more relevant than dry measurements (Angker *et al.*, 2004; Marshall *et al.*, 2001), because they are sensitive to the interaction between the organic and inorganic components of the dentin and because teeth function in a hydrated state. The addition of 22 mM carbonate (Tung, 1995) to the remineralization solutions (2 and 5) did not have an effect on remineralization, even though carbonate increases remineralization rate by gradually increasing the pH as CO₂ evaporates. Alternatively if we look at the time points more closely, we can see that for solution 2, which contained 22 mM CO₃²⁻ but no fluoride, the first 4 time points (1 day, 3 days, 5 days and 7 days) had significant increases in hydrated nanomechanical properties, whereas solution 1, which had the same composition as solution 2, but did not contain CO₃²⁻, the first 4 time points did not have significant increases. This effect was not seen with the solutions that contained fluoride (solutions 4 and 5), perhaps because the addition of fluoride decreased the pH of the solutions and thus changed the rate of the reaction that forms carbon dioxide from CO₃²⁻ in solution.

As expected, the addition of 2 ppm fluoride to the remineralization solutions had a marked effect on remineralization rate. It has been demonstrated that fluoride can increase remineralization rates (Hicks *et al.*, 2004; Lagerweij and ten Cate, 2002; Mukai and ten Cate, 2002). Fluoride ions then incorporate into the carbonated hydroxyapatite mineral, becoming fluorapatite, which is less

soluble to cariogenic acids (Featherstone, 1999; Hicks *et al.*, 2004; Larsen and Jensen, 1989).

Remineralized artificial carious dentin lesion pink zones had significantly higher hydrated elastic modulus and hardness than that in natural caries after 28 days of remineralization with one of the fluoride solutions. This difference is likely due to differences in the artificial caries model and natural caries. The differences between artificial and natural lesions include: 1) the presence of bacteria and collagenases that could disrupt the collagen network in the pink zone of natural lesions; 2) the lack of remineralization and demineralization cycles, as occurs in natural caries; 3) artificial lesions were uniformly demineralized, while natural lesions contained varying amounts of residual extrafibrillar (EF) mineral, intrafibrillar (IF) mineral and negatively charged NCPs, which might interfere with remineralization by attracting the positively charged calcium ions. EF, instead of IF mineral could act as nucleation sites for remineralization, causing a decrease in hydrated mechanical properties because of the poor attachment of EF mineral to the collagenous matrix. It is important to consider these factors in a clinical setting. Therefore it may be necessary to alter the artificial carious dentin lesion model we have used.

In an effort to reduce variables, the artificial carious dentin model (Chapter 3) does not take into account many biochemical factors in the saliva that contribute to the caries balance (Featherstone, 2004). For example, the artificial carious dentin lesions in this study were generated by constant demineralization in a buffer at pH 5.0, while the pH in the mouth cycles between acidic (~pH 5)

and basic (~pH 8), depending on the presence of cariogenic acid produced by the bacteria that ferment ingested carbohydrates. This fluctuation in pH causes a unique and varied morphology of most carious dentin lesions, which contain transparent dentin, the transparency caused by occlusion of the dentinal tubules by reprecipitated mineral (Fusayama, 1991). Because our model was not pH-cycled and did not provide any activity from odontoblasts, our artificial lesions more or less had only two zones, pink and normal, with very small light pink zones (Chapter 3) and no transparent zone. Another reason that our artificial lesions only contained two zones may have to do with the fact that the lesions were created in extracted non-vital teeth with the pulp removed. According to Fusayama (Fusayama, 1993) carious dentin from pulp-less teeth do not have a light pink CD-stained or “inner” carious dentin and there is a sudden drop in hardness properties from the normal dentin to the pink CD-stained or “outer” carious dentin. Therefore, pH-cycles including demineralization and remineralization approaches have been (Featherstone, 1996; ten Cate, 1995) and should be used in the future to generate more clinically applicable data for dentin remineralization studies.

In conclusion, artificial carious dentin lesions were partially remineralizable, as measured by increases in hydrated nanomechanical properties from demineralized to remineralized dentin. Remineralization was enhanced by the addition of fluoride to the remineralization solution. Natural carious dentin lesions were also partially remineralizable, but not nearly to the same extent as the artificial lesions. These data have potential clinical

implications in favor of preservation of pink CD-stained dentin by the dentist for remineralization, instead of removal before placement of the restoration.

D. REFERENCES

Angker L, Nijhof N, Swain MV, Kilpatrick NM (2004). Influence of hydration and mechanical characterization of carious primary dentine using an ultra-micro indentation system (UMIS). *Eur J Oral Sci* 112(3):231-6.

Balooch M, Wu-Magidi IC, Balazs A, Lundkvist AS, Marshall SJ, Marshall GW, *et al.* (1998). Viscoelastic properties of demineralized human dentin measured in water with atomic force microscope (AFM)-based indentation. *J Biomed Mater Res* 40(4):539-44.

Clarkson BH, Chang SR, Holland GR (1998). Phosphoprotein analysis of sequential extracts of human dentin and the determination of the subsequent remineralization potential of these dentin matrices. *Caries Res* 32(5):357-64.

Daculsi G, Kerebel B, Kerebel LM (1979). Mechanisms of acid dissolution of biological and synthetic apatite crystals at the lattice pattern level. *Caries Res* 13(5):277-89.

Doerner W (1986). A method for interpreting the data from depth-sensing indentation instruments. *J Mater Res* 1(601-615).

Featherstone JD, Glena R, Shariati M, Shields CP (1990). Dependence of in vitro demineralization of apatite and remineralization of dental enamel on fluoride concentration. *J Dent Res* 69 Spec No(620-5; discussion 634-6).

Featherstone JD (1996). Modeling the caries-inhibitory effects of dental materials. *Dent Mater* 12(3):194-7.

Featherstone JD (1999). Prevention and reversal of dental caries: role of low level fluoride. *Community Dent Oral Epidemiol* 27(1):31-40.

Fusayama T (1991). Intratubular crystal deposition and remineralization of carious dentin. *J Biol Buccale* 19(3):255-62.

Fusayama T (1993). New Concepts in the Pathology and treatment of dental caries. In: A Simple Pain-Free Adhesive Restorative System by Minimal Reduction and Total Etching. Tokyo, St. Louis: Ishiyaku EuroAmerica, Inc. Publishers, pp. 1-20.

Hicks J, Garcia-Godoy F, Flaitz C (2004). Biological factors in dental caries: role of remineralization and fluoride in the dynamic process of demineralization and remineralization (part 3). *J Clin Pediatr Dent* 28(3):203-14.

Hunter GK, Goldberg HA (1994). Modulation of crystal formation by bone phosphoproteins: role of glutamic acid-rich sequences in the nucleation of hydroxyapatite by bone sialoprotein. *Biochem J* 302 (Pt 1)(175-9.

Kinney JH, Pople JA, Driessen CH, Breunig TM, Marshall GW, Marshall SJ (2001). Intrafibrillar mineral may be absent in dentinogenesis imperfecta type II (DI-II). *J Dent Res* 80(6):1555-9.

Kinney JH, Habelitz S, Marshall SJ, Marshall GW (2003). The importance of intrafibrillar mineralization of collagen on the mechanical properties of dentin. *J Dent Res* 82(12):957-61.

Klont B, ten Cate JM (1991). Susceptibility of the collagenous matrix from bovine incisor roots to proteolysis after in vitro lesion formation. *Caries Res* 25(1):46-50.

Lagerweij MD, ten Cate JM (2002). Remineralisation of enamel lesions with daily applications of a high-concentration fluoride gel and a fluoridated toothpaste: an in situ study. *Caries Res* 36(4):270-4.

Larsen MJ, Jensen SJ (1989). Solubility, unit cell dimensions and crystallinity of fluoridated human dental enamel. *Arch Oral Biol* 34(12):969-73.

Levine RS, Rowles SL (1973). Further studies on the remineralization of human carious dentine in vitro. *Arch Oral Biol* 18(11):1351-6.

Marshall GW, Habelitz S, Gallagher R, Balooch M, Balooch G, Marshall SJ (2001). Nanomechanical properties of hydrated carious human dentin. *J Dent Res* 80(8):1768-71.

McIntyre JM, Featherstone JD, Fu J (2000). Studies of dental root surface caries. 1: Comparison of natural and artificial root caries lesions. *Aust Dent J* 45(1):24-30.

Mukai Y, ten Cate JM (2002). Remineralization of advanced root dentin lesions in vitro. *Caries Res* 36(4):275-80.

Oliver W, Pharr, GM (1992). An improved technique for determining hardness and elastic modulus using load and displacement sensing indentation experiments. *J Mater Res* 7(1564.

Stetler-Stevenson WG, Veis A (1986). Type I collagen shows a specific binding affinity for bovine dentin phosphophoryn. *Calcif Tissue Int* 38(3):135-41.

ten Cate JMB, M.J.; Damen, J.J. (1995). pH-cycling of enamel and dentin lesions in the presence of low concentrations of fluoride. *Eur J Oral Sci* 103(6):362-7.

White JM, Goodis HE, Marshall SJ, Marshall GW (1994). Sterilization of teeth by gamma radiation. *J Dent Res* 73(9):1560-7.

Figures and Tables

Table 5-1. Metastable supersaturated remineralization solutions.

Solution	Ca ²⁺ (mM)	PO ₄ ³⁻ (mM)	KCl (mM)	CO ₃ ²⁻ (mM)	pH	F (ppm)	Saturation ⁴
1 ¹	2.2	1.45	150	0	7.4	0	13.1 (HAP)
2 ^{1,2}	2.2	1.45	150	22	Initial 5.5- 8.5	0	Initial 1.57 (HAP)
3 ³	1.5	0.9	150	0	7.4	0	9.96 (HAP)
4	2.2	1.45	150	0	7.4	2	13.1 (HAP) 16.8 (FAP)
5	2.2	1.45	150	22	Initial 5.5- 8.5	2	1.56 (HAP) 7.14 (FAP)
6 ³	1.5	0.9	150	0	7.4	2	9.96 (HAP) 14.1 (FAP)

¹ Saito, T, Arsenault, AL, Yamauchi, M, *et al.* (1997). Mineral induction by immobilized phosphoproteins. *Bone*, 21(4), 305-11.

² Tung, Ming S. (1995) Carbonated solutions for treating, mineralizing, and fluoridating calcified tissues and methods for their use. United States Patent 5,427, 768.

³ Featherstone JDB (1996). Modeling the caries-inhibitory effects of dental materials. *Dent Mater* 12 (3): 194-7.

⁴ Larsen J (2001). Ion products of calcium phosphate solutions. Aarhus, Denmark: Royal Dental College.

Table 5-2. Hydrated elastic modulus in GPa of artificial carious dentin lesions treated with remineralization solutions.

Remin time (days)	Elastic modulus (GPa) (sd)					
	Solution 1	Solution 2	Solution 3	Solution 4	Solution 5	Solution 6
	2.2 mM Ca ²⁺ /1.45 mM PO ₄ ³⁻ pH7.4 (n=3)	2.2 mM Ca ²⁺ /1.45 mM PO ₄ ³⁻ / 22 mM CO ₃ ²⁻ pH5.5- 8.5 (n=3)	1.5 mM Ca ²⁺ / 0.9 mM PO ₄ ³⁻ pH7.4 (n=3)	2.2 mM Ca ²⁺ /1.45 mM PO ₄ ³⁻ , 2ppm F, pH7.4 (n=3)	2.2 mM Ca ²⁺ /1.45 mM PO ₄ ³⁻ / 22 mM CO ₃ ²⁻ , 2 ppm F pH5.5-8.5 (n=3)	1.5 mM Ca ²⁺ / 0.9 mM PO ₄ ³⁻ , 2 ppm F, pH 7.4 (n=3)
1	0.4 (0.2)	0.7 (0.4)*	0.3 (0.2)	1.2 (0.5)*	0.3 (0.3)	1.0 (0.6)*
3	0.3 (0.2)	2.2 (1.2)*	0.9 (0.1)*	2.0 (3.0)	1.3 (0.8)*	1 (0.6)*
5	0.3 (0.1)	2.9 (1.3)*	1.8 (2)*	2.6 (1.2)*	1.1 (1.0)*	2.4 (1.5)*
7	0.2 (0.1)	3.3 (1.8)*	0.7 (0.3)*	4.6 (3.8)*	0.9 (1.2)	2.7 (1.2)*
14	2.0 (2.7)*	0.3 (0.4)	2 (1.8)*	4.9 (2.8)*	6.6 (7.5)*	2 (1.8)*
21	1.1 (1.4)*	0.2 (0.3)	0.9 (1)*	9.7 (3.7)*	5.6 (4.6)*	4.1 (3)*
28	2.7 (3.3)*	3.3 (4.4)*	3.3 (2.1)*	12.4 (3.4)*	2.2 (1.4)*	6.7 (5.7)*

* indicates a significant difference from baseline demineralized dentin (p<0.05).

Table 5-3. Hydrated nanohardness in GPa of artificial carious dentin lesions treated with remineralization solutions.

Remin time (days)	Nanohardness (GPa) (sd)					
	Solution 1	Solution 2	Solution 3	Solution 4	Solution 5	Solution 6
	2.2 mM Ca ²⁺ /1.45 mM PO ₄ ³⁻ pH7.4 (n=3)	2.2 mM Ca ²⁺ /1.45 mM PO ₄ ³⁻ / 22 mM CO ₃ ²⁻ pH5.5-8.5 (n=3)	1.5 mM Ca ²⁺ / 0.9 mM PO ₄ ³⁻ pH7.4 (n=3)	2.2 mM Ca ²⁺ /1.45 mM PO ₄ ³⁻ , 2ppm F, pH7.4 (n=3)	2.2 mM Ca ²⁺ /1.45 mM PO ₄ ³⁻ / 22 mM CO ₃ ²⁻ , 2 ppm F pH5.5-8.5 (n=3)	1.5 mM Ca ²⁺ / 0.9 mM PO ₄ ³⁻ , 2 ppm F, pH 7.4 (n=3)
1	0.02 (0.01)	0.02 (0.01)	0.02 (0.01)	0.05 (0.02)*	0.02 (0.01)	0.03 (0.02)
3	0.02 (0.01)	0.06 (0.06)*	0.04 (0.01)*	0.05 (0.05)	0.05 (0.03)*	0.07 (0.05)*
5	0.02 (0.01)	0.07 (0.08)*	0.06 (0.09)	0.09 (0.08)*	0.05 (0.04)*	0.07 (0.03)*
7	0.02 (0.01)	0.07 (0.08)*	0.03 (0.01)	0.13 (0.11)*	0.03 (0.04)	0.08 (0.09)*
14	0.05 (0.05)	0.01 (0.01)	0.07 (0.07)*	0.12 (0.07)*	0.19 (0.27)*	0.11 (0.10)*
21	0.03 (0.04)	0.02 (0.02)	0.03 (0.03)	0.22 (0.13)*	0.28 (0.23)*	0.09 (0.05)*
28	0.04 (0.02)*	0.12 (0.15)*	0.10 (0.08)*	0.37 (0.14)*	0.07 (0.14)*	0.12 (0.10)*

* indicates a significant difference from baseline demineralized dentin (p<0.05).

Table 5-4. Increase in hydrated elastic modulus and nanohardness in GPa of natural carious dentin lesions treated with one remineralization solution (2.2 mM Ca²⁺/1.45 mM PO₄³⁻, 2ppm F, pH7.4 (n=3).

Remineralization time (Days)	Increase in E (GPa)	Increase in H (GPa)
1	0.2 (0.1)	0.01 (0.01)
3	0.3 (0.2)	0.02 (0.01)
5	0.3 (0.2)	0.04 (0.02)
7	1.0 (1.0)*	0.06 (0.03)*
14	1.5 (0.9)*	0.14 (0.02)*
21	0.6 (0.2)*	0.08 (0.08)*
28	2.9 (1.7)*	0.26 (0.18)*

* indicates a significant difference from baseline demineralized dentin (p<0.05).

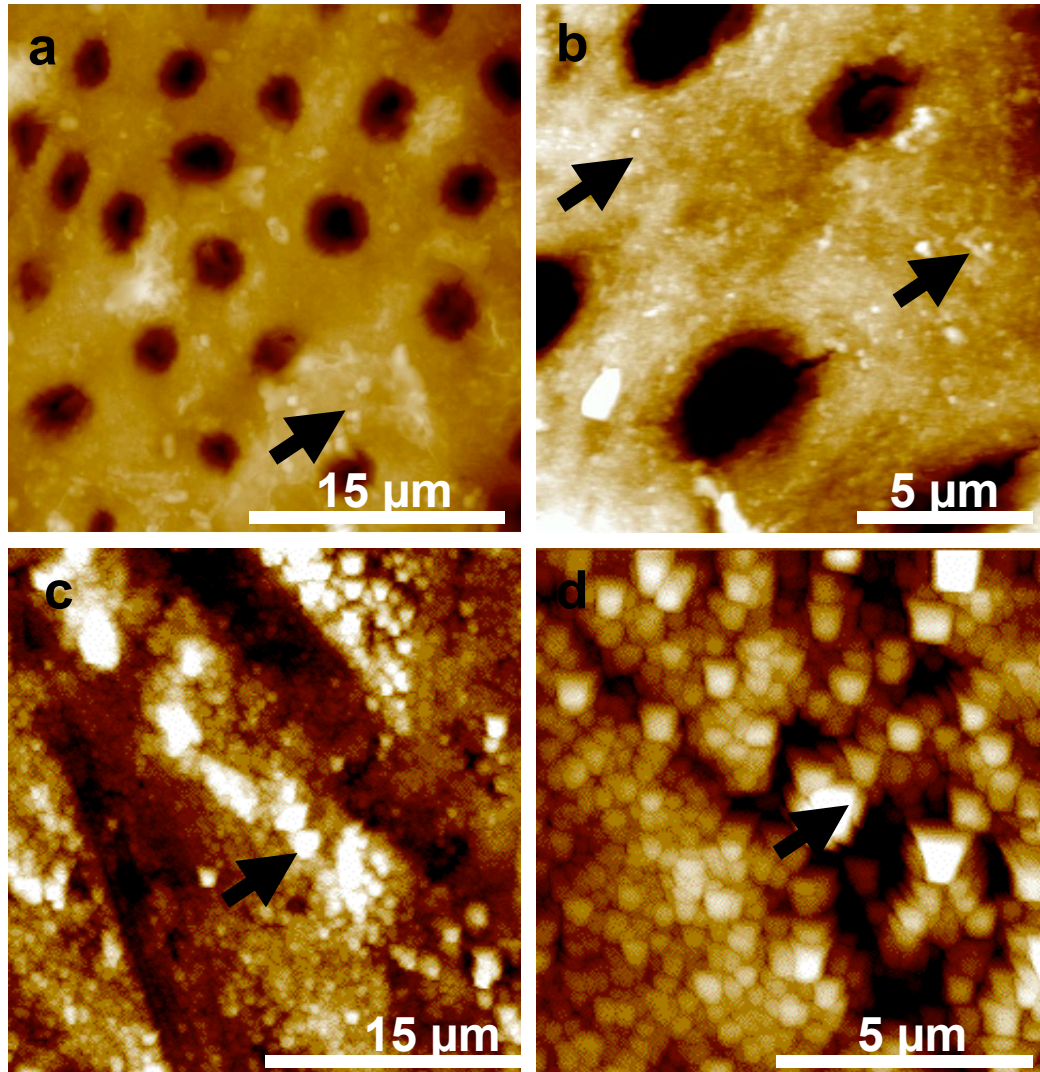


Figure 5-1. AFM topographic images of baseline (demineralized) dentin and dentin treated with remineralization solution. a) Baseline, demineralized dentin treated with 0.05 M acetate buffer with 2.2 mM Ca and PO_4 at pH 5.0 for 8 hours, black arrowhead shows remaining mineral on the surface; b) demineralized dentin treated with remineralization solution (2.2 mM Ca, 1.45 mM PO_4 , 150 mM KCl, pH 7.4) for 1 day; c) 7 days; and d) 7 days at high resolution. Black arrowheads in b, c and d indicate mineral deposited in intertubular dentin after remineralization treatment. Mineral deposition increased over time, even without fluoride.

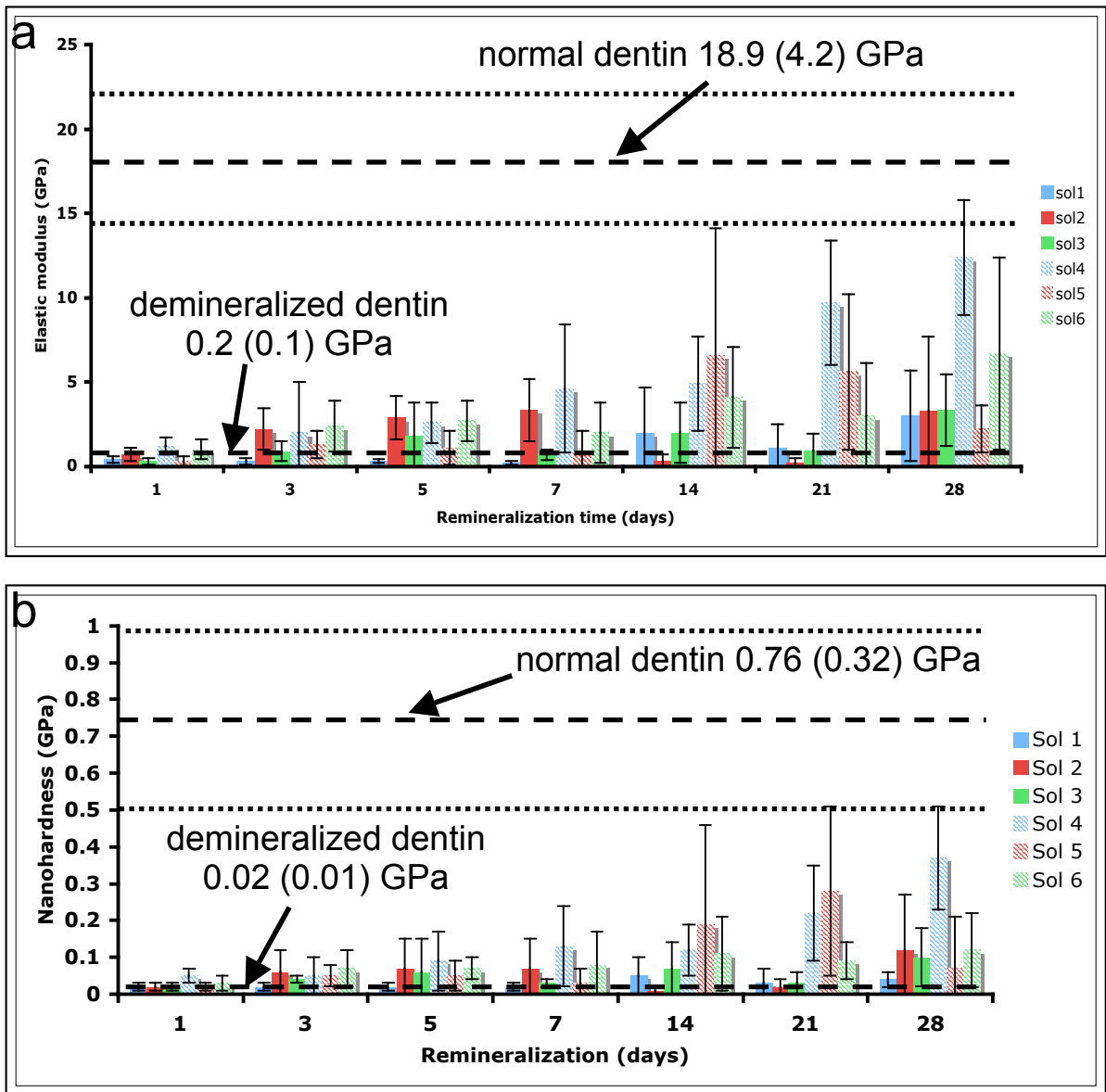


Figure 5-2. Hydrated nanomechanical properties from AFM-based nanoindentation of artificial carious dentin lesions (n=3) treated with remineralization solutions. a) Elastic modulus (E) of lesions with baseline (0.2 GPa) and normal (18.9 GPa) values; b) Nanoindentation hardness (H) of lesions with baseline (0.02 GPa) and normal (0.76 GPa) values. Both E and H increased with time, and were enhanced by the addition of fluoride to the remineralization solutions. CO_3^{2-} increased E and H without fluoride addition but not with fluoride. Average values for baseline demineralized dentin and normal dentin (with sd) indicated by dashed line.

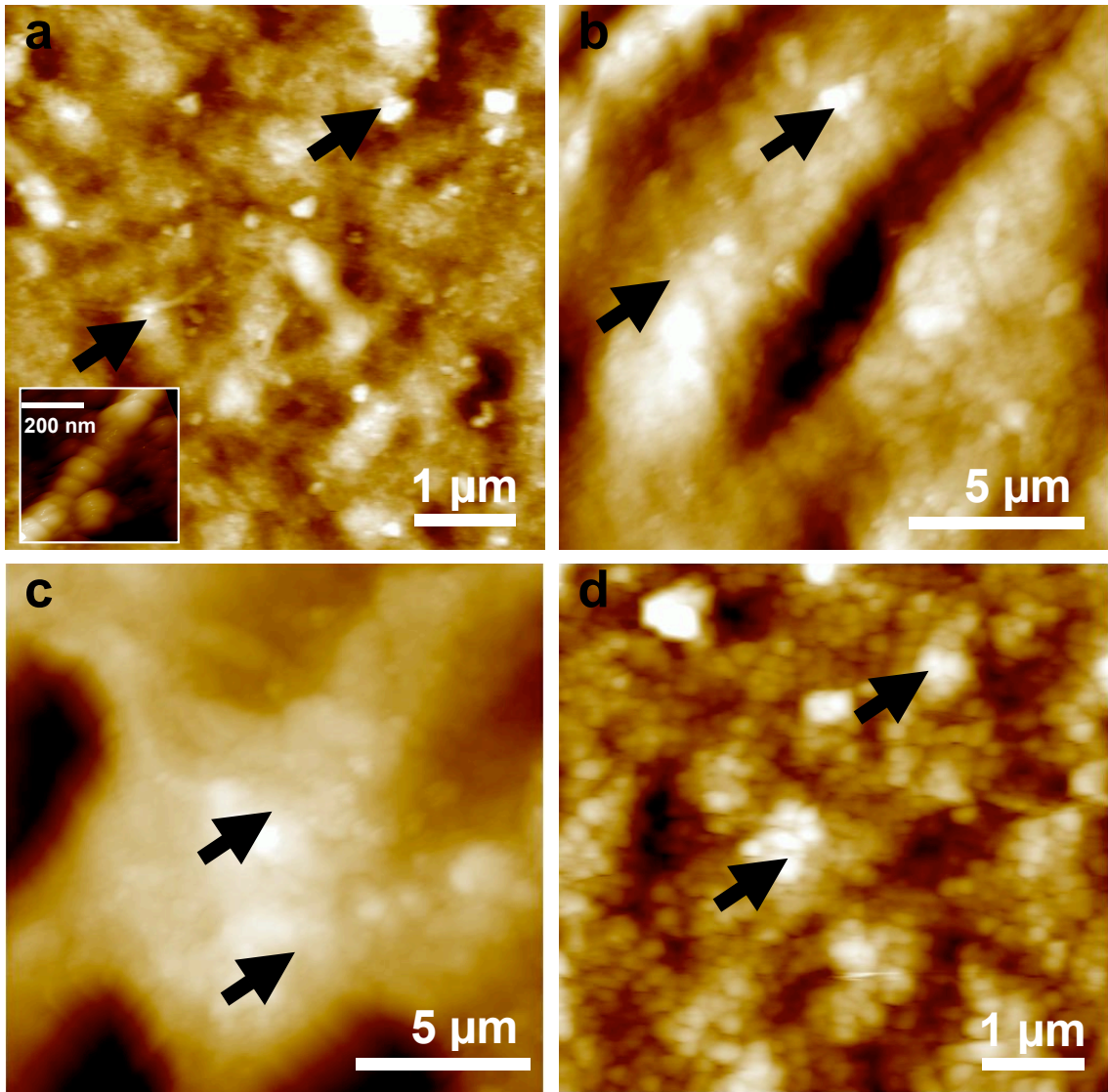


Figure 5-3. AFM topographic images of natural carious dentin lesions before and after treatment with remineralization solution 4 (2.2 mM Ca^{2+} , 1.45 mM PO_4^{3-} , 150 mM KCl, 2 ppm NaF, pH 7.4). a) baseline (carious) dentin shows residual mineral (black arrowhead) and collagen fibrils (black arrowhead and inset) in intertubular dentin; b) carious dentin treated with remineralization solution 4 for 7 days newly formed mineral in intertubular dentin (black arrowheads); c) 28 days newly formed mineral in intertubular dentin (black arrowheads); and d) 28 days at high resolution, newly formed mineral in intertubular dentin (black arrowheads). Mineral formation in intertubular dentin increased slowly over time after treatment with remineralization solution.

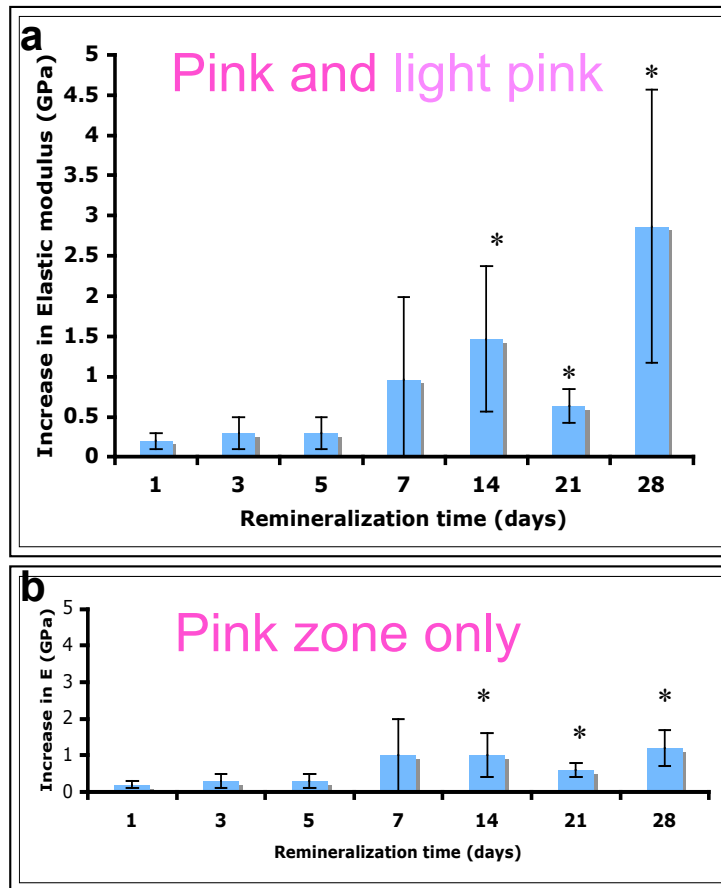


Figure 5-4. Increase in hydrated elastic modulus in GPa from baseline nanoindentation measurements of natural carious dentin lesions. a) Data from both pink and light pink zones of carious dentin; b) data from only pink zone of carious dentin. With the data from the light pink zones of remineralized dentin subtracted, increase in elastic modulus in pink zones was lower. * indicates significant differences from baseline demineralized dentin ($p < 0.05$).

Chapter 6

Summary and future directions

Summary and Discussion

Dental caries is one of the most common of all disorders, second only to the common cold with 94% of all adults having evidence of treated or untreated coronal caries (Winn *et al.*, 1996). Caries, a transmissible disease, occurs when plaque that is on the surface of the tooth contains bacteria that produce acids as a byproduct of fermentable carbohydrate metabolism (Loesche, 1986). The organic acids produced by the bacteria diffuse into the enamel and dentin, dissolving the apatite mineral (LeGeros, 1991).

Traditionally, dentists treat caries by using invasive techniques to remove the diseased and surrounding dental tissue and restore the lesion with a synthetic material, ideally preventing further progression of decay. Unfortunately dentists currently spend more time retreating restored teeth than treating primary decay and the cycle of re-restoration significantly weakens teeth and causes additional pulpal insult (Anusavice, 1988; Brantley *et al.*, 1995). Therefore modern management of caries stresses non-invasive techniques whenever possible for maximum protection of sound tooth structure. The decision to initiate operative intervention is significant because it is irreversible and restorations have a finite lifespan (McComb, 2001).

A primary goal of dental tissue engineering is the biological reconstruction of tooth substrate destroyed by caries. Success in strategies associated with remineralization of enamel and root caries (Featherstone and Rodgers, 1981; O'Reilly and Featherstone, 1987), and studies on the roles of calcified matrix proteins in *de novo* mineralization of bone or dentin have contributed to the less

invasive possibility of remineralization of carious lesions extending into dentin (Hunter and Goldberg, 1993; Lussi *et al.*, 1988; Mukai and ten Cate, 2002). Studies have shown that insoluble phosphoprotein tightly bound to collagen may nucleate mineral crystal growth within the collagen fibrils, so-called intrafibrillar mineral (IF), as opposed to extrafibrillar mineral (EF), which forms outside of or around the collagen fibrils (Bradt JH, 1995; Landis *et al.*, 1993; Olszta *et al.*, 2003). The primary role of teeth is mastication and therefore their main function is mechanical. We thus define functional remineralization as remineralization that restores the original mechanical properties of the tissue. Functional remineralization of dentin is considered ideal because it should maintain the unique association between organic (type I collagen network with NCPs) and inorganic matrices (carbonated apatite crystals) in dentin.

In Chapter 2, Caries Detector (CD) stain was shown to distinguish zones within the caries with different elastic modulus (E), nanohardness (H) and mineral content. As expected, mineral content was correlated with E and H. A significant finding from this chapter is that the pink zone of these carious dentin lesions contained about 25% of the mineral content of normal dentin. Previous studies of bone have shown that the mineral of the calcified tissue is partitioned between two sites: intrafibrillar mineral, which is confined within the gap zones of the collagen fibrils; and extrafibrillar mineral, which lies within the interstitial spaces separating the fibrils (Landis *et al.*, 1996). Extrafibrillar mineral, makes up as much as 75% of the total mineral (Bonar *et al.*, 1985), leaving 25% intrafibrillar mineral. Therefore, in our study, the pink zone may have remaining intrafibrillar

mineral, which may have important consequences on remineralization and restoration of mechanical properties since it has been shown that if dentin lacks the IF, mechanical properties are drastically lowered when measured under hydrated conditions (Kinney *et al.*, 2003).

In Chapter 3, artificial carious dentin lesions had similar elastic modulus, hardness and mineral content in the pink zones as natural carious dentin lesions. Artificial lesions also had similar correlations between elastic modulus, hardness and mineral content. Some notable differences between the lesions generated by the artificial carious dentin model used in this study and natural carious dentin lesions are that there is little to no light pink zone, as well as the lack of the transparent zone in artificial lesions. This results in a sharper gradient in elastic modulus and mineral content reduction between normal dentin and the most demineralized (pink zone) dentin. The discrepancies between the artificial lesions generated by our model and natural lesions could be explained by the fact that our model used constant demineralization instead of pH-cycling, which is more clinically relevant (Featherstone *et al.*, 1990; ten Cate, 1982). We chose to use constant demineralization because we wanted a simple model at first, so we could control variables and make changes as needed. Our results indicate that pH-cycling should be utilized.

In Chapter 4, trichrome staining, which was used to identify collagen in carious dentin, identified the same four zones as distinguished by Caries Detector staining. High-resolution AFM imaging of carious dentin collagen in the pink zone revealed partially demineralized fibrils that display the characteristic

~67 nm periodicity. These collagen fibrils had gap-overlap depths of 2.7 nm, suggesting remaining intrafibrillar mineral, since unmineralized collagen has a gap-overlap depth of 7 nm (Balooch *et al.* 2004).

UVRRS of demineralized dentin collagen and artificial and natural carious dentin demonstrated that the intrafibrillar collagen environment in dentin is affected by demineralization and drying, as the demineralized collagen matrix collapses with dehydration. SAXS data showed similarities between natural and artificial lesions but did not confirm the presence of mineral crystallites in the gap zones of collagen fibrils in the most demineralized pink zone of caries. It is possible that the SAXS measurements of the carious dentin were not accurate since they were taken under dry conditions, in which the demineralized dentin collagen matrix will collapse (Marshall *et al.*, 1998). According to Kinney *et al.* (2001), for SAXS to identify the 67 nm periodicity of mineral in the collagen fibrils, the x-ray beam must be perpendicular to the tubule axes, since in a hydrated or mineralized state the collagen fibrils are perpendicular to the tubules.

In summary, the collagen from the pink zones of arrested natural carious dentin lesions seemed intact with some remaining intrafibrillar mineral. Arrested lesions may not contain activated collagenases and the artificial lesions were not treated with collagenase. However, active lesions are known to contain active collagenases that degrade the carious dentin matrix (Tjaderhane *et al.*, 1998), decreasing the remineralization potential because degraded collagen cannot be bound to a phosphoprotein (Clarkson *et al.*, 1998) or intrafibrillar mineral. Further

characterization of the collagen in carious dentin is necessary, especially in active lesions.

In Chapter 5, when artificial lesions were treated with 6 different remineralization solutions, CO_3^{2-} had no effect with fluoride, but did have an effect without F^- at shorter time points. Artificial carious dentin lesions were partially remineralizable (~65% of normal dentin), as measured by increases in hydrated nanomechanical properties from demineralized to remineralized dentin. Remineralization was enhanced by the addition of fluoride to the remineralization solution.

Natural carious dentin lesions were also partially remineralizable (~15% of normal dentin), but not nearly to the same extent as the artificial lesions. The natural lesions may have had uncontrollable variables such as residual extrafibrillar mineral crystals on the lesion surface that may have attracted the mineral ions instead of allowing them to attach to intrafibrillar mineral, causing the lower mechanical properties of the partially remineralized natural carious dentin lesions. These extrafibrillar mineral crystals, were in fact observed by AFM imaging of the most demineralized pink zones, revealing a heterogeneous surface in contrast to the surface of the artificially demineralized dentin. This emphasizes the benefit of using an artificial lesion model for *in vitro* remineralization studies, to fully understand the different variables involved in the process of natural dentin caries formation. These data have potential clinical implications in favor of preservation of pink CD-stained dentin by the dentist for remineralization, instead of removal before placement of the restoration.

In carious dentin lesions, the existing mineral nuclei or crystals may facilitate *functional* mineral growth, from within collagen fibrils (IF) and continuing outward to the EF compartment (Kinney *et al.*, 2003). Without existing nuclei, in completely demineralized collagen, remineralized tissue is likely the result of *precipitative* mineral growth, filling only the extrafibrillar compartment with mineral. This tissue may have structural and nanomechanical similarities to DI-II dentin. Functional remineralization is considered to be optimal.

The clinical applications of this area of biomineralization are vast, including therapies for defective bone and dentin diseases, such as dental caries. Theoretically, it would be possible to remineralize dentin demineralized by cariogenic acids, as long as the mechanisms and components involved in initial dentin mineralization were understood and the remaining components in the carious lesions were known. Caries-demineralized dentin generally contains varying and unknown concentrations of residual mineral. Therefore, it is important to identify the remaining components in carious dentin lesions and their effects on remineralization within different regions of the lesions, such that optimal remineralization conditions are determined, and future caries treatments can be minimally invasive.

One significant clinical consideration involved in dentin caries remineralization that has not been discussed thus far in this thesis is bacterial infection. Although traditional restorative intervention of caries may eliminate the bacteria at the restoration site, the bacteria are able to recolonize in the rest of

the mouth, continuing the progression of other carious lesions (Wright *et al.*, 1992). Antibacterial therapy, such as chlorhexidine treatment as a caries preventative measure is rarely used in the US (Featherstone, 2000), even though it has been shown to markedly reduce cariogenic bacteria (Anderson *et al.*, 1993). It is therefore essential to address the bacterial challenge when employing remineralization protocols clinically.

Future Directions

Active carious dentin lesions

An important distinction to make is that the results from this research primarily come from arrested lesions, which clinically differ significantly from active lesions in severity, morphology, rate of mineral loss and level of bacterial infection. Therefore, the experiments in this dissertation should be performed on active carious dentin lesions, including caries detector zone characterization by mechanical properties and mineral content, comparison with an artificial carious dentin model, collagen characterization by SAXS and high-resolution AFM imaging, and remineralization. These results should be compared with data from arrested lesions.

Artificial dentin caries model

As discussed in Chapter 3, the artificial carious dentin lesions produced by demineralization, with 0.05M acetate with 2.2 mM Ca/PO₄ at pH 5, had no transparent zone and much smaller light pink zones than arrested natural carious

dentin lesions. The saliva in the mouth undergoes pH cycling as a result of the balance between pathological factors (acid challenge) and protective factors, which determine the progression or reversal of caries (Featherstone, 2000). The dynamic nature of the dentin caries process has been simulated by several pH cycling models (Featherstone *et al.*, 1990; ten Cate, 1982). Due to the changes in pH from pathological factors promoting demineralization and protective factors promoting remineralization (Featherstone, 2000), pH-cycling during demineralization may be more clinically relevant for the model. pH-cycling could potentially produce artificial carious dentin lesions with larger light pink zones and transparent zones. During the remineralization cycle, the supersaturated remineralization solution will deposit calcium and phosphate in the form of apatite on the demineralized dentin surface, thus reducing the substrate's porosity and potentially filling the dentinal tubules to form transparent dentin. When using an artificial demineralization pH-cycling model to simulate active carious dentin lesions, collagenases should be incorporated into the model (Tjaderhane *et al.*, 1998).

AFM nanoindentation load-displacement curve analysis

Nanoindentation load-displacement curves provide information of materials response to contact deformation. Most nanoindentation theory and instruments have been developed for smooth, solid, elastic or elastic-plastic materials, but biological tissues are hydrated viscoelastic materials with irregular geometries. The shape of the unloading portion of the curve should be linear and determines

the Young's modulus of the material. However, when the material displays viscoelastic behavior as the load is removed, then the unloading curve fits no existing model particularly well. This results in considerable difficulty in obtaining valid mechanical property data for these types of materials. The most demineralized zones of artificial and natural carious dentin lesions (Chapters 2, 3, 4 and 5) exhibited obvious indications of such viscoelastic behavior, with non-linear unloading portions from nanoindentation load-displacement curves (Figure 6-1). Furthermore, it is important to note that nanoindentation measurements of very soft dentin caries may not be accurate since the actual Young's modulus may be below the lower limit of the AFM instrumentation, which in the case of our microscope is ~200 MPa.

Collagen gap-overlap height difference measurements

High-resolution AFM-based measurements of gap-overlap height differences in collagen fibrils from light pink, transparent and normal dentin should be compared with data from the pink zone in this study. Imaged surfaces should remain untreated, but this may not be possible in the more mineralized zones such as light pink, transparent, and apparently normal because collagen fibrils generally cannot be resolved without treatment with citric acid and NaOCl (Habelitz *et al.*, 2002), or EDTA (Pugach *et al.* IADR abstract, 2004) to remove NCPs and any remaining mineral coating the fibril surface. Unfortunately these treatments could cause artifacts for measuring gap-overlap height differences. Normal dentin treated with citric acid and NaOCl to reveal the collagen fibrils

exhibited gap depths of 3 to 7 nm (Habelitz *et al.*, 2002).

TEM analysis of carious dentin

Since SAXS measurements of carious dentin did not confirm the presence of mineral crystallites in the gap zones of collagen fibrils in the most demineralized (pink) zones (Chapter 4), TEM should be utilized to image the crystallites at high resolution. TEM has been used to visualize the mineral-collagen interactions in bone, tendon (Prostak and Lees, 1996), and dentin (Nalla *et al.*, 2005).

Significance of this research

The results presented in this dissertation emphasize minimally invasive dentistry- based treatment of carious lesions extending into the dentin. The regions of carious dentin lesions that are typically removed by dentists, and stain pink with Caries Detector stain, are possibly infected with cariogenic bacteria, and historically have been considered non-remineralizable (Fusayama, 1988). However, the research in this dissertation suggests that these region of carious dentin that stain pink, do in fact contain mineral, possibly within the collagen fibrils and are partially remineralizable. Remineralization was measured as an increase in nanomechanical properties of the demineralized dentin treated with remineralization solutions. Both elastic modulus and hardness increased in partially remineralized dentin and remineralization was therefore considered functional. This effect was enhanced by the addition of fluoride in the remineralizing solution. However, functional remineralization should occur slowly

in order to allow for the interaction of calcium, phosphate and fluoride ions from either the dental pulp or the occlusal lesion surface, with collagen and prevent apatite precipitation on the lesion surface, as evidenced by the artificial lesions from this study that remineralized to 2/3 of normal dentin mechanical properties.

The artificial carious dentin lesion model used in this research produced lesions that resembled active carious dentin lesions in Caries Detector zones and mineral gradients, and resembled arrested lesion in pink zone properties. The lesions were remineralizable to a much greater extent than the arrested natural carious dentin lesions. This discrepancy may have occurred because residual extrafibrillar mineral in the pink zone of the arrested lesions may have attracted the calcium, phosphate, and fluoride ions from the remineralization solution, prevent them from binding to the remaining intrafibrillar mineral. These studies emphasize the importance of using an artificial lesion model for studying dentin remineralization, since it allows for a better understanding of the variables involved in the dentin caries process.

Conclusions

In this thesis for the first time, the Caries Detector stained zones of arrested carious dentin lesions have been characterized in terms of mechanical properties, mineral content and collagen characteristics. Furthermore the remineralization potential of each zone was tested. The most demineralized pink zone, which is commonly removed prior to restoration, contains considerable residual mineral and is remineralizable.

D. REFERENCES

Anderson MH, Bales DJ, Omnell KA (1993). Modern management of dental caries: the cutting edge is not the dental bur. *J Am Dent Assoc* 124(6):36-44.

Anusavice KJ (1988). Criteria for placement and replacement of dental restorations. *Fla Dent J* 59(2):30-1.

Balooch MB, G; Habelitz, S; Marshal, SJ; and Marshall, GW (2004). Intrafibrillar demineralization study of single human dentin collagen fibrils by AFM. *MRS Symposium Proceedings*.

Bonar LC, Lees S, Mook HA (1985). Neutron diffraction studies of collagen in fully mineralized bone. *J Mol Biol* 181(2):265-70.

Bradt JH MM, Teresiak A, Pompe W (1995). Biomimetic mineralization of collagen by combine fibril assembly and calcium phosphate formation. *Chem Mater* 11(2694-2701).

Brantley CF, Bader JD, Shugars DA, Nesbit SP (1995). Does the cycle of reresoration lead to larger restorations? *J Am Dent Assoc* 126(10):1407-13.

Clarkson BH, Chang SR, Holland GR (1998). Phosphoprotein analysis of sequential extracts of human dentin and the determination of the subsequent remineralization potential of these dentin matrices. *Caries Res* 32(5):357-64.

Featherstone JD, Rodgers BE (1981). Effect of acetic, lactic and other organic acids on the formation of artificial carious lesions. *Caries Res* 15(5):377-85.

Featherstone JD, Glena R, Shariati M, Shields CP (1990). Dependence of in vitro demineralization of apatite and remineralization of dental enamel on fluoride concentration. *J Dent Res* 69 Spec No(620-5; discussion 634-6.

Featherstone JD (2000). The science and practice of caries prevention. *J Am Dent Assoc* 131(7):887-99.

Fusayama T. (1988). Clinical guide for removing caries using a caries-detecting solution. *Quint Int* 19:397-401.

Habelitz S, Balooch M, Marshall SJ, Balooch G, Marshall GW, Jr. (2002). In situ atomic force microscopy of partially demineralized human dentin collagen fibrils. *J Struct Biol* 138(3):227-36.

Hunter GK, Goldberg HA (1993). Nucleation of hydroxyapatite by bone sialoprotein. *Proc Natl Acad Sci U S A* 90(18):8562-5.

- Kinney JH, Pople JA, Marshall GW, Marshall SJ (2001). Collagen orientation and crystallite size in human dentin: a small angle X-ray scattering study. *Calcif Tissue Int* 69(1):31-7.
- Kinney JH, Habelitz S, Marshall SJ, Marshall GW (2003). The importance of intrafibrillar mineralization of collagen on the mechanical properties of dentin. *J Dent Res* 82(12):957-61.
- Landis WJ, Song MJ, Leith A, McEwen L, McEwen BF (1993). Mineral and organic matrix interaction in normally calcifying tendon visualized in three dimensions by high-voltage electron microscopic tomography and graphic image reconstruction. *J Struct Biol* 110(1):39-54.
- Landis WJ, Hodgens KJ, Arena J, Song MJ, McEwen BF (1996). Structural relations between collagen and mineral in bone as determined by high voltage electron microscopic tomography. *Microsc Res Tech* 33(2):192-202.
- LeGeros RZ (1991). Calcium phosphates in oral biology and medicine. *Monogr Oral Sci* 15(1-201).
- Loesche WJ (1986). Role of *Streptococcus mutans* in human dental decay. *Microbiol Rev* 50(4):353-80.
- Lussi A, Crenshaw MA, Linde A (1988). Induction and inhibition of hydroxyapatite formation by rat dentine phosphoprotein in vitro. *Arch Oral Biol* 33(9):685-91.
- Marshall GW, Jr., Wu-Magidi IC, Watanabe LG, Inai N, Balooch M, Kinney JH, et al. (1998). Effect of citric acid concentration on dentin demineralization, dehydration, and rehydration: atomic force microscopy study. *J Biomed Mater Res* 42(4):500-7.
- McComb D (2001). Systematic review of conservative operative caries management strategies. *J Dent Educ* 65(10):1154-61.
- Mukai Y, ten Cate JM (2002). Remineralization of advanced root dentin lesions in vitro. *Caries Res* 36(4):275-80.
- Nalla RK, Porter AE, Daraio C, Minor AM, Radmilovic V, Stach EA, et al. (2005). Ultrastructural examination of dentin using focused ion-beam cross-sectioning and transmission electron microscopy. *Micron* 36(7-8):672-80.
- O'Reilly MM, Featherstone JD (1987). Demineralization and remineralization around orthodontic appliances: an in vivo study. *Am J Orthod Dentofacial Orthop* 92(1):33-40.

Olszta MJ, Douglas EP, Gower LB (2003). Scanning electron microscopic analysis of the mineralization of type I collagen via a polymer-induced liquid-precursor (PILP) process. *Calcif Tissue Int* 72(5):583-91.

Prostak KS, Lees S (1996). Visualization of crystal-matrix structure. In situ demineralization of mineralized turkey leg tendon and bone. *Calcif Tissue Int* 59(6):474-9.

Pugach MK, Li W, Habelitz S, Marshall SJ, and Marshall GW. In Vitro Dentin Demineralization by Acetic Acid or EDTA. J Dent Res IADR abstract #893, 2004

ten Cate JMaD, P.P. (1982). Alternating demineralization and remineralization of artificial enamel lesions. . *Caries Res* 16(201-210).

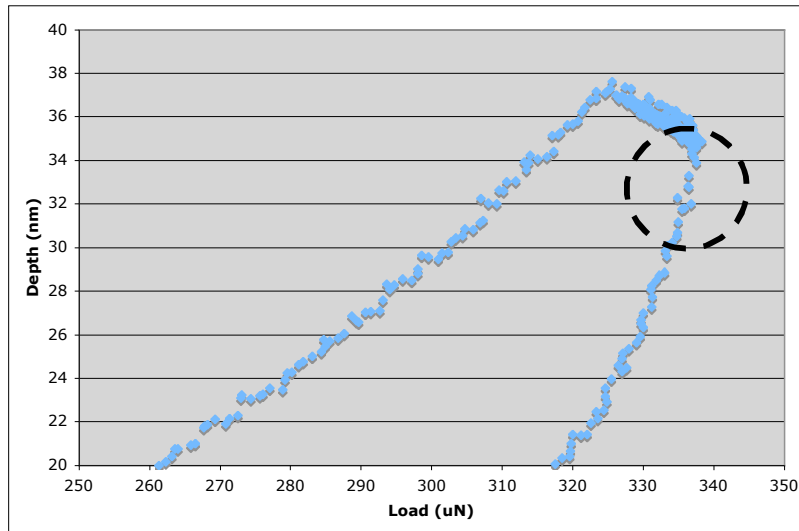
Tjaderhane L, Larjava H, Sorsa T, Uitto VJ, Larmas M, Salo T (1998). The activation and function of host matrix metalloproteinases in dentin matrix breakdown in caries lesions. *J Dent Res* 77(8):1622-9.

Winn DM, Brunelle JA, Selwitz RH, Kaste LM, Oldakowski RJ, Kingman A, *et al.* (1996). Coronal and root caries in the dentition of adults in the United States, 1988-1991. *J Dent Res* 75 Spec No(642-51).

Wright JT, Cutter GR, Dasanayake AP, Stiles HM, Caufield PW (1992). Effect of conventional dental restorative treatment on bacteria in saliva. *Community Dent Oral Epidemiol* 20(3):138-43.

Figure 6-1

(a) Carious Dentin



(b) Non-carious Dentin

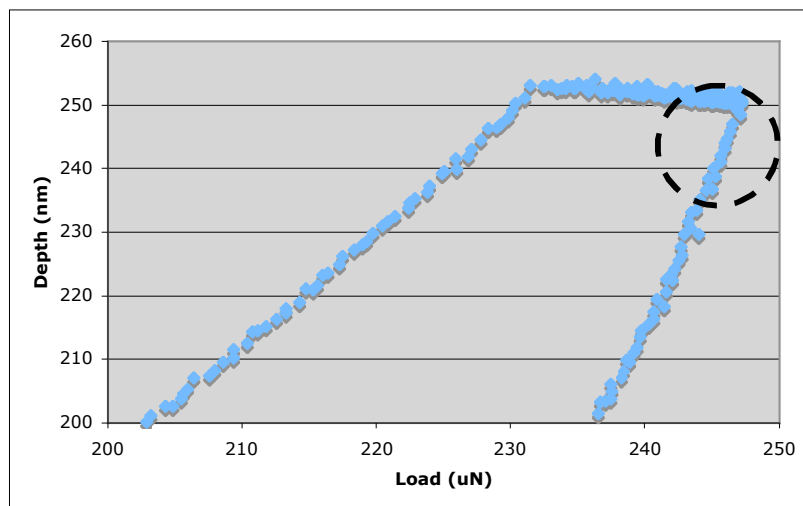


Figure 6-1. Load-displacement curves from AFM nanoindentation of (a) carious and (b) non-carious dentin. (a) Carious dentin exhibits non-linear viscoelastic behavior in the unloading portion of curve, while (b) non-carious dentin has a linear unloading portion of the curve. Unloading portions are indicated by dashed circle.

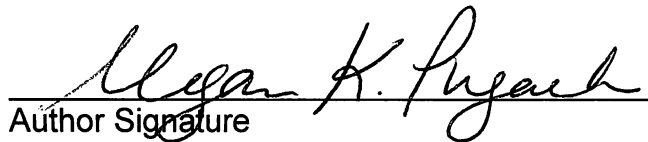
UCSF Library Release

Publishing Agreement

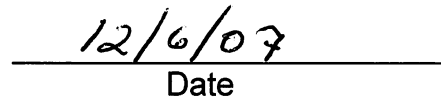
It is the policy of the University to encourage the distribution of all theses and dissertations. Copies of all UCSF theses and dissertations will be routed to the library via the Graduate Division. The library will make all theses and dissertations accessible to the public and will preserve these to the best of their abilities, in perpetuity.

Please sign the following statement:

I hereby grant permission to the Graduate Division of the University of California, San Francisco to release copies of my thesis or dissertation to the Campus Library to provide access and preservation, in whole or in part, in perpetuity.



Author Signature



Date